Analysis of spatiotemporal patterns of plastics in the Baltic Sea

Master Thesis in Physics

Written by *Ella Jacobsen*

December 31, 2020

Supervised by
Markus Jochum

University of Copenhagen

UNIVERSITY OF COPENHAGEN

NAME OF INSTITUTE:	KU-SCIENCE
NAME OF DEPARTMENT:	Niels Bohr Institute
AUTHOR(S):	Ella Jacobsen
EMAIL:	xjw372@alumni.ku.dk
TITLE AND SUBTITLE:	Analysis of spatiotemporal patterns of plastics in the Baltic Sea -
SUPERVISOR(S):	Markus Jochum
HANDED IN:	December 31, 2020
DEFENDED:	January 13, 2021

NAME ______________________________

SIGNATURE __________________________

DATE ______________________________

Acknowledgements

I would like to thank my supervisor, Professor Markus Jochum, for helping me with the direction of my thesis project. The original plan for my thesis did not work out, and Professor Jochum provided the necessary guidance to let me continue with a new direction, after which he provided a lot of useful feedback.

I would also like to thank Xaver Lange from Team Ocean, who ran the GETM simulations in the project on my behalf, and who took the time throughout the project to help me with data analysis and simulations.

Abstract

Marine plastic pollution has become an increasing area of concern in recent years. In spite of this, there are still gaps in our knowledge about the distribution and transport of plastics in the sea. In this thesis project, our aim is to analyze the spatiotemporal patterns of plastics via a summary of data from the literature and a simulation of plastic transport. We will restrict our attention to the Baltic Sea for the literature review, and to the Gullmar Fjord in Sweden for the simulation, in order to limit the scope of the project. The main finding from the literature is that microplastic particles tend to be more abundant in shallow waters, followed by near the ocean floor, with few particles in intermediate layers. The main finding from the simulation case study is that wind transport tends to be the most important factor in plastic transport when wind is present, and that otherwise tidal effects play a large role.

Contents

Part I
Introduction

1 Project overview

Plastics are defined as those polymers which can be molded, and which soften upon heating. They are inexpensive, light and durable, and also a very versatile class of materials since different plastic polymers can have a wide array of useful properties. As a result of this, they are used to manufacture a variety of different household and industrial products. (Ilyas et al. 2018)

The durability of plastics unfortunately comes with a downside, namely that they are difficult to dispose of. Plastic items degrade when exposed to UV light or subject to mechanical abrasion, however this degradation occurs slowly, and plastic particles can remain in the environment for a long time. Because of their utility, plastic pollution is widespread globally, with plastic fragments found in urban areas but also in soil samples and bodies of water. (Thompson et al. 2009)

In this project, the focus will be on plastic pollution in the marine environment. This is a relevant topic for consideration as the amount of plastic pollution entering the ocean is large, and it degrades slowly. It can have a negative impact on marine environments due to ingestion or entanglement by marine animals, and thus harm marine ecosystems. This can further affect humans and other species which consume marine organisms such as fish or plankton (Ilyas et al. 2018). We therefore wish to have an idea as to the magnitude of the problem, if something is to be done about plastic pollution in the future.

Plastic pollution in world oceans is a large topic for consideration. There may be global differences in sources and amounts of pollution, as this depends heavily on local factors such as plastic consumption and the quality of sewage treatment facilities. Additionally, there are different relevant transport mechanisms in the movement of plastics that depend on the size of the body of water under consideration. In order to limit the scope of the project to something more feasible, we will consider plastic pollution in the Baltic Sea, which is relatively small and enclosed.

Even if we restrict our focus to a single geographical area, there are many relevant questions we can ask that have yet to be resolved in the literature. A few examples include an accurate evaluation of the sources of plastic pollution in the sea, which areas have higher abundance of plastic litter, what the relevant transport mechanisms are, what the sinks are for plastic litter, and what the effect is on marine ecosystems. Each of these issues is challenging to address, and so we once again restrict our attention to only a couple of these aspects. The focus on this project will therefore be to assess the abundance of plastic litter in the Baltic Sea, as well as to learn more about the transport pathways of plastic.

We will use different methods for each of these two tasks. In order to learn about the abundance of plastic pollution in the Baltic Sea, we will conduct a literature review of studies in which samples were taken in the Baltic Sea to determine pollution levels. These studies attempt to collect information about the concentration of especially microplastics in the Sea. They do not, however, provide information on how long the collected particles had been at sea, or provide any evidence as to the path by which particles had reached these locations. To explore the transport pathways of plastic particles, we therefore conduct a simulation of plastic particle releases over a week of wind-driven currents. As obtaining the wind-driven currents was computationally expensive, we selected to run the simulations only for the Gullmar Fjord in Sweden, which is near the transition between the Baltic and North Seas.

In conclusion, the main aims of this project are to critically evaluate what we can conclude about the abundance of plastic litter in the Baltic Sea from the literature, as well as to examine the dominant transport pathways and patterns of plastic particles released in a case study in the Gullmar Fjord.

2 Structure of the thesis

We have structured the thesis in order to satisfy these two aims as clearly as possible. First, we will start with a brief section detailing some of the relevant theory and background which we will need for the rest of the project. This includes an overview of basic concepts from fluid mechanics, a description of the Eulerian and Lagrangian views of fluid motion, and a look at some of the known transport pathways for plastic pollution.

Next, we will attempt to determine the distribution of plastic pollution in the Baltic Sea, to satisfy the first aim of the project. The focus here will be on pollution of microplastic particles, which are defined as those plastic particles which have a diameter smaller than 5 mm, as this is the type of litter for which most literature data is available. We will cover how data is collected and analyzed in these studies, including the benefits and limitations of the different methods. After this we will describe what conclusions can be drawn in a review of the literature data regarding the distribution of microplastics both horizontally and vertically in the water column, with consideration to the limitations in the data collection.

We will then try to fulfill the second aim of the project, to learn more about the transport pathways of plastic litter via a case study in the Gullmar Fjord. In order to do this, we will first analyze the wind conditions in this area with regards to typical wind speeds and directions, as well as the steadiness of the wind velocity. Then we will further describe the implementation details for the simulation, followed by results. In the results, we will examine the accumulation patterns of plastics when several different wind directions were applied, as well as the difference in the results if we had taken a boxcar average over a time scale greater than the tidal period. This was done to determine the effect of different wind directions, as well as to attempt to evaluate the relative magnitude of wind and tidal effects.

Finally, we will conclude on the findings in the thesis project, and assess whether we have answered our aims. We will examine what the limitations are of the methods we have used, and consequently of our conclusions. We will finish off with ideas for further research on abundance and transport of plastic litter in the Baltic, and also on the topic of plastic pollution more generally.

Part II

Theory and Background

Before proceeding to discuss plastic pollution in the Baltic Sea, we include a basic overview of some basic concepts and equations of fluid mechanics. These equations will be used later, mostly to simulate the currents in the Gullmar Fjord for different wind velocities.

We will then give a brief background for some of the transport processes which are listed in the literature as being relevant for plastic pollution in the ocean. This will provide some context for the transport mechanisms examined in the Gullmar Fjord simulation, as well as when discussing abundance patterns of plastic in the Baltic Sea.

3 Theory

In this section, we will go through some of the basic equations of fluid mechanics which form the backbone of ocean simulation. We will begin with the fluid equations of motion, which are the translations of the classical equations conservation of mass and momentum for a fluid medium, and go through how to modify these to include effects of the Earth's rotation. We will also go through the Boussinesq approximation, which is applied in order to simplify the equation of momentum conservation in simulations. Finally, we will end with a brief discussion of turbulence. The main source for this section was the book Vallis 2017, and so unless otherwise stated we follow the general methods used in this book.

3.1 Conservation of mass

The first equation of motion for a fluid stems from the principle of conservation of mass. In classical mechanics of rigid bodies we know that mass is conserved, however fluids may flow and change in densities more easily, and so it is necessary to have an equation which accounts for the flow of mass. We will derive this equation using vector calculus from an Eulerian framework.

To this end, consider some arbitrary volume V bound by a closed surface S which is fixed in space. Let S be pointing towards the outside of V. The rate of fluid loss due to flow through S is then given by the integral

$$\int_S \rho v \cdot \mathrm{d}S\,,$$

where ρ is the density of the fluid and v is the velocity field at the fluid surface. Using the divergence theorem, we can rewrite the above integral as

$$\int_S \rho v \cdot \mathrm{d}S = \int_V \nabla \cdot (\rho v)\, \mathrm{d}V\,. \tag{1}$$

The rate of fluid loss must correspond to some change in the mass M of the fluid contained in V, which we can express mathematically as $-\,\mathrm{d}M/\mathrm{d}t$. As the volume V is fixed, and so it is only the density of fluid that can change when we change M, we can obtain another integral equation for rate of fluid loss:

$$-\frac{\mathrm{d}M}{\mathrm{d}t} = -\frac{\mathrm{d}}{\mathrm{d}t}\int_V \rho\, \mathrm{d}V = -\int_V \frac{\partial \rho}{\partial t}\, \mathrm{d}V\,. \tag{2}$$

Since equations (1) and (2) are both expressions for the same thing, the rate of fluid loss, we can equate them, yielding the expression

$$\int_V \left(\frac{\partial \rho}{\partial t} + \nabla \cdot (\rho v)\right) \mathrm{d}V = 0.$$

We picked an arbitrary control volume, and so if the above equation is to hold in general, then the integrand must equal zero:

$$\frac{\partial \rho}{\partial t} + \nabla \cdot (\rho v) = 0, \tag{3}$$

which is an equation for conservation of mass in a fluid.

3.2 The momentum equation

In this section we cover how to express Newtons's second law for a continuum. Let $m = m(x, y, z, t)$ be the momentum per unit volume of a fluid, also called the momentum-density field. It holds that $m = \rho v$, and that the total momentum of the fluid is given by the volume integral of m.

The rate of change of momentum for a fluid is given by the material derivative, which for a general tensor field $h = h(x, y, z, t)$ is defined by

$$\frac{Dh}{Dt} = \frac{\partial y}{\partial t} + v \cdot \nabla h,$$

and so we have that

$$\frac{Dm}{Dt} = \frac{D}{Dt}\int_V m \,\mathrm{d}V = \frac{D}{Dt}\int_V \rho v \,\mathrm{d}V = \int_V \rho \frac{Dv}{Dt}\,\mathrm{d}V\,,$$

where the last equality follows from the product rule for material derivatives and constant mass of a fluid element. We furthermore know from Newton's second law that the rate of change of momentum of the fluid is equal to the force F acting on it, and thus

$$\int_V \rho \frac{Dv}{Dt}\,\mathrm{d}V = \int_V F\,\mathrm{d}V\,.$$

Subtracting the left integral from both sides, and using that the integrand must vanish since we have used an arbitrary volume V, we obtain conservation of momentum for a fluid:

$$\rho \frac{Dv}{Dt} = F. \tag{4}$$

The above equation in conjunction with equation (3) for conservation of mass are collectively referred to as the Navier-Stokes equations.

For rigid bodies, we consider F to be the sum of external forces acting upon the body, however for a fluid, not all relevant forces will be external. Due to contact between fluid parcels, we have pressure and viscous forces to consider as well. We proceed with a heuristic derivation of these forces, starting with pressure forces.

Pressure: Pressure is defined as the normal force per unit area due to molecular motion, and thus the pressure force F_p can be expressed as

$$dF_p = -p\,\mathrm{d}S\,,$$

where p is the pressure. To obtain the pressure force on a volume of fluid, we then simply integrate over its boundary. If we apply the divergence theorem following this, we obtain that

$$F_p = -\int_V \nabla p\,\mathrm{d}V\,,$$

and so the pressure force per unit volume is simply given by $-\nabla p$.

3.2.1 Viscosity

Viscosity forces in a fluid occur due to the friction that may arise when adjacent fluid parcels are in relative motion. The viscous force per unit volume for a Newtonian fluid is approximately given by $\mu \nabla^2 v$, where μ is the viscosity of the fluid. This expression is only approximate, as it relies on an assumption of incompressibility of the fluid, i.e. that the density is constant within a fluid parcel.

Incorporating both the pressure force and the viscosity force, and dividing through by the fluid density in eq. (4) gives

$$\frac{Dv}{Dt} = -\frac{1}{\rho}\nabla p + \nu \nabla^2 v + F_b, \tag{5}$$

where $\nu = \mu/\rho$ and F_b is a term describing external forces per unit mass, such as gravity.

A perfect fluid is one which has zero viscosity. In practice this is not observed in nature, however it is sometimes convenient for the sake of calculation to neglect the viscosity term, thereby assuming a perfect fluid. For water, we have that $\nu \approx 1.1 \cdot 10^{-6}$ m^2 s^{-1}, and often other terms in the momentum equation will be of larger order of magnitude, so we neglect the viscosity term.

3.2.2 Hydrostatic balance

For a perfect fluid subject to no external forces, the vertical component of the momentum equation is

$$\frac{Dw}{Dt} = -\frac{1}{\rho}\frac{\partial p}{\partial z} - g,$$

where w is the velocity in the z-direction. If the fluid is at rest, so that $Dw/Dt = 0$, then

$$\frac{\partial p}{\partial z} = -\rho g,$$

so that the pressure at a given depth is due to the weight above it (assuming $p = 0$ at the surface). This is called hydrostatic balance.

3.3 The equation of state

An equation of state relates different thermodynamic quantities to each other. We desire such an expression since the mass conservation equation and the momentum equation together have five unknowns (density, pressure and three components of velocity), but provide only four equations (one for mass and three for momentum).

The ocean does not behave as an ideal gas, and any alternate expressions to the ideal gas law which relate pressure, temperature and density are more difficult to find. Empirically, the density of ocean water depends on pressure, temperature and salinity, and so we can write a general equation of state as

$$\rho = \rho(T, S, p),$$

where T is temperature, S is salinity and p is pressure. We may also more conveniently work with a relation for $\alpha = 1/\rho$, $\alpha = \alpha(T, S, p)$.

A small change around a reference value gives

$$\begin{aligned} \mathrm{d}\alpha &= \left(\frac{\partial \alpha}{\partial T}\right)_{S,p} \mathrm{d}T + \left(\frac{\partial \alpha}{\partial S}\right)_{T,p} \mathrm{d}S + \left(\frac{\partial \alpha}{\partial p}\right)_{T,S} \mathrm{d}p \\ &= \alpha(\beta_T \,\mathrm{d}T - \beta_S \,\mathrm{d}S - \beta_p \,\mathrm{d}p), \end{aligned}$$

where the thermal expansion coefficient β_T, the saline contraction coefficient β_S and the compressibility coefficient β_p are defined in such a way that the above equality holds, and α_0 is a reference reciprocal density value. The β-coefficients are in general not constants, but may be considered as such for small variations, and we have

$$\alpha = \alpha_0 \left[1 + \beta_T(T - T_0) - \beta_S(S - S_0) - \beta_p(p - p_0)\right].$$

In the ocean these coefficients have typical values of $\beta_T \approx 2(\pm1.5) \cdot 10^{-4}$ K^{-1}, $\beta_S \approx 7.6(\pm0.2) \cdot 10^{-4}$ ppt^{-1} and $\beta_p \approx 4.4(\pm0.5) \cdot 10^{-10}$ Pa^{-1}.

If we are indeed dealing with small variations, then

$$\rho = \rho_0 \left[1 - \beta_T(T - T_0) + \beta_S(S - S_0) + \beta_p p\right].$$

This is a decent equation of state for intuitive, qualitative analysis, however it is insufficiently accurate for drawing quantitative conclusions.

3.4 Rotation effects

Our expression in eq. (5) is not sufficient as an equation of motion for the ocean as a fluid, as it does not take into account the Earth's rotation. Since the Earth rotates about its own axis with a period of roughly 24 hours, it is not an inertial frame of reference, and so a naïve application of Newton's second law will not apply.

We first present the result for the rate of change of a vector in a rotating frame of reference. Consider a vector C which is measured in both an inertial and a rotating frame of reference. Let the angular velocity of the rotating frame of reference be Ω. Then the rate of change of C is given by

$$\left(\frac{\mathrm{d}C}{\mathrm{d}t}\right)_I = \left(\frac{\mathrm{d}C}{\mathrm{d}t}\right)_R + \Omega \times C, \tag{6}$$

where the subscript I is used to denote the quantity in the inertial frame of reference, and the subscript R to denote the frame in relative motion to the inertial frame.

We can use eq. (6) to relate the velocity in an inertial frame to that in a rotating frame by putting the position of a fluid parcel, which we denote by r, in the position of C, giving

$$v_I = v_R + \Omega \times r, \tag{7}$$

where v_I is the velocity in the inertial frame and v_R the velocity in the rotating frame.

We now wish to find an expression relating the rate of change of the velocity in the two frames of reference. We use eq. (6) once again and obtain that

$$\left(\frac{\mathrm{d}v_R}{\mathrm{d}t}\right)_I = \left(\frac{\mathrm{d}v_R}{\mathrm{d}t}\right)_R + \Omega \times v_R.$$

We can then insert the result for v_I in eq. (7) into the above equation, giving that

$$\left(\frac{\mathrm{d}}{\mathrm{d}t}\left(v_I - \Omega \times r\right)\right)_I = \left(\frac{\mathrm{d}v_R}{\mathrm{d}t}\right)_R + \Omega \times v_R.$$

If we expand the terms on the left hand side in this equation, we get that

$$\left(\frac{\mathrm{d}v_I}{\mathrm{d}t}\right)_I = \left(\frac{\mathrm{d}v_R}{\mathrm{d}t}\right)_R + \Omega \times v_R + \frac{\mathrm{d}\Omega}{\mathrm{d}t} \times r + \Omega \times \left(\frac{\mathrm{d}r}{\mathrm{d}t}\right)_I.$$

We can further simplify this equation using two things. The first is that $(\mathrm{d}r/\mathrm{d}t)_I$ is equal to v_I, and we can thus use eq. (7) to relate it to v_R. The second is that we assume Ω is constant. Combining these gives the form

$$\left(\frac{\mathrm{d}v_R}{\mathrm{d}t}\right)_R = \left(\frac{\mathrm{d}v_I}{\mathrm{d}t}\right)_I - 2\Omega \times v_R - \Omega \times (\Omega \times r).$$

This final equation gives us the rate of change of the velocity in the rotating frame by relating it to the acceleration in the inertial frame (equal by Newton's second law to force per unit mass) along with two acceleration terms to correct for the rotation. The former is called the Coriolis acceleration, and the latter the centrifugal acceleration.

The centrifugal force per unit mass may more conveniently be written in the form of a gradient of a scalar potential. Let $r_\perp$ be the displacement perpendicular to the axis of rotation. Then $\Omega \times r = \Omega \times r_\perp$, and we use an identity for triple vector product to see that

$$F_{ce} = -\Omega \times (\Omega \times r_\perp) = (\Omega \cdot \Omega) r_\perp - (\Omega \cdot r_\perp)\Omega,$$

where F_{ce} is the centrifugal force per unit mass. As $r_\perp$ is perpendicular to Ω by definition, the dot product of the two quantities vanishes, and we are left with

$$F_{ce} = \Omega^2 r_\perp = -\nabla \Phi_{ce},$$

where we define $\phi_{ce} = -(\Omega \times r_\perp)^2/2$.

Combining all of these elements, the momentum equation in a rotating frame of reference can thus be written as

$$\frac{Dv}{Dt} + 2\Omega \times v = -\frac{1}{\rho}\nabla p - \nabla \Phi,$$

where we eliminate the subscript R from v_R and henceforth consider v to be in the rotating frame of reference unless otherwise stated, and where the potential Φ consists of the centrifugal term as well as other possible external forces. Finally, we make note of the fact (but do not show) that the mass conservation equation is unaltered when taking the rotation of the Earth into account.

3.5 The Boussinesq approximation

Our equations of motion so far can be quite complicated to solve as they are, and so we wish to make some further assumptions in order to achieve simpler expressions. The Boussinesq approximation, which we will derive, involves exploiting the small variation in density of the ocean.

Let the density consist of a constant and a deviation from this constant which may vary in space and time, i.e. $\rho(x, y, z, t) = \rho_0 + \delta\rho(x, y, z, t)$. Assume that the variation in density is of a typical magnitude of $\epsilon\rho_0$, where $\epsilon \ll 1$, so that $|\delta\rho| \ll \rho_0$. We use this to write

$$\delta\rho = (\epsilon\rho_0)\delta\tilde{\rho}, \tag{8}$$

where the tilde denotes a dimensionless quantity, and $\delta\tilde{\rho}$ is $\mathcal{O}(1)$. Using this rewrite the density becomes

$$\rho = \rho_0(1 + \epsilon\delta\tilde{\rho}).$$

As the rotation and viscosity terms in the momentum equation do not depend directly on density variations, we omit them for simplicity. The vertical component of the momentum equation, using our density variation notation, is then

$$(\rho_0 + \delta\rho)\frac{Dw}{Dt} = -\frac{\partial p}{\partial z} - (\rho_0 + \delta\rho)g, \tag{9}$$

where w is the vertical component of the velocity and g is the gravitational acceleration.

We wish to create a series expansion of our above terms according to powers of ϵ, and keep the leading orders. To do this, we first write several of the variables above as non-dimensional quantities, similar to eq. (8) for $\delta\rho$. We must make some decisions about which scales are reasonable in this expansion. First we do this to the displacement and velocity variables,

$$\begin{aligned}(x, y, z) &= L(\tilde{x}, \tilde{y}, \tilde{z}),\\ (u, v, w) &= U(\tilde{u}, \tilde{v}, \tilde{w}),\end{aligned}$$

where u and v are the velocities in the x and y directions, respectively. We use L and U to do the same for the time, pressure and gravitational acceleration:

$$\begin{aligned}t &= \frac{L}{U}\tilde{t},\\ p &= \rho_0\frac{U^2}{\epsilon}\tilde{p},\\ g &= \frac{U^2}{\epsilon L}\tilde{g}.\end{aligned}$$

Throughout, the quantities with a tilde are dimensionless and presumed to be $\mathcal{O}(1)$. Using these rewrites of our terms, eq. (9) becomes

$$(1 + \epsilon\delta\tilde{\rho})\frac{D\tilde{w}}{D\tilde{t}} = -\frac{1}{\epsilon}\frac{\partial\tilde{p}}{\partial\tilde{z}} - \frac{1}{\epsilon}(1 + \epsilon\delta\tilde{\rho})\tilde{g}. \tag{10}$$

We now expand our dimensionless terms in orders of ϵ:

$$\begin{aligned}\delta\tilde{\rho} &= \delta\tilde{\rho}_0 + \epsilon\delta\tilde{\rho}_1 + \epsilon^2\tilde{\rho}_2 + \dots\\ \tilde{p} &= \tilde{p}_0 + \epsilon\tilde{p}_1 + \epsilon^2\tilde{p}_2 + \dots\\ \tilde{w} &= \tilde{w}_0 + \epsilon\tilde{w}_1 + \epsilon^2\tilde{w}_2 + \dots\end{aligned}$$

and similar for $\tilde{u}$ and $\tilde{v}$. Replacing these expansions instead of our dimensionless quantities in eq. (10) and collecting like terms in powers of ϵ gives the lowest order term, which is of ϵ^{-1}, and reduces to the equation:

$$\frac{\partial\tilde{p}_0}{\partial\tilde{z}} = -\tilde{g}. \tag{11}$$

The next order up is those terms which have coefficient of ϵ^0, which together give equation

$$\frac{D\tilde{w}_0}{D\tilde{t}} = -\frac{\partial\tilde{p}_1}{\partial\tilde{z}} - \delta\tilde{\rho}_0\tilde{g}. \tag{12}$$

We neglect terms of higher order in ϵ.

Returning to dimensional quantities, we see that eq. 11 becomes

$$p_0(z) = -\rho_0 g z$$

and that eq. (12) becomes

$$\frac{Dw}{Dt} = -\frac{1}{\rho_0}\frac{\partial p'}{\partial z} - \frac{\delta\rho}{\rho_0}g,$$

where p' is a deviation from the pressure p_0, which is hydrostatic. Introducing the terms $\phi = p'/\rho_0$ and the buoyancy $b = -g\delta\rho/\rho_0$, we can rewrite this into a simpler expression

$$\frac{Dw}{Dt} = -\frac{\partial\phi}{\partial z} + b.$$

Upon similar considerations, we may obtain a similar expression for the velocities in the horizontal directions (although simpler since p_0 is a function of z only). We may combine these into one expression for the three-dimensional velocity v:

$$\frac{Dv}{Dt} = -\nabla\phi + bk,$$

where k is the unit vector in the z-direction. To this we may add viscosity and rotation terms, obtaining our final momentum equation with Boussinesq approximation:

$$\frac{Dv}{Dt} + 2\Omega \times v = -\nabla\phi + \nu\nabla^2 v + bk.$$

The mass continuity equation also becomes simpler under the Boussinesq approximation. Using our rewrite $\rho = \rho_0 + \delta\rho$ we get

$$\frac{D}{Dt}(\rho_0 + \delta\rho) + (\rho_0 + \delta\rho)\nabla \cdot v = 0.$$

We spot that $D\rho_0/Dt = 0$ since ρ_0 is a constant. Furthermore, since ρ_0 is of greater magnitude in ϵ than $\delta\rho$, the leading order term in the mass conservation equation is

$$\nabla \cdot v = 0.$$

Using the Boussinesq approximation thus leads us to the assumption that we are working with a divergence-free fluid.

3.5.1 Quality of the Boussinesq approximation

In all of the above, we have proceeded under the assumption that density variations in the ocean are small. Before applying the equations we have consequently derived, we must ask how correct the assumption is. To do this, we evaluate the three effects which produce density changes in the ocean: compression of water due to pressure (denoted by $\Delta_p\rho$), thermal expansion due to temperature changes ($\Delta_T\rho$), and changes due to salinity ($\Delta_S\rho$). These are related to density ρ via the equation of state

$$\rho = \rho_0 \left[1 - \beta_T(T - T_0) + \beta_S(S - S_0) + \beta_p p\right].$$

The values of the constants in the above equation are $\beta_T \approx 2 \cdot 10^4$ K^{-1}, $\beta_S \approx 10^{-3}$ (g/kg)$^{-1}$ and $\beta_p \approx 4.4 \cdot 10^{-10}$ Pa^{-1}.

Thermal effects: The thermal change in density is given by $\Delta_T\rho \approx -\beta_T\rho_0\Delta T$, which gives

$$\frac{|\Delta_T\rho|}{\rho_0} \approx \beta_T\Delta_T \approx 4 \cdot 10^{-3}$$

for a temperature change of 20 K. In order for the above quotient to be of order one, we would require ΔT to be around 5000 K, which is clearly unrealistic.

Salinity effects: Changes in density due to salinity changes are given by $\Delta_S\rho \approx \beta_S\rho_0\Delta S$, giving

$$\frac{|\Delta_S\rho|}{\rho_0} \approx \beta_S\Delta S \approx 1.5 \cdot 10^{-3}$$

with $\Delta S = 5$ g kg^{-1}.

Pressure effects: Density change due to pressure is given using the hydrostatic approximation by $\Delta_p\rho \approx \Delta p/c_s^2 \approx \rho_0 gH/c_s^2$, where $c_s \approx 1500$ m s^{-1} is the speed of sound, and H is the depth. We get

$$\frac{|\Delta_p\rho|}{\rho_0} \approx \frac{gH}{c_s^2} \approx 4 \cdot 10^{-2}$$

for $H = 8$ km. Hence the pressure even at the bottom of the ocean is insufficient to cause a large density change.

The combination of these three effects shows that changes in density are small, of order 10^{-2} at most, and so the Boussinesq approximation may result in equations that, while less exact, are still quite useful.

3.6 Turbulence

Turbulent flow is nonlinear and disordered both spatially and as a function of time. In this section, we aim to give a brief description of turbulent flow as is relevant to the simulations we that we have conducted. As part of this, we will define the Reynolds number and introduce the Reynolds-averaged Navier-Stokes equations.

3.6.1 The Reynolds number

The Reynolds number is a property of a fluid used to characterize its flow, characterizing the ratio between viscous and inertial forces in the fluid. It is defined by

$$\mathrm{Re} = \frac{\rho u L}{\mu},$$

where ρ is the fluid density in kg m^{-3}, u is the flow speed in m s^{-1}, L is a characteristic length scale of the system in metres, and μ is the dynamic viscosity of the fluid in kg m^{-1} s^{-1}. The Reynolds number is thus a dimensionless quantity. When the Reynolds number is low the flow tends to be smoother, and is called laminar. Such flow is dominated by viscous forces. When the Reynolds number is high, on the other hand, turbulent flow arises, and inertial forces are more dominant.

The Reynolds number arises naturally when we take the momentum equation (5) and make it dimensionless. We begin with this equation:

$$\frac{Dv}{Dt} = -\frac{1}{\rho}\nabla p + \nu \nabla^2 v + F_b.$$

In order to make the above equation dimensionless, we first introduce the characteristic length scale of the system L, which is in metres, and the velocity V relative to the fluid, in metres per second. We then define the dimensionless quantities $\tilde{v} = v/V$, $\tilde{p} = p/(\rho V^2)$ and $\tilde{F_b} = FL/V^2$, as well as the operators $\partial/\partial\tilde{t} = L/V\ \partial/\partial t$ and $\tilde{\nabla} = L\nabla$. Using these operators and quantities, we rewrite the momentum equation as

$$\frac{V^2}{L}\frac{D\tilde{v}}{D\tilde{t}} = -\frac{V^2}{L}\tilde{\nabla}\tilde{p} + \frac{\nu V}{L^2}\tilde{\nabla}^2\tilde{v} + \frac{V^2}{L}\tilde{F_b}.$$

Multiplying through with L/V^2 and recalling that $\nu = \mu/\rho$, we get the dimensionless equation

$$\frac{D\tilde{v}}{D\tilde{t}} = -\tilde{\nabla}\tilde{p} + \frac{\mu}{\rho L V}\tilde{\nabla}^2\tilde{v} + \tilde{F_b}.$$

The coefficient to the term $\tilde{\nabla}^2\tilde{v}$ (the viscosity term) is equal to the reciprocal of the Reynolds number. As a consequence of this result, we see that incompressible flows with similar Reynolds number will behave in similar ways. We also see that as the Reynolds number tends to zero, the viscosity term goes to infinity, confirming what we said earlier about low Reynolds number corresponding to viscous flow. On the other hand as the Reynolds number tends to infinity, the viscosity goes to zero, confirming that in this case inertial forces dominate.

3.6.2 Reynolds averaging

Turbulent flow is nonlinear and difficult to predict. Because of this, we often want to learn more about the statistical properties of the flow. To that aim we break the velocity field into a mean and a deviation from the mean, $v = \overline{v} + v'$, where $\overline{v}$ is the mean velocity and v' is the deviation. Note that the mean could be taken over time but also over space.

On the other hand this approach can introduce other problems. To see this, consider the Navier-Stokes equations in one spatial direction only, for instance in the x-direction. For simplicity assume that $\rho = 1$ and that there are no external forces. The equation for an averaged flow (known as Reynolds averaging) then becomes

$$\frac{\partial \overline{u}}{\partial t} + (\overline{v} \cdot \nabla)\overline{u} = -\frac{\partial \overline{p}}{\partial x} - \nabla \cdot \overline{v'u'},$$

where v is a three-dimensional velocity, whereas u is the x-component of velocity. We pay special attention to the last term, involving the divergence of $\overline{v'u'}$. By definition of the deviation from the mean, $\overline{u'} = 0$ and $\overline{v'} = 0$, however the average of the two multiplied gives the average correlation between the deviations, which is not in general zero.

We could attempt to compute this term by taking higher order derivatives, but then we would merely end up with third order rather than second order correlations to compute, and so on for higher orders. This term, and those like it in the y- and z-equations, are called the Reynolds stress terms. The problem of trying to represent these terms with respect to the mean flow is known as the closure problem, and so far cannot be solved without introducing physical assumptions.

3.6.3 The $k - \epsilon$ closure scheme

As mentioned above, the closure problem cannot be solved using only the Reynolds averaged Navier-Stokes equations; rather we require some extra information to solve it. There are therefore a number of different closure schemes representing different assumptions which we can use to solve these equations. In this section, we will describe one of these closure schemes, the $k - \epsilon$ scheme, in greater detail, as this is the one which we will later make use of. We follow a similar presentation as (Argyropoulos and Markatos 2015).

The $k - \epsilon$ model has the underlying assumption that the ratio between the Reynolds stress terms and the average strain rate is isotropic. This assumption can be thought of in analogy with molecular diffusion, in which fluid parcels collide like molecules which obey the kinetic theory of gases. Reynolds stress terms are modelled as

$$\tau_{ij} = \overline{u_i' u_j'} = \frac{2}{3} k \delta_{ij} - \nu_t \left(\frac{\partial \overline{u_i}}{\partial x_j} + \frac{\partial \overline{u_j}}{\partial x_i} \right),$$
$$k = \frac{1}{2} \overline{u_i' u_i'} = \frac{1}{2} (\overline{u_1'^2} + \overline{u_2'^2} + \overline{u_3'^2}),$$

where τ_{ij} is a component of Reynolds stress, the u_i variables are velocity components, k is the turbulent kinetic energy, and δ_{ij} is the Kronecker delta. ν_t is the eddy viscosity, which is not constant but rather depends on the flow. We can substitute the first of these two equations for the Reynolds stress terms into the Reynolds averaged momentum equation expressed in Cartesian coordinates and obtain

$$\frac{\partial \overline{u_i}}{\partial t} \frac{\partial}{\partial x_j} = -\frac{1}{\rho} \frac{\partial \overline{p}}{\partial x_i} + \frac{\partial}{\partial x_j} \left[(\nu + \nu_t) \frac{\partial \overline{u_i}}{\partial x_j} \right],$$

where the kinetic energy term has been absorbed into $\overline{p}$.

It still remains to figure out an expression for ν_t. We begin by noting that, by dimensional analysis, ν_t is proportional to LV, the product of the characteristic length and velocity scales. Even knowing this, however, we could ask what L and V are equal to for a given flow. The $k - \epsilon$ model is a two-equation closure scheme, which means that it introduces two differential equations to find two variables (the turbulent kinetic energy, and the rate of dissipation of turbulence), and then a third and final equation to compute the eddy viscosity using these two variables.

The $k - \epsilon$ model ends up being defined by the following three equations: the turbulence kinetic energy equation, the turbulence dissipation rate equation, and the kinematic eddy viscosity equation. The turbulence kinetic energy equation for k is

$$\frac{\partial k}{\partial t} + \overline{u_j}\frac{\partial k}{\partial x_j} = \frac{\partial}{\partial x_j}\left[\frac{\nu + \nu_t}{\sigma_k}\frac{\partial k}{\partial x_j}\right] + \tau_{ij}\frac{\partial \overline{u_i}}{\partial x_j} - \epsilon,$$

where ϵ is the turbulence dissipation rate and $\sigma_k = 1.0$ is a constant. The turbulence dissipation rate equation for ϵ is

$$\frac{\partial \epsilon}{\partial t} + \overline{u_j}\frac{\partial \epsilon}{\partial x_j} = \frac{\partial}{\partial x_j}\left[\frac{\nu + \nu_t}{\sigma_\epsilon}\frac{\partial \epsilon}{\partial x_j}\right] + C_{\epsilon 1}\frac{\epsilon}{k}\tau_{ij}\frac{\partial \overline{u_i}}{\partial x_j} - C_{\epsilon 2}\frac{\epsilon^2}{k},$$

where $\sigma_\epsilon = 1.3$ is a constant, and so are $C_{\epsilon 1} = 1.44$ and $C_{\epsilon 2} = 1.92$. The general structure of these two equations is that on the left hand side we have the rate of change of k or ϵ plus the transport by advection of k/ϵ, and on the right hand side we have that this is equal to the diffusive transport of k/ϵ plus the rate of production of k/ϵ, from which we subtract the rate of removal of k/ϵ. To these two equations we add the kinematic viscosity equation,

$$\nu_t = C_\mu \frac{k^2}{\epsilon},$$

where $C_\mu = 0.09$ is a constant. These three equations allow us to compute the Reynolds stress terms, and thus solve the Reynolds averaged momentum equation.

4 Lagrangian ocean analysis

Before we move on to transport processes, we move on to a more applied part of our theory. This is the difference between the Lagrangian and Eulerian views of fluid flow, which we will define shortly. This discussion will become relevant when discussing transport mechanisms in the following section, and again when describing the simulations we will run. We follow a similar presentation to (van Sebille, Griffies, et al. 2018).

In order to simulate the movement of plastic particles in the ocean, we must first have a grasp on how to simulate the movement of water between ocean regions more generally. There are broadly speaking two frameworks for doing this: the Eulerian approach and the Lagrangian approach. In the Eulerian approach, we consider how a concentration of particles evolves over time in different cells of a fixed grid. The Lagrangian approach, in contrast to this, involves an ensemble of particles which move according to a prescribed velocity field in a frame of reference that moves along with fluid parcels (infinitesimal particles of fluid).

Both approaches have different advantages. The Eulerian approach is more natural for considering the evolution of particle concentrations over time, but makes it more challenging to view particle trajectory histories. The Lagrangian approach allows for convenient storage of particle trajectories, as well as analysing only those trajectories which satisfy various user-chosen criteria, but is more unwieldy for computing aggregate quantities. Computationally, the two methods also scale differently – movement of a particle takes only one set of computations each time step, while calculating particle concentrations takes one set of computations for each grid cell per time step. In the Lagrangian method the time scaling is thus according to number of particles, while in the Eulerian approach it depends heavily on the number of grid cells.

In our simulations which will be described later in the thesis project, we will use the Lagrangian approach, with velocity fields obtained from another simulation forced with user-specified wind velocities. We will therefore proceed with a more thorough explanation of kinematic theory and relevant computational algorithms for this approach.

Assume we have a point particle which behaves in accordance with classical physics. It may have a position vector $x(t)$, which depends on time t. The curve in space describing the path of the particle is referred to as its trajectory. We may also have an ensemble of discrete particles, each of which has a position vector, and we can combine these vectors using the notation $x^n(t)$, where n is a natural number which ranges over all the particles in our ensemble. If the particles, rather than being discrete, are assumed to form a continuum, n becomes a continuous label, and we describe the motion of particles in the continuum by $x = x(a, t)$, where a is commonly selected to be the position at some reference time $t = t_0$. a is called the material coordinate.

We also wish to introduce the concept of a fluid parcel, which is a collection of molecules of microscopic scale. The velocity of a fluid parcel is given by the mass-weighted mean of velocities of the individual molecules. Alternatively, under the continuum hypothesis a fluid parcel can be considered a small (but not microscopic) volume of continuous matter. The velocity of a fluid parcel can be found be taking the time derivative of the trajectory, holding a fixed, i.e.

$$v(x,t) = \left(\frac{\partial x(a,t)}{\partial t}\right)_a ,$$

where v is the velocity and $x = x(a, t)$.

In order to obtain a more complete kinematic description, we also wish to compute changes in an arbitrary function of the trajectory $\psi = \psi(x, t)$. Using the chain rule we get

$$\frac{\partial \psi(x(a,t),t)}{\partial t} = \left[\left(\frac{\partial}{\partial t}\right)_x + v(x(a,t),t) \cdot \nabla\right] \psi(x(a,t),t). \tag{13}$$

Finally, we wish to consider how the Lagrangian and Eulerian approaches are related mathematically. An Eulerian field, such as a velocity field, is given as some general function f of position and time, $f = f(x, t)$. On the other hand in the Lagrangian view, fluid parcels are labelled by the material coordinate a. Examining the flow velocity $u(x, t)$ in the Eulerian view, it is related to the Lagrangian velocity by

$$u(x(a,t),t) = \frac{\partial x}{\partial t}. \tag{14}$$

Returning to a general Eulerian field $f(x, t)$, we wish to know how the rate of change of f is experienced by a fluid parcel. As f is just a function of the trajectory, we can apply the result from eq. (13) to obtain that this change in f is given by its material derivative

$$\frac{Df}{Dt} = \frac{\partial f}{\partial t} + (u \cdot \nabla) f. \tag{15}$$

5 Plastic drift processes

We now proceed to describe some transport processes in the ocean which are relevant to plastic drift. Our aim is to describe the more dominant processes, especially as it pertains to the Baltic Sea, which is inland.

5.1 Large-scale ocean processes

Large-scale drift refers to those drift processes which transport tracer particles horizontally on a global scale. These are less relevant to transport of plastics in the Baltic Sea, and more to transport between and within world oceans.

In large-scale drift processes, currents are driven primarily by surface winds and further affected by the Coriolis effect, which causes the surface currents to be approximately 45 degrees offset from the wind direction, the deflection being to the right of the wind in the Northern hemisphere, and the left of the wind in the Southern hemisphere. (van Sebille, Aliani, et al. 2020)

Due to friction between the surface layer being moved by surface wind with respect to to the layer beneath, there arises a current in the next layer as well, and so on for subsequent layers. There is however energy lost in the processes with each subsequent layers, so the drift becomes smaller with each layer, and motion usually ceases at depths below 100m. The net ocean current moving through layers of the sea then forms a spiral shape, known as an Ekman spiral.

This causes another effect wherein Ekman transport causes convergence of currents, and ocean water piles up in a sort of hill. It flows down away from the convergence due to gravity, but is deflected due to the Coriolis Effect. This is called a geostrophic flow, and it is clockwise in the Northern Hemisphere, and counterclockwise in the Southern Hemisphere. In the absence of waves or wind, tracer particles will thus accumulate in places where surface waters converge. (Webb 2020)

Surface water has a net downward velocity in an Ekman spiral, so it is relevant to examine whether this mechanism causes sinking of surface plastics. The downward velocity is typically on the order of tens of metres per year, which is lower than the sinking velocity of buoyant plastics (Reisser et al. 2015). It is thus thought that the buoyant plastic remains at the surface but is transported horizontally.

The theory of Ekman transport and geotrophic flow being a dominant factor in the transport of plastics in the ocean is well-supported by empirical evidence (Kubota 1994; Martinez, Maamaatuaiahutapu, and Taillandier 2009; Onink et al. 2019).

While this theory has predictive power regarding the accumulation zones of plastic in the world's oceans, it does not predict the exact pathways which the particles take to get there. It also does not predict the time-scale from source to arrival at an accumulation zone (van Sebille, Aliani, et al. 2020). As the Baltic Sea is relatively closed off from the Atlantic Ocean, there are no predicted accumulation zones from such processes which are in the Baltic sea.

5.2 Mesoscale open ocean processes

On a scale which is smaller than global, there is the transport of plastics by mesoscale eddies. These eddies are vortices with diameters of hundreds of kilometers, depths of hundreds to thousands of metres, and time-scales of weeks to years (van Sebille, Aliani, et al. 2020). The maximum width of the Baltic Sea is around 190 km, and the maximum depth under 500 m (Alice F.A. Mutton, Alastair Dougal Couper 2019), and so mesoscale open ocean processes are also less relevant to the Baltic Sea.

Mesoscale eddies are formed due to a balance of a pressure gradient (which comes from density differences in bodies of water) and the Coriolis force (Alistair Adcroft, Stephen Griffies, Robert Halberg n.d.). There are two types of eddies: cyclonic, where the radial component of the surface flow is directed outwards, and anti-cyclonic where the radial component is directed inwards. Cyclonic eddies rotate counter-clockwise in the Northern hemisphere, and clockwise in the Southern hemisphere; the rotation directions are reversed for anti-cyclonic eddies (van Sebille, Aliani, et al. 2020). Anti-cyclonic eddies are found to have higher concentrations of plastics than cyclonic eddies (Brach et al. 2018), which is perhaps explained by the direction of the radial component.

Mesoscale eddies can in themselves retain debris, however as the eddy is potentially long-lived and also travels, it can become another global transport mechanism of tracer particles in the sea. The exact role and importance of mesoscale eddies in plastic transport is unknown (van Sebille, Aliani, et al. 2020).

5.3 Open ocean Stokes drift

Stokes drift velocity is in general defined as the difference between the average Lagrangian velocity of a fluid parcel, and the average Eulerian flow velocity as measured at a fixed point in space (Monismith 2020). We recall the relation between the two descriptions by eq. (14). If we take the average of each of the two velocities over a certain period of time, for example a wave period, we get an average given by

$$\overline{u}_E = \overline{u(x,t)}$$

for the Eulerian velocity and

$$\overline{u}_L = \overline{\frac{\partial X}{\partial t}} = \overline{u(X(a,t),t)}$$

for the Lagrangian velocity, where the bar denotes an average, and the subscripts E and L stand for Eulerian and Lagrangian, respectively. The Stokes drift $\overline{u}_S$ is then given by

$$\overline{u}_S = \overline{u}_L - \overline{u}_E.$$

More specific to the context of plastic particle drift, we consider a particle floating on the surface of a wave. Due to Stokes drift, this particle will have a net velocity in the direction of wave propagation. The waves relevant to plastic transport are surface gravity waves, which arise from the interface between the atmosphere and ocean when the forces of gravity or buoyancy restore equilibrium, such as when there is wind. (Bremer and Ø. Breivik 2018)

As surface gravity waves are mostly due to wind, it is sometimes assumed that any tracer particles carried by such waves travel at some fraction of the wind speed in the given wind direction (Weber 1983). This assumption is not entirely accurate, however, as waves both build strength and dissipate more slowly than winds, and so the wind waves at one point in space and time may be due to earlier wind at another point in space. (Hanley, Belcher, and Sullivan 2010)

The extent to which plastic litter in the sea is transported via Stokes drift is still unknown, especially as it pertains to particles of different densities, shapes and sizes (van Sebille, Aliani, et al. 2020). If objects are small, submerged, and of similar density to the surrounding fluid, then their transport will be described by the Lagrangian flow (Maxey and Riley 1982). It has also been shown for fully submerged particles that lighter particles can be transported faster than the Stokes drift of the fluid in which they are submerged, and that the opposite holds true for heavier particles (Eames 2008; Santamaria et al. 2013). The shape of particles may not necessarily alter their Stokes drift velocity. (DiBenedetto and Ouellette 2018)

It is generally difficult to assess how affected particles are by Stokes drift, as it rarely occurs in isolation from other transport mechanisms. The interplay between Stokes drift and other transport mechanisms is also poorly understood (van Sebille, Aliani, et al. 2020). In spite of this, Stokes drift has been shown to be significant for the modelling of transport of various objects in the sea. Examples of this include drifters (Meyerjürgens et al. 2019) and oil spills (Röhrs et al. 2018). A study using numerical modeling of surface currents and wind waves off the Japanese coast found that Stokes drift can contribute to plastic particles moving 5-10 mm towards the coast during winter (Iwasaki et al. 2017).

The Stokes drift is a second order effect in the steepness of the waves, and so changes in wave shape can contribute to changes in particle transport. This becomes important especially along the coast as waves break, and during storms. (van Sebille, Aliani, et al. 2020)

5.4 Tides

Tides are a rise and fall in the sea level due to gravitational effects. Most commonly discussed in this context is the gravitational pull of the Moon on the Earth, which causes a tidal force. When the tidal force is applied to a particle, it is equal to the difference between the gravitational force that the moon exerts on the particle and the gravitational force that the particle would experience if it were located at the Earth's centre of mass. This results in a tidal bulge, with regions of the Earth closest to and furthest from the Moon experiencing the largest net force away from the Earth's centre of mass, causing the sea levels in this area to rise. This rise is known as high tide, with the other regions that do not experience a positive tidal force in the direction away from Earth experiencing low tide.

As the Earth rotates about its own axis, and the Moon and Earth both rotate about a common centre of mass (which is in practice inside the Earth), the position of the tidal bulges changes. The Moon revolves about the Earth-Moon centre of mass with a period of 27.3 days, and the Earth rotates about its own axis every 24 hours in the same direction, resulting in a lunar day of 24 hours and 50 minutes, which is the period of the Earth's rotation with respect to the Moon. As the tidal bulge occurs both where the Earth is closest to and furthest from the Moon, a given location will move through high tide (and low tide) twice in a lunar day. This gives a tidal period of approximately 12 hours and 25 minutes. (The Open University 1999)

The effect of tides on plastic pollution drift, especially as it pertains to plastic washing up along the shore, has been explored before. An example is in the paper (Turrell 2018) which attempts to create a model to explain the role of tides and other transport mechanisms wash litter ashore on a Scottish coastal region. This model was able to predict the amount of litter collected on beaches with good accuracy using this tide and wind-based effects. We will also examine the role of tidal effects when we examine the role of different transport mecanisms in a simulation of the Gullmar Fjord.

5.5 Windage

Marine debris may be transported due to direct wind force, which is known as windage and affects items which portrude out of the water (van Sebille, Aliani, et al. 2020). This is therefore a more relevant effect for macroplastics. Typically this is combined with Stokes drift, as both transport mechanisms arise from similar circumstances. (Øyvind Breivik et al. 2011)

Windage arises from a combination of two drag forces. The first of these is skin drag, which is due to viscous friction on the surface of an object. The second is form drag, and it arises due to wind pressure on the part of the object which is not submerged in water. It depends significantly on the shape of the object as well as its density (Houghton et al. 2017). Both effects combine into the drag equation, given by

$$F_D = \frac{1}{2}\rho v^2 A C_D,$$

where ρ is the atmospheric density, v is the wind velocity relative to the object, A is the area of the object exposed to wind, and C_D is the drag coefficient. As it can be complicated to determine the area of an object exposed to wind, as well as the drag coefficient of various plastic objects at sea (this would be determined experimentally for complex shapes) this equation is impractical for our simulation purposes, although it can provide greater qualitative insight into this phenomenon.

5.6 Langmuir circulation

Langmuir circulation happens in the surface layers of the ocean, and describes a certain type of flow where pairs of vertically counter-rotating vortices align horizontally. Windrows form due to Langmuir circulation, which are lines of bubbles, debris and plankton that form on the surface in the convergence zones of the pairs of vortices, and these can therefore be used to recognize Langmuir circulation.

This type of circulation arises due to the interaction of Stokes drift and and shear flow caused by wind. First, wind blows across the ocean surface, resulting in a shear force. This force has variations due to variations in the wind. This variability of the shear flow can create vertical vortices, which are then transported due to Stokes drift. Stokes drift will result in greater transport towards the sea surface rather than deeper down, and the top portions of the vortices become aligned parallel to the wind direction. A diagram depicting the dynamics of Langmuir circulation can be seen in fig. (1). Langmuir cells generally arise when the wind speed is above around 3-5 m s^{-1}, and tend to disintegrate when wind speeds are higher than around 13 m s^{-1}. They tend to form over the course of several minutes, although the surface convergence zones are only apparent after about 15-20 minutes. (Thorpe 2005)

Langmuir circulation is a possible explanation for observations from ships of high flotsam concentrations in 2-3 metre wide bands that stretch into the horizon (Faller 1964). The vertical flows in Langmuir cells may be strong, and contribute to vertical transport of especially smaller plastic items (Kukulka and Brunner 2015). As plankton accumulate in the convergence zones which result from Langmuir circulation, this can lead to increased biofouling of smaller marine debris particles. It could also increase the chances that marine organisms get entangled in or ingest flotsam. (Gove et al. 2019)

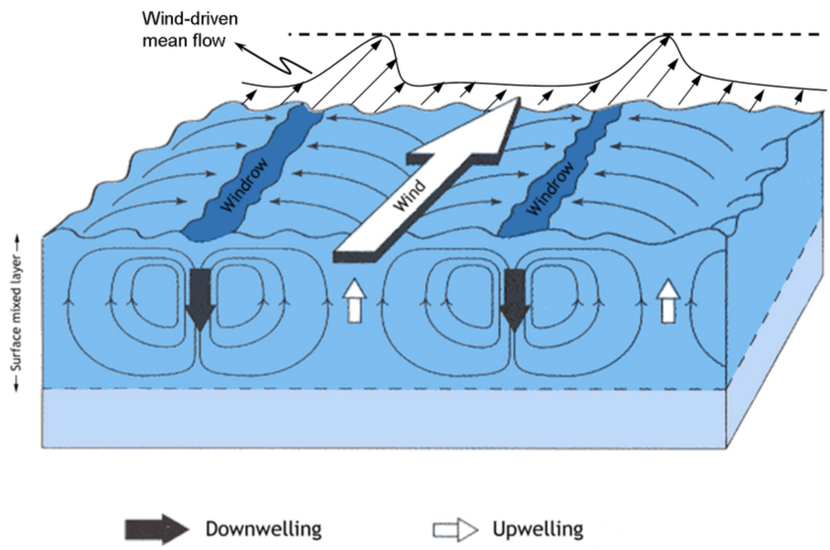

Figure 1: A diagram depicting dynamics of Langmuir circulation, sourced from Akan 2012.

5.7 Ice formation, melting and drift

The Baltic Sea has a typical annual maximum ice coverage of about $170,000$ km^2, which represents about 40% of its area. Ice coverage begins in the northern parts of the Sea in the Bothnian Bay, and then spreads towards the south (see figure 2 for a map of the Baltic Sea with subbasins). Normally during the winter the ice spread will reach to the Gulf of Finland, the Archipelago Sea, and parts of the Northern

Baltic Proper (FMI 2016). Ice formation, melting and drift could therefore be a relevant factor in the transport processes of plastic litter in the Baltic Sea. This could influence the results of studies which attempt to determine abundance of microplastics in the Baltic Sea, and also for the Gullmar Fjord, which tends to freeze over in January to February (Länsstyrelsen Västra Götaland n.d.).

Microplastics in particular may be concentrated in sea ice by 1-2 orders of magnitude relative to seawater, in a process called scavenging. When seawater freezes, small elongated ice crystals of about 3-4 mm in length form, which are known as frazil ice. Frazil ice has a much lower salinity than seawater salt, and salt is released into the sea as these ice crystals form. They are usually found on the sea surface, although due to turbulence they can also occur at depths of up to several metres. As more crystals form they tend to cluster together and form an ice layer. Convection due to both thermal and haline effects causes vertical transport, which means that both floating litter and that which was floating several metres beneath the sea surface can become trapped in the ice. (Obbard et al. 2014)

Once the plastics are trapped in ice, they can be transported across the sea surface when the ice drifts, and released again into the sea surface as the ice melts.

5.8 Estuarine circulation

Estuarine circulation results from density differences which occur as a result of salinity differences in different bodies of water that comes into contact. Saltwater is denser than freshwater, and so if for example a river flows into the sea, some seawater will also flow towards the river as a result of this difference in density. The exact circulation pattern will depend on the bathymetry. (Maccready 2004)

In addition to river mouths, estuarine circulation can also occur in Fjords, which may be relevant in the transport patterns we observe in our simulation of the Gullmar Fjord. It may be less relevant to the Baltic Sea than other seas, however, as the Baltic Sea has brackish waters. (Alice F.A. Mutton, Alastair Dougal Couper 2019)

5.9 Rivers

Rivers can be a major transport mechanism moving plastic litter from inhabited areas to the sea (Lebreton et al. 2017), especially as it pertains to sources such as city dust from cities along the river (Boucher and Friot 2017). River plumes form when river and ocean water come in contact, resulting in fronts which can stretch out for tens or even hundreds of kilometres. Floating debris tends to accumulate at these fronts. (Atwood et al. 2019)

Rivers can also transport debris to settle along river banks or on seashores (Acha et al. 2003). It has been found that rivers have higher density of pollution downstream of the flow relative to upstream (Acha et al. 2003; P. K. Cheung, L. T. O. Cheung, and Fok 2016). This means that we would expect higher concentrations of plastic pollution at river mouths where rivers flow into the Baltic Sea, or into the Gullmar Fjord.

5.10 Beaching

Ocean transport in coastal regions is mostly influenced by wind, waves and tides. Transport is furthermore influenced by the bathymetry as waters tend to be shallow in coastal areas.

Waves become altered as the water becomes shallower: they become steeper and less symmetrical relative to how they are in deeper waters (Doering and Bowen 1995). This can in turn alter the strength of Stokes drift. This phenomenon increases until the waves break along the coast, which causes increased mixing due to turbulence (Hsu et al. 2019). Marine debris that is carried along the waves may thus be beached. Buoyant plastic particles tend to float on the surface and are therefore more likely to be beached than smaller particles, which tend to mix into the water column and be transported offshore (Hinata et al. 2017). Beached litter may then degrade due to weathering, and smaller fragments may be transported back into the sea.

There is not a large amount of information on the beaching of marine debris. Some estimates relying on neural networks have been used with input data from beach clean-up surveys. Other estimates rely on the more well-studied transport of different types of sediment. Beaches can also, as previously discussed, be a source of plastic sea litter, due to weathering of plastics left on the beach (van Sebille, Aliani, et al. 2020).

The importance of beaching as an effect depends heavily on coastal features, such as the presence of cliffs. We would thus expect it to have some impact as a plastic sink in certain areas of the Baltic Sea, however less impact in the Gullmar Fjord specifically, which has cliffs. That said, however, the magnitude of the effect is not well-studied and thus difficult to estimate.

5.11 Transport by organisms

Marine animals may ingest smaller plastic particles, or become entangled in larger pieces of plastic (Bråte et al. 2017). This plastic may end up ashore due for example due to predation (Ryan and Fraser 1988) and feeding of chicks. It can also be redistributed in the sea due to migration of animals, or become fragmented into smaller pieces due to digestion. Consumption by organisms can therefore function as a transport mechanism for plastic particles, but it can also function as a sink, for example if the animals are removed from the marine environment for the purposes of human consumption.

Microorganisms and algae may also grow on plastic objects as they are at sea, in a process called biofouling. Microplastics which initially are buoyant may sink as a result of this, as they become denser than seawater with the addition of algae or other organisms. This means that plastic particles which would otherwise float may sink deeper in the water column. (Kaiser, Kowalski, and J. Waniek 2017)

Transport by organisms therefore involves several factors (ingestion, entanglement and biofouling), the role of which is unclear. It seems likely that these factors could significantly alter the patterns of microplastic distribution at sea, however the approximate magnitude of these effects is unknown. Especially biofouling seems like it could be a big potential cause for sinking of microplastics, although this is not known for sure.

Part III

Microplastic distribution in the Baltic Sea

6 Aim and scope

The aim of this part of the thesis project is to examine the data from the literature in order to assess the state of pollution of microplastic particles in the Baltic sea. We will attempt to examine the distribution of plastic litter vertically in the water column, and horizontally across the surface layer. Care will be taken to assess the reliability and limitations of the data used, and the areas where necessary data may be missing in order to form conclusions.

We will focus only on microplastic litter in the sea, defined as plastic particles in the sea which are smaller than 5 mm in size. Such particles have distinct sources, sinks and transport processes which are less relevant for large plastic particles (macroplastics), which we will discuss in further detail. The choice to only include microplastic pollution occurs since information in the literature on macroplastic pollution in the sea (rather than for example on beaches) is scant.

We will furthermore restrict our attention to conditions in the Baltic Sea, which is an arm of the Atlantic Sea and is located in Europe. The entrance to the Baltic Sea is considered to be at the parallel of Skaw in the Skagerrak (at 57.75194 degrees North), at which it borders the North Sea (HELCOM 1992). The Baltic Sea is otherwise bordered by land. A map of the Baltic Sea with divisions into subbasins can be seen in figure 2.

In this part, we will begin by looking at the sources of plastic pollution in the Sea, as well as plastic sinks, especially in relation to some of the transport mechanisms which we described in section 5. We will then examine the different methods by which sea samples with plastic are collected. Finally, we will look to the data in the literature to see whether there are any patterns in microplastic litter distribution in the Baltic Sea.

7 Sources and sinks

Studies on plastic abundance in the sea in general involve an attempt to take samples at different locations and times in order to determine the concentration of plastic particles per volume unit. Before designing and conducting such a study, it is relevant to consider hypotheses of where we would expect plastic to enter the sea, and how we might expect plastic to exit the sea. We might expect that plastic pollution levels would be higher near sources, and in any expected accumulation zones. We will therefore begin by discussing where we might expect waste to enter the Baltic Sea (sources), as well as the pathways by which it exits the Baltic Sea (sinks). We will take a look at sources first, followed by sinks.

7.1 Sources

The relevant sources of plastic waste in the sea depend on a number of factors. The first is the size of the released particles: plastic waste can enter the sea as microplastic particles, or as larger macroscopic pieces of plastic. These larger plastics can then degrade due to weathering and waves, UV-radiation and oxidation to release microplastic particles (Boucher and Friot 2017). These microplastics which arrive at sea through degradation of larger plastic objects are referred to as secondary microplastics, as opposed to primary microplastics which enter the sea as small particles. Our division is thus between macroplastics

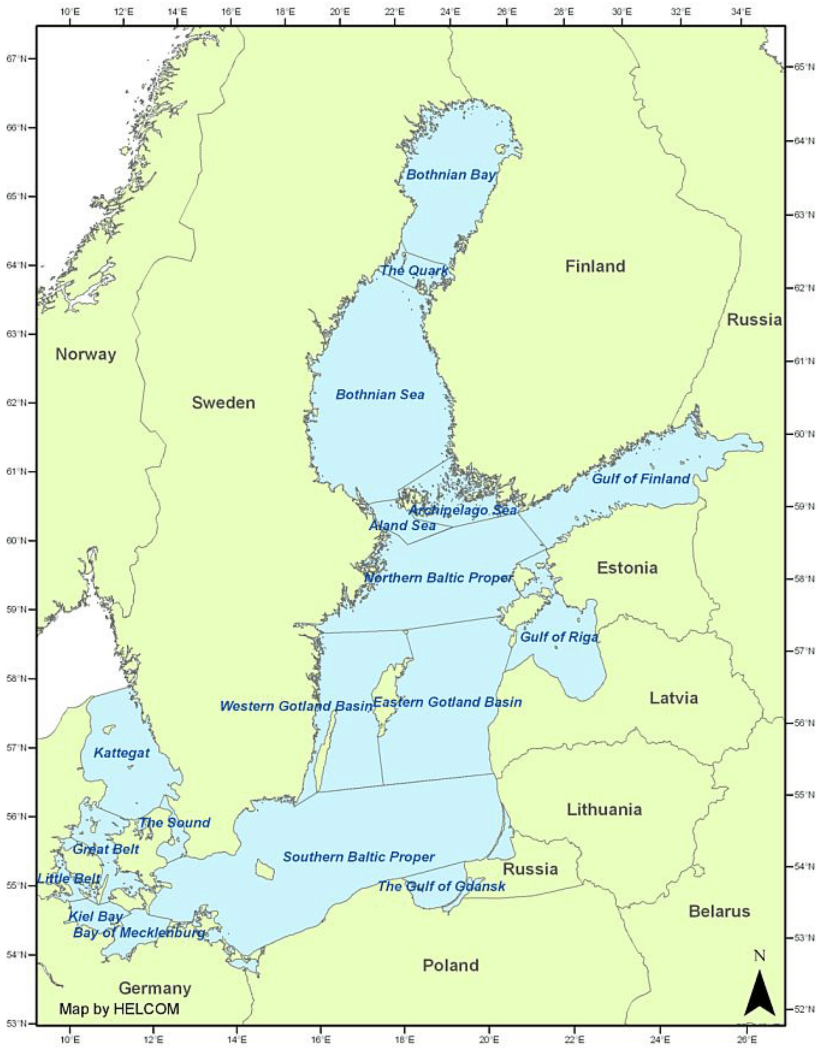

Figure 2: A map of the Baltic Sea, with subbasins indicated. Found from Tedesco 2009.

and microplastics, and furthermore into primary and secondary microplastics. We note that one source which is common to both of these types is entrance to the Baltic Sea via the North Sea, but unfortunately we could not find quantification for this.

7.1.1 Macroplastic sources

Even though most of the data from the literature on plastic pollution in the Baltic Sea is about microplastics, we still consider macroplastic sources as larger plastic objects can degrade into secondary microplastics. Estimating the sources and sinks of larger plastic objects is also easier than that for small particles, as they are simpler to detect. The main method of plastic waste detection in this case is via waste collection along public beaches. For beaches visited regularly by people, this is assumed to be due to littering which takes place at the beach. In contrast to this, when plastic waste is found on beaches which are secluded or not frequently visited, the assumption is that this waste has washed up on the coast from the sea (Programme 2013). We note that these assumptions are reasonable but not verified; in the absence of more detailed evidence-based information they are useful.

Macroplastics are further divided into those which are from sea-based sources or land-based sources. Sea-based sources include shipping, fishing vessels, offshore platforms and other boats and infrastructure in the ocean. Land-based sources include beach litter, landfills on the coast, and any other sources which are on land but from which plastic can arrive in the sea. It is estimated that, on a global scale, around 80% of plastic litter is due to land-based sources, and 20% is due to sea-based sources (UNEP 2005). This estimate can vary in different places; a study which sampled beach litter in the Baltic and Mediterranean seas found that between 75% and 90% of the plastic pollution could be attributed to land-based sources (Mehlhart and Blepp 2012). In the Baltic sea, the major land-based sources of macroplastics are coastal tourism, river fishery and waste dumping. The major sea-based sources are commercial shipping and tourism-related ships. (Strand et al. 2015)

7.1.2 Microplastic sources

Secondary microplastics arise due to degradation of macroplastics, and they therefore have common sources with macroplastics. We will therefore focus on primary microplastics. The data available for this are not necessarily collected for the Baltic sea, but rather in larger regions or globally. We will list the sources in order of abundance of marine microplastic pollution by mass stemming from each for the region of Europe and Central Asia. All information in this part was sourced from (Boucher and Friot 2017).

Tyre wear (54% of litter): Tyres of cars, trucks and other vehicles are usually made of synthetic rubber, natural rubber and a number of other additives. As the tyres are used, the rubber erodes, leaving tyre dust that is swept away by wind or washed away by rain.

Synthetic textiles (25% of litter): Laundering synthetic textiles, both in an industrial and private capacity, releases primary microplastics through abrasions and tears in the fabric. These microplastics then end up in sewage water, through which they may enter the ocean.

Road markings (15% of litter): Markings on roads may contain plastic particles, and due to weathering they erode. Similar to tyre wear, these particles are swept away by wind or washed away by rain.

Marine coatings (4% of litter): Ships and other vessels are typically painted or otherwise coated. This coating may contain plastic, and erodes over time due to weathering, whereupon it enters the sea.

Personal care products (1% of litter): Cosmetic and personal hygiene products often contain plastic particles. Once these are used by an individual, they are typically washed down the drain, and may enter the sea through sewage water.

Plastic pellets (1% of litter): Plastic pellets are used in manufacturing larger plastic products. They are shipped to factories for this purpose, however occasionally there is a spill from ships which releases these pellets into the ocean before they reach their intended destination.

The total amount of primary microplastics released into the sea in Europe and Central Asia is around $2.43 \cdot 10^5$ tonnes per year, although of course this is a large area and only a fraction of this will be in the Baltic Sea specifically.

7.2 Sinks

As with sources, there are a number of sinks for plastic litter in the sea. Some plastic particles are denser than seawater, but there is also evidence of buoyant particles in the water column and in sediments (Bergmann et al. 2017; Song et al. 2018). Sinking of buoyant plastic litter is what we wish to consider, as the transport is less obvious.

Particularly microplastics may stick to marine snow, which is a shower of small organic particles from the upper to the lower layers of the water column. Some observations indicate that up to 70% aggregates of marine snow contained microplastics (Zhao et al. 2018; de Haan, Sanchez-Vidal, and Canals 2019). Some plastics may enter the seafloor sediment (Näkki, Setälä, and Lehtiniemi 2019; UNEP 2005), especially if they are small particles that are negatively-buoyant. Microplastics may also be ingested by marine animals such as fish and birds (Bråte et al. 2017), whereupon they may be transported across distances, and then incorporated in fecal pellets which increases the sinking velocity (Cole et al. 2016). Beaching is another sink, i.e. plastic objects or fragments washing up along the coast (Programme 2013). In the case of the Baltic Sea, plastics could also move to the North Sea, and leave the ocean only later.

The relative importance of each plastic sink depends partly on the timescale involved, that is, how long it takes for a plastic particle to sink in that particular way. Unfortunately the time involved for several of these sinks, such as beaching or biota ingestion, is difficult to study. One sink that is more well-studied is sedimentation of microplastic particles.

Evidence from a simulation indicates that sedimentation time for microplastics can take anywhere from minutes to hundreds of years to sink, depending on particle size and density (larger and denser particles sink faster), and presumably also depth of the sea (Kooi et al. 2017). Particles between 1μm and 1 mm were simulated. An experimental procedure testing sinking velocities for larger microplastics (of the size of a couple of millimetres) in Baltic seawater found velocities of between 6 and $91 \cdot 10^{-3}$ m s^{-1} (Kowalski, Reichardt, and J. J. Waniek 2016). Given even the maximum depth of 459 m in the Baltic Sea (Alice F.A. Mutton, Alastair Dougal Couper 2019), this would give a very rapid sinking time of a few seconds to a few minutes, although this is in the absence of currents and other transport processes. Another experiment using regular-shaped plastic particles of between 0.5 and 5 mm in diameter found sinking velocities of $5 \cdot 10^{-3}$ and $127 \cdot 10^{-3}$ m s^{-1}, which indicates similar sinking times of several minutes for the maximum depth of the Baltic Sea (Khatmullina and Isachenko 2017).

Figuring out where plastics end up finally is challenging, as plastic decomposes so slowly (with half-lives in the range of decades to hundreds of years) (Chamas et al. 2020), and when plastic is found in a marine environment it can be difficult to estimate how long the litter has been at sea. There may furthermore be interaction between Some of the sinks, as e.g. the decomposition of plastic would occur more slowly than that of any marine animal which ingested the plastic. Estimates based on data collected in the North sea and Australia indicate that around 70% of marine litter which enter the sea end up on the seabed, whereas 15% wash up on the coast and 15% float on the surface (UNEP 2005), although this source makes it unclear which sizes of plastic were investigated. Another paper focusing on the Baltic Sea indicates that sedimentation is a major sink in this area, with subsequent biota ingestion being uncommon (Näkki, Setälä, and Lehtiniemi 2019).

8 Data collection methods

We wish to present some findings from the literature about the distribution of microplastics in the Baltic Sea, but in order to assess the quality of these findings, as well as determine how valid the comparison is between different articles with different methodologies, we must first consider how data is collected. Note that we have included literature data only on microplastic particles, i.e. only those plastics which are less than 5 mm in diameter. We have furthermore only looked at observations from plastic in the water, so articles on abundance of plastic particles in the beach or sediments, as well as that which has been ingested by marine animals, were not considered. This is because it is challenging to relate these in a direct way to abundance of particles in the Sea itself.

The three forms of data collection on concentrations of plastic particles in the Baltic sea itself are manta trawls, water pumps and bulk collection. In the following sections we will consider each of these in greater detail.

8.1 Manta trawls

Trawling is a method of sea litter collection which involves a moving ship equipped with a surface sampler, usually some form of net, where the net moves along the surface of the water. This method is useful to obtain samples from the sea surface, especially if one is interested in collecting small pieces of debris. Several of the microplastic studies conducted in the Baltic sea use this technique: Gewert et al. 2017, Tamminga, Hengstmann, and Fischer 2018, K. Norén, Haikonen, and F. Norén 2015, Setala et al. 2016, F. Norén 2007. In addition, we used data from the EU project CLAIM, which aims to develop new technologies to clean plastic marine litter in the Baltic and Mediterranean Seas. The data from this project was collected in the Gulf of Finland in 2014 using manta trawls.

Another source for a more general description of how manta trawl data is collected and analyzed is Ribic, Dixon, and Vining 1992.

In trawling the sea surface, data is collected by a moving ship with a net that moves along the water surface. A given area is designated, and the ship moves through this area with a relatively slow speed, usually in the range of 2-3 knots, though in any case less than 5 knots. (Ribic, Dixon, and Vining 1992)

The net is placed either to the side or to the front of the ship, to minimize the disturbance in debris patterns caused by motion of the ship. It is generally trapezium shaped, with the wider base in front. The width of this side of the net determines the width of the strip of sea which is sampled. The length of the strip sampled is determined by how far the ship travels, though a maximum length is when the net is full. If the trawl continues beyond this point, then results may be inaccurate, as the volume sampled will be overestimated. Trawled distances tend to be less than 5 km, with many being significantly shorter than this (e.g. Tamminga, Hengstmann, and Fischer 2018 or the CLAIM data). The size of debris which can be collected is determined by the fineness of the net mesh, commonly about 300μm, which was roughly the size for most of the trawling studies in the Baltic Sea.

Concentration of plastic particles found during a trawl is calculated by counting the plastic particles caught in the net, and then dividing by the volume of water sampled. Sampled water volume can be calculated using the area of the net opening which is submerged in water, multiplied by the distance travelled. This method can potentially have uncertainties as the presence of waves can change the degree to which the net is submerged. In some studies, e.g. in the CLAIM data set, the net is equipped with a flowmeter, which can directly measure the volume of water passing through the net. A large concentration of debris can, however, interfere with the flowmeter, making the results of this tool less accurate.

When undertaking a study of marine debris using this method, one must take care to choose periods of time with calmer weather conditions. A high wind speed and large waves may mean that the net is completely submerged, or completely outside of the water, which will skew measurements (Ribic, Dixon, and Vining 1992). This is a limitation of the method, as most data is as a consequence collected in calmer periods of the year, which means that data is lacking for seasonal comparison.

Care must also be taken to select an area which is appropriate to study, if one wishes to find concentration of marine debris and plastics more specifically, rather than just small organic particles of lifeforms. In particular, trawls are sometimes used to monitor plankton populations, and areas which are known to have high concentration of plankton may be unsuitable for collection of plastic litter. Even if debris is collected, some attention must be given to the fact that it may not be plastic litter, if this type of litter is the only one of concern in the study. (Ribic, Dixon, and Vining 1992)

Once the samples are collected in the net, they are either bottled, or preserved in some manner and then bottled. Preservation methods include freezing, storing in alcohol, or storing in a seawater-formalin mixture. Freezing the sample is generally the least reliable of these methods, since it may alter the shape of debris fragments. (Ribic, Dixon, and Vining 1992)

Once the data is collected, a calculation of density of the debris can be made according to the formula

$$\hat{D} = \frac{n}{La},$$

where $\hat{D}$ is the density in amount per cubic metre, L is the length of the trawl in metres, and a is the area of the net submerged in water, in square metres. n is either the number of debris particles, or the total mass of debris particles of a given type. Of the studies on the Baltic sea, all papers reported concentrations of particle number rather than mass. The length L of the trawl is given either by the straight-line distance between the start- and end-coordinates, taking into account any periods where data was not being collected, or by multiplying the ship speed and the duration of the trawl.

8.2 Water pumps

Another method of sea litter collection is sailing a ship with an attached water pump that is submerged beneath the sea surface. Water pumps are used to stream ocean water through a filter, which separates out debris or organic particles above a certain size. This method is normally used for depths up to half a metre below the water surface (Karlsson et al. 2019). The studies in the Baltic sea which use water pumps are: Setala et al. 2016, Magnusson and F. Norén 2011.

In general, various locations are selected at which to take samples, and a fixed quantity of water is fed through a pump into a filter at each location. A variety of filter sizes can be used to further obtain size categories of the different microplastics which are present. One advantage of water pumps over manta trawls is that the mesh fineness can often be much smaller, in some cases down to 10μm. A finer mesh can catch more plastic particles, although since more particles are in the collection range, the filter will get full faster, so a smaller volume of water can be filtered. This can lead to larger uncertainties when finding plastic concentrations, since we take average particle number per cubic metre over a smaller sample. Once the samples are collected, they can be taken to a lab for further analysis.

8.3 Bulk sampling

Bulk sampling involves collection of a volume of water from the sea in some sort of collection device, whereupon the water is filtered. Unlike trawling, the sample is collected from a ship which is anchored, rather than in motion. Unlike both trawling and water pumps, the filtering is done after the sample is collected, rather than concurrently. As a result, there is more flexibility in the choice of filter, which will determine the smallest particles which can be detected during data collection. (GESAMP 2019)

In the Baltic sea, bulk sampling has been used to collect data about microplastic concentrations in the papers: Tamminga, Hengstmann, and Fischer 2018, K. Norén, Haikonen, and F. Norén 2015, Bagaev, Khatmullina, and Chubarenko 2018. A different type of collection device is used in each: an integrated water sampler is used in the former two, while Niskin bottles are used in the latter.

An integrated water sampler is a clear plastic tube with a piston inside. The piston mechanism is controlled electronically to open at a certain depth or time, and can then be closed again (RMB

Environmental Laboratories, Inc. n.d.). A Niskin bottle is made of plastic with a rubber stopper at each end, which allows for collection of water from a specific depth of the sea, without mixing of water from other depths. The bottles can lowered to the desired depth using a cable. A small weight is then released down the cable, striking a release mechanism. The release mechanism pulls the two stoppers into the ends of the bottle, allowing entry of water. Several bottles can be grouped together and opened at different depths, allowing for samples at different depths at the same location. (Flanders Marine Institute (VLIZ) n.d.)

One big advantage of bulk sampling over trawling or using a water pump is that sampling can be done at many different depths. The other two methods are restricted to near-surface samples. Using a round of Niskin bottles, it is possible to take several samples at different depths, using which we can create depth profiles at a given location.

A disadvantage of bulk sampling is the small volume of water collected for a sample. In general, bottles can collect between 2-12 litres (or $2 \cdot 10^{-3}$ to $12 \cdot 10^{-3}$ cubic metres) per sample (Flanders Marine Institute (VLIZ) n.d.; RMB Environmental Laboratories, Inc. n.d.). In contrast, pumps can sample over several cubic metres, and trawls can sample over up to hundreds of cubic metres – the volume of sample in this case depends on when the filter is full and no longer able to collect, rather than a pre-determined size of bottle. (GESAMP 2019)

Additionally, bulk sampling devices such as integrated water samplers and niskin bottles are normally made of plastic, and so there is a chance of contamination of the samples. As only a small volume is sampled each time, even one or two particles contaminating the sample can have a large effect on which concentration of plastics is discovered. It is therefore necessary when designing bulk sampling experiments to be cognizant of contamination, and measure the base rate of plastic particles released from the equipment when filtering pure water which is known to be unpolluted.

8.4 Other methods

We have focused on the methods which can be used to assess the abundance of plastic microlitter in the sea, however there are other methods to examine litter quantities which may be relevant in other contexts. These methods are sediment collection, beach sampling and marine animal dissection.

Sediment collection can used to determine the abundance of microplastics in either beach sediments or in the ocean floor. Sediment samples are extracted by divers, or using ROVs or surface vehicles. The volume of each sample is measured, and the abundance of plastic within this sediment is determined in a lab (GESAMP 2019). Examples of papers which use sediment observations in the Baltic Sea are Stolte et al. 2015 and Zobkov and Esiukova 2017.

Beach sampling is the collection of plastic and other anthropogenic objects left as litter on beaches, in order to determine the level of pollution on beaches. Objects are collected by eye, and so only macroplastics and other large litter objects are considered. Examples of studies which use beach observations along the Baltic coast are Programme 2013 and E. Esiukova 2017.

Dissection of marine animals is done to study whether these animals have ingested plastic particles, and possibly the effect these particles have had, if any, on the health of the animals. Usually animals such as fish or seagoing birds are selected for these studies. Examples of papers which use these methods in the Baltic Sea are Skóra et al. 2012 and Sørensen et al. 2013.

9 Results

In this section we will summarize some of the key trends found in the literature on abundance of plastic particles in the Baltic Sea.

9.1 Comparison of sampling methods

When analyzing the data on the Baltic sea, we wish to combine the results of several different studies which use different sampling methods, looking at both the mesh size used in the studies, as well as different measuring techniques. This will help us to evaluate whether different studies in the literature which use different mesh sizes or different sampling methods are comparable.

9.1.1 Mesh size

The mesh size used to filter the water sample was one of the biggest determinants of how much plastic was found in the sample. Samples obtained with a finer mesh sometimes had higher concentrations of microplastic by several orders of magnitude.

In one study (F. Norén 2007), manta trawls with both an 80 μm and a 450 μm net were used, and concentrations of between 0.01 and 0.14 particles per cubic metre were found with the larger mesh size, compared to between 150 and 2400 particles per cubic metre with the finer mesh. The sampling was done over similar regions in a similar time frame, and so it seems reasonable that this very large disparity is in fact due to the mesh size, even though only a single trawl was conducted with each mesh size at each location.

Another study (Setala et al. 2016) used a water pump with both a 100 μm mesh and a 300 μm mesh to take samples at twelve different stations. They found that concentrations were between 0 and 4 particles per cubic metre with the finer mesh and between 0 and 9 particles per cubic metre with the coarser mesh, and comparing the results side by side it appears that higher concentrations were normally found with the smaller mesh size. Additionally, with the finer mesh size the composition of particles changed to include more fibres. It is theorized in the paper that fibres can slip through a coarser mesh more easily than fragments can, and that this is the reason for the discrepancy. This is a much less dramatic difference than the former study, and as only a single measurement was taken at each location with each of the two mesh sizes, it is difficult to evaluate whether there is statistical significance.

Other studies did not assess the effect of mesh size directly, but comparing between studies it does appear that mesh size has an effect. All other studies in the Baltic which used a manta trawl had a mesh fineness of around 300 μm, and found concentrations of around 0-8 particles per cubic metre (e.g. Tamminga, Hengstmann, and Fischer 2018; Gewert et al. 2017). Samples from different studies which were taken at different locations and years thus had similar orders of magnitude in their results. On the other hand in one study (K. Norén, Haikonen, and F. Norén 2015) which used a water sampler with a 10 μm filter, concentrations of between 1,000 and 27,000 particles per cubic metre were found.

Such comparisons are relatively weak, since there are so many differences between these experiments, and therefore several factors to which we could attribute this large disparity. The first is differences in location or time of sampling, but it seems unlikely that this would produce orders of magnitude of difference when we consider that the trawl studies with similar mesh sizes found similar orders of magnitudes in microplastic concentrations. The second is that some of the difference is caused by differences between bulk sampling, which uses a small volume and is therefore more prone to counting error, and manta trawls. We will compare bulk sampling to manta trawls later to see if there is indeed a difference in the two methods.

In conclusion, there is likely some difference in microplastic concentration depending on the size of the mesh used. As we do not have data to obtain statistical significance it would usually not be possible to say either way, however results like in F. Norén 2007 which have orders of magnitude in difference provide decent evidence even without more repetitions to be sure. If indeed it is true that we find higher concentrations with a finer mesh, this would provide evidence that most microplastics in the Baltic Sea are smaller than 0.3-0.45 mm (300-450 μm).

9.1.2 Manta trawls and water pumps

We also wish to compare whether manta trawls and water pumps give comparable results. There is one paper making this comparison in the Baltic Sea, Setala et al. 2016. They used a manta trawl with mesh size of 333μm, a water pump with filter size of 300μm, and a water pump with filter size of 100μm. Twelve stations in the Gulf of Finland were selected, and each device was used at all twelve stations to measure the surface plastic concentration at that station. All samples were taken over the same week in August, 2013, which reportedly had calm weather conditions.

According to this paper, the water pump and manta samples with similar filter fineness gave similar results, whereas using the water pump with a 100μm mesh gave a higher concentration of particles, as reported in the previous section on the effect of mesh fineness.

We conducted a Kruskal-Wallis test for the difference in medians of the data sets compiled using each of the three sampling methods. This statistical test was selected because in each case the distribution of concentrations appeared similar, but skewed so that assuming a normal distribution would likely be faulty. The results were that the difference between the manta trawl samples and those of the 300μm pump were deemed insignificant at the 95% level (p-value 0.07), the difference between the trawl and the 100μm pump was insignificant (p-value 0.17), and the difference between the pumps with different filters was also insignificant (p-value 0.77). This provides some evidence that the three methods were indistinguishable.

Another study which compares trawling and water pumps is Karlsson et al. 2019 which was conducted in the Gullmar Fjord in the North Sea. This study used a 300 μm mesh size for both the water pump and the trawl, and concluded that water pumps have a higher accuracy in the volume measurement, however the trawl sampled more volume and so there were fewer uncertainties due to counting errors or contamination. Samples taken with a trawl had higher concentrations due to sampling the sea surface rather than being completely submerged.

9.1.3 Manta trawls and bulk sampling

There were two studies in the Baltic Sea which used both trawls and bulk sampling (Tamminga, Hengstmann, and Fischer 2018; K. Norén, Haikonen, and F. Norén 2015). Unfortunately the latter of these used a different mesh size for the trawl (300 μm) relative to the integrated water sampler (10 μm) and so even though higher concentrations were found with the water sampler by several orders of magnitude, it is difficult to know what the cause of the difference is.

We therefore examine only the first of these studies, which had 10 samples taken with a manta trawl, and 31 samples taken with an integrated water sampler. The bulk samples were taken with a mesh fineness of 300 μm, and the manta net fineness is unfortunately not noted in the paper – since the values seem to align with other manta trawl studies in the Baltic which used a mesh size of about 300 μm and this is the standard size, we assume that this is the case in this paper, although of course this is less than ideal. Of the 31 bulk samples, 4 were taken at harbors between trawling routes at a depth of 0.5 m, and the remaining 27 were divided into 9 stations along the trawling routes, at which samples were taken at depths of 0.5, 2 and 5 m. As the vertical distribution of microplastics could potentially be a factor, as suggested in e.g. Karlsson et al. 2019, we compare only the manta samples with the samples taken at the most shallow depth using an integrated water sampler.

The samples taken with a manta trawl had very low plastic concentrations, of between 0.04 and 0.09 particles per cubic metre. The bulk samples, however, had particle concentrations of between 350 and 2800 particles per cubic metre. This order of magnitude difference indicates that the two sampling methods are not directly comparable, as it seems implausible that there would be very low concentrations on the surface, yet much higher concentrations at a depth of 0.5 m.

Part of this difference could be due to the way samples are taken using the two methods. The estimated sample volume for the manta trawls was between 127 and 193 cubic metres, however the integrated water sampler had a volume of 5 litres ($5 \cdot 10^{-3}$ cubic metres). This means that even if only a single plastic particle was found in a bulk sample, the minimum concentration would be 200 particles per cubic metre. Thus any single particle which entered the sample due to contamination would have a large effect on the results relative to the trawl sample. On the other hand, when using a manta net there can be a large uncertainty due to the movement of the manta net in the water, clogging of the net, and so on, which can lead to undercounting of particles or errors in the reported sample volume. Both sampling methods have their advantages and disadvantages, and while it seems clear that it is incorrect to directly compare samples taken using these methods, it is unclear that one of them is necessarily preferable.

9.1.4 Water pumps and bulk sampling

We found no studies in the Baltic Sea which directly compared bulk sampling with water pumps. From the previous discussion it appears that usage of manta trawls and water pumps produce results of similar orders of magnitude, whereas bulk samples tend to have much higher concentrations, so we can draw a tentative hypothesis that usage of bulk sampling would produce higher concentrations than use of a water pump. Without data either way, though, it is hard to know for sure.

9.2 Vertical distribution

The sampling technique most suited to an analysis of the vertical distribution is bulk sampling, as it allows for the collection of samples at varying depths. Two papers in the Baltic Sea examined different depths using bulk sampling, Tamminga, Hengstmann, and Fischer 2018 and Bagaev, Khatmullina, and Chubarenko 2018.

The first of these papers involved the use of a 5 litre (0.005 cubic metres) integrated water sampler with a mesh size of 300 μm, with three depths at 9 locations (0.5, 2 and 5 metres) sampled, and an additional 4 locations sampled at 0.5 metres. Each of the nine sets with three depths was sampled at the same time, which makes it easier to compare them. The median concentration for each of the three depths ranging from shallowest to deepest is respectively 1070, 400 and 600 particles per cubic metre.

We wish to know whether there is some statistical difference between the concentrations at different depths to see if this difference in medians is meaningful. The data at each depth tested appear to be skewed, and thus we use the Kruskal-Wallis test for difference in medians, which only assumes that other than the difference in medians, the distribution of the samples is identical. This assumption is not completely justified, since it appears that the sample standard deviation in the three distributions for the different depths is not identical (in order of shallowest to deepest the values are 834, 814 and 881 particles per cubic metres), and since we do not have enough data points to determine whether the distributions are otherwise of the same shape. On the other hand, the distributions are all skewed towards lower concentrations, with some higher outliers. In order to see whether we can draw some conclusion, we therefore make an assumption of identical distributions as we proceed.

The results of the Kruskal-Wallis test are overall that at 95% significance, there are no statistical differences between samples from the three depths. When conducting the test for all three samples together, the resulting H-value was 3.573, with a corresponding p-value of 0.17. The closest to a statistically significant result is the difference between the samples at 0.5 m and at 2 m, which have an H-value of 2.974, with a corresponding p-value of 0.08. This sample size is fairly small, though, and perhaps there is a real difference that could not be captured with only nine samples in each category.

The study Bagaev, Khatmullina, and Chubarenko 2018 was conducted using Niskin bottles with a volume of 10 litres and a 174 μm mesh. There were 95 samples taken on six different cruises over the course of about a year, which is the largest sample size of any study conducted in the Baltic Sea. The samples were taken from various depths, locations and times.

If we look at the aggregate data only in terms of depth, and more specifically the sampling depth divided by the depth of the seabed, we see a pattern as depicted in figure 3. Most of the samples in the study appear to have been taken at either a shallow depth (depth fraction closer to zero) or quite deep (depth fraction closer to one) with relatively few samples in between. At a depth fraction of under 0.05 (29 observations), we see a spread of concentrations ranging from 0 to around 2400 particles per cubic metres. At a depth fraction of between 0.05 and 0.8 (12 observations) we see lower concentrations of between 0 and 400 particles per cubic metre. Between a depth fraction of 0.8 and 1 we see a couple of outliers which have very high concentrations, of over 2000 particles per cubic metres, with the majority of observations otherwise lying between 0 and 1000 particles per cubic metres.

If we divide the data up by depth fractions and examine only the shallowest tenth and the deepest tenth of the sea, we see that both of these have concentration distributions which are skewed towards lower concentrations, with some higher values. The median for the shallowest tenth (with 32 observations) is 600 particles per cubic metre; for the deepest tenth (with 48 observations) it is 100 particles per cubic metres. A Kruskal-Wallis test for the difference in medians between these two samples has an H-value of 10.60, with a corresponding p-value of 0.001. This indicates that the difference in medians of particle concentrations between the two layers is statistically significant at a 95% level, and that the shallower layer has the higher amount of microplastics. It furthermore appears from the study that layers in between these have the lowest concentrations of microplastic by a factor of 3–6.

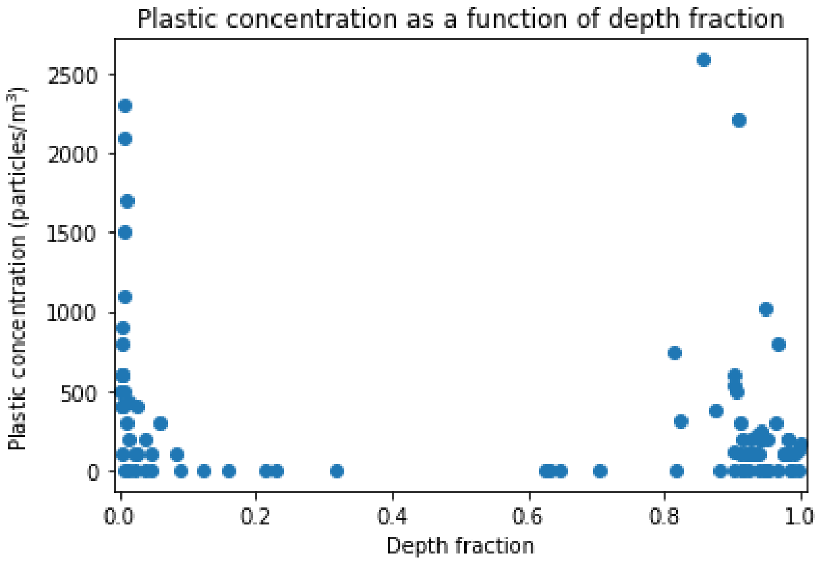

Figure 3: A graph depicting the microplastic concentration, in particles per cubic metres, as a function of the depth fraction (equal to sampling depth over depth of the seabed) for each of the 95 samples in the study Bagaev, Khatmullina, and Chubarenko 2018.

9.3 Horizontal and temporal distributions

When considering how microplastics are distributed in the Baltic Sea, we wish to know what the horizontal distribution is, i.e. if there are locations which tend to have higher or lower concentrations than others, especially in the surface waters. We also wish to know the temporal distribution, i.e. whether the concentration of particles in a given location tends to increase or decrease, and in what fashion, over time. Although these are both separate questions, we combine them in one section because using the data from the literature on the Baltic Sea, it is challenging to answer both of these questions for the same reasons, which is a lack of controls in the data and lack of repeated samples.

We will use an example to illustrate this using the CLAIM data set on the Gulf of Finland, which contains 58 trawl samples over 9 locations. There are thus repeated samples at several stations on different months. One such repetition is at the station Paljassaare, for which two samples were taken on the same day (04/06/2014) giving respective concentrations of 3.59 and 3.27 particles per cubic metre. Another sample was taken at the same location eight days later (12/06/2014) which had a concentration of 0.89 particles per cubic metre. Other samples were taken even more sparsely, with for the most part no more than one observation taken at a single station for a given month. The total range of concentrations found in the study was 0.21 to 3.59 particles per cubic metre, and so the span in this one station within these eight days indicates that the variations within a single month can potentially be large, enough so that it can overwhelm the long-term differences between different months and locations.

This example shows the importance of control variables and repeated experiments. Most other studies of this kind conducted in the Baltic Sea, e.g. Tamminga, Hengstmann, and Fischer 2018 or Gewert et al. 2017, involved single samples at different locations at different times, and used this as evidence to conclude on which areas are more or less polluted than others. In fact, it appears from the CLAIM data that such conclusions are premature without further samples taken for confirmation.

The one observation which is backed by several studies (e.g. K. Norén, Haikonen, and F. Norén 2015; F. Norén 2007; Gewert et al. 2017), is that outliers with very high concentrations, sometimes orders of magnitude higher than the other measurements in the same study, tend to be located at industrial harbours or urban centres. This fits with our common sense expectations, as places with industrial development and human habitation are more likely to be sources for plastic pollution.

9.4 Quality of the data

Unfortunately, the data gathered in the literature has a number of shortcomings which makes it difficult to form conclusions.

Two of these shortcomings have already been discussed in the previous section on horizontal and temporal patterns in microplastic distributions. The first is the lack of controls in the experiments. Often, several samples were taken altering both location and the day of the sample between them. This limits the ability to form conclusions about whether the plastic concentrations are different due to different locations, or different times. Another example of lack of controls is in the paper K. Norén, Haikonen, and F. Norén 2015, where they took both bulk samples and trawl samples, and varied the mesh size between them, so it is impossible to say for sure whether the reason for the difference between the results is due to a different mesh, or a different sampling technique. Some of the studies such as F. Norén 2007 and K. Norén, Haikonen, and F. Norén 2015 are structured more as surveys of pollution rather than experiments, which means that they are not designed to test any particular hypothesis, and so are not done in a controlled fashion. Although this can be useful, it also introduces a lot of noise, and so any result found by such a study must be especially clear in order to form conclusions.

The other frequent shortcoming which we have previously touched on is the lack of repetitions or other attempts to find errors in the samples. There can be many sources of error in the types of studies used to measure microplastic concentration in the sea, for example error in volume of water sifted by a manta trawl, contamination from equipment, or errors from misidentification of particles in the lab. Most of the studies made some attempt to determine error due to contamination, although none of them gave estimates for any other type of error which could have been involved in the process, e.g. by also giving a count of the number of particles for which classification was ambiguous, or trying to estimate some error bounds for the flow volume in trawl studies.

In addition to this, it would be extremely useful to see repeated measurements taken at very close locations at the same time, or taken at different times on the same day at the same location. This would allow us to calculate a statistical spread in results and come up with an informed margin of error, and would also allow for better ability to compare between different studies. One reason for why this might not be done is because analyzing samples, especially from trawls, is laborious, and so researchers may not be willing or able to perform such repetitions. Without them, though, the quality of the study is greatly diminished.

Finally, another shortcoming is due to the nature of such studies. Although it is certainly useful to have an idea of which regions are especially polluted, they do not tell us about the dominant transport mechanisms for microplastic particles, their lifetime in the water column, their sinking time in different seasons, or other similar questions. These questions are relevant, however they are difficult to answer experimentally, which is why we use simulations to try to answer them instead.

Part IV

Macroplastic drift in the Gullmar Fjord

10 Aim and scope

In this previous part, we discussed the literature on abundance of microplastic particles in the Baltic Sea in general. We came to a few conclusions. The first is that there were significant differences in measured quantities that seemed like they were a direct result of methodological differences between studies, such as use of different mesh sizes in filtering. The second is that it seems as though plastic concentrations tend to be higher in shallower water, then in deeper waters, and that very low concentrations are found in between.

We also found that there were several areas where we could not come to any definitive conclusions. It would have been relevant to learn more about the horizontal and temporal distributions of microplastics in the Baltic Sea, however due to a lack of systematic measurements and methodological differences between studies, we could only draw very limited conclusion on this. Due to the general nature of studies that measure plastic abundance, we also could not determine the likely transport patterns of plastic particles, how long they had been in the marine environment, or other information that involved the movement of plastic particles in time.

Due to the limited information on the transport patterns of plastic pollution in the Baltic Sea, as well as the lack of high quality data about horizontal distribution of plastics in the literature, we need to answer these questions in another way. In this part, we will aim to answer these questions by doing a simulation of plastic particles in the Gullmar Fjord in Sweden, which is near the entrance to the Baltic Sea from the North Sea. The simulation is not meant to be predictive of which plastic concentrations we would find at different places of the Gullmar Fjord, but rather to examine how particles move over a week with current fields representative of different wind directions.

The scope of the simulations run in this part will be limited in a number of ways. One of these is the location – we have chosen, due to computation time, to limit the scope to the Gullmar Fjord, rather than conducting the simulation over a larger area such as the Baltic Sea. We will run the simulation only for the duration of a week, with wind velocity being held constant for this time, due to simplicity and computational ease. We will also restrict our focus only to the horizontal current fields when releasing particles, meaning that the simulation is only valid for buoyant particles, and we do not consider causes of sinking in the water column.

We will begin this part by introducing the Gullmar Fjord and examining the wind conditions near the Gullmar Fjord, including typical wind speeds and directions, and wind steadiness. Then we will move on to discussing the numerical simulations, focusing on the details of implementation. Finally, we will discuss the results of the simulations, including any conclusions we can draw as well as shortcomings.

11 The Gullmar Fjord

The Gullmar Fjord is on the west coast of Sweden and outflows into the Skagerrak strait in the North Sea. A map of this Fjord, with its location in Sweden, can be seen in figure 4. It is 25 km long, with a width ranging between 1 to 3 km. It has a depth of 45 m at its mouth were it enters Skagerrak, and a maximum depth of 125 m. (Länsstyrelsen Västra Götaland n.d.)

The largest city on the Gullmar Fjord is Lysekil, located at the mouth of the Fjord. Lysekil has a population of around 14,400 people as of October 2020 (Statistikmyndigheten SCB 2020). The Gullmar Fjord is also the location of the Stora Bornö island, where the Bornö Marine Research Station is located. This research station is used by scientists at the University of Copenhagen as well as other universities to conduct research in physical-chemical oceanography, and is the reason that the Gullmar Fjord is of particular interest, and why it was selected as a case study in this project. Both the Bornö Marine Research Station and Lysekil are indicated in figure 4.

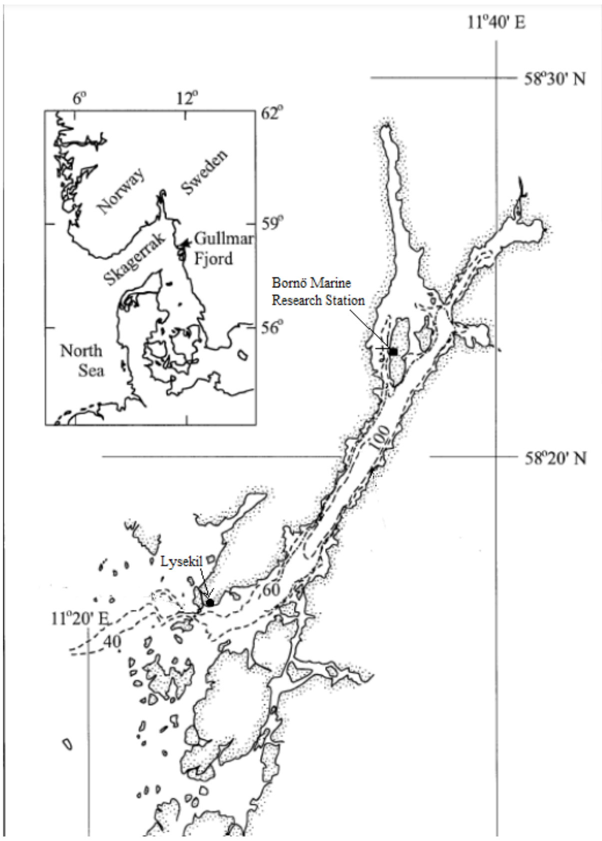

Figure 4: A map of the Gullmar Fjord, with a smaller map of the location of the Fjord in Sweden. The largest city on the Fjord, Lysekil, is indicated, as well as the Bornö Marine Research Station. Adapted from a map found in (Arneborg et al. 2004).

12 Meteorological properties of the Gullmar Fjord

Before simulating the currents in the Gullmar fjord, we first need to find out more about the wind speeds and directions which are most frequently occurring in this area. We will do this using data provided by the Swedish Meteorological and Hydrological Institute (SMHI), for the stations Måseskär between the years 1949 and 1995, and Måseskär A from 1995 to the present. Both stations are near each other, and so we will treat the data from the two stations together. Note that this station is outside of the Gullmar Fjord, located about 19 km away from the Fjord in the SSW direction along the coast of Sweden. We use data from this station as it is the closest available source, however the wind conditions on this island could differ in a systematic way to the conditions in the Gullmar Fjord, especially since the station is not surrounded by land to the same extent.

The data consists of wind speed measurements in metres per second, as well as wind direction measurements. We will first obtain a profile of which wind speeds are most commonly occurring in the region, and subsequently examine which wind directions occur more frequently in conjunction with different wind strengths. This will later allow us to use these values to generate a current profile in the Gullmar Fjord that matches different wind velocities of relevance to this area. After this, we will examine how steady the wind is, i.e. what the likelihood is of the wind having changed after a certain number of hours have elapsed. This is in order to see which time scales are realistic for a simulation using ocean currents simulated using only a single wind velocity.

12.1 Wind speeds

We begin by examining the wind speed distribution of the data, taken between January 1949 and December 2019. Note that data from the year 2020 was omitted, as the data was not available for all months of the year at the time of the analysis, and so conducting the analysis including this year was thought to potentially skew the results. There were a total of 296,771 points in the data set. Until October 1995, when data was taken at the station Måseskär, measurements were taken thrice per day, at 6 AM, 12 PM and 18 PM UTC+1. Upon the switch to the newer station Måseskär A, measurements were recorded hourly.

The overall mean of the data is 7.4 m s^{-1}, with a sample standard deviation of 3.9 m s^{-1}. The data is skewed, with a median of 7.0 m s^{-1}, differing from the mean. The skew is also apparent when viewing a histogram of the data, as in figure 5(c). This skew is expected, as it is known that windspeed follows a Weibull distribution (Mahmood, Resen, and Khamees 2020), which is asymmetrical and has a probability density function of

$$f(x;\lambda,k) = \begin{cases} \frac{k}{\lambda}\left(\frac{x}{\lambda}\right)^{k-1}\exp\left(-\left(\frac{x}{\lambda}\right)^{k}\right) & x > 0 \\ 0 & x \leq 0, \end{cases}$$

where x is in our case the wind speed in metres per second, λ is a scale parameter with units of metres per second, and k is a shape parameter with no units.

The Weibull distribution is a generalization of the Rayleigh distribution, which is a special case of the Weibull distribution with $k = 2$. The Rayleigh distribution arises when we take the norm of a two-dimensional vector with normally distributed components which are independent, centred at zero, and of equal variance. As our wind velocities are only considered in two dimensions, we could in theory get a pure Rayleigh distribution. In practice, however, some of the assumptions in producing a Rayleigh distribution may have been violated, and so we instead obtain a Weibull distribution. We expect, however, that the shape parameter of the Weibull distribution to be of the same order as $k = 2$ or closer.

We can display all of the wind speed data in a single figure as a two-dimensional histogram over speeds, as well as an overall distribution of the wind speeds for all years combined, and a comparison of the annual values of mean, median and 90th percentile wind strengths for each year. This can be seen in figure 5. Note that in this figure, we have only presented data from between 1969 and 2019. This is because the meteorological data is sorted into high and low quality data, and we have kept only the high quality data points here. Some years had too few high quality data points to be included in the comparison, so we began the analysis at the year 1969, for which there are over a thousand high quality measurements. For all years combined from 1969 and through 2019, we have 178,681 data points. This figure can help us form several conclusions about the wind speed distribution at the Måseskär meteorological stations.

Firstly, we can observe the best fit Weibull distribution for these data, and extract the fit parameters and obtain an estimate for the mean, median and 90th percentile wind speeds at this location. For the combined data, the mean, median and 90th percentile were 7.35, 6.69 and 13.3 metres per second, respectively. These are the values obtained for the Weibull distribution which was determined as the best fit for our data, depicted as the blue line in figure 5(c). Lines indicating the mean, median and 90th percentile are also shown in the figure. This fit has shape parameter 1.75 and scale parameter 8.27 m/s, which accords with our expectation that the shape parameter will be close to 2.

Secondly, we can compare whether there is a noticeable temporal change in the distribution of speeds. This is relevant in two regards: whether there is a change before and after 1996, which is the first year for which all data were obtained using the updated measuring methods, and whether there is a large annual change between the wind speeds every year, or if the data are more stable. In determining this, we examine figure 5(a), which shows the mean, median and 90th percentile values for the best fit Weibull distribution in each year.

The data does appear, by eye, to be different before and after 1996, indicated by a black vertical line in figure 5(a). Before 1996, there appears to be more spread in the data, with more wind speed values that were especially high or low, as can be seen in the two dimensional histogram in figure 5(b). The data collected in 1996 and after appears more peaked between the values of around 4 to 10 metres per second. The plot in figure 5(a) seems by eye to confirm this trend, with higher 90th percentile values in multiple years before 1996 than observed after. We can see whether this observation holds up numerically by finding the average mean, median and 90th percentile wind speeds before and after 1996, as well as the year-by-year variance in these values. The results are displayed in table 1, and seem to confirm the impression given from looking at fig. 5(b). The mean and 90th percentile wind speed are both higher in the data before 1996, and the median is the same in both samples. The standard deviation is in all cases higher before 1996 rather than after, which indicates that the wind speed distribution varies less each year.

If the data before and after 1996 appear different, then we should preferably form conclusions based on the more recent data, since there are more data points gathered using better measuring techniques. We see that this data has low standard deviations in values of mean, median and 90th percentile, and thus that the distribution for each year is similar. We do see a higher standard deviation in the case of 90th percentile values, which is to be expected since these speeds occur less frequently and there is thus a smaller sample size. The total range of the data was between 0 metres per second and 31 metres per second, with the maximum value representing a very large outlier.

Year	Mean (m/s)	Median (m/s)	90th percentile (m/s)
Before 1996	7.65 ± 0.50	6.67 ± 0.69	14.58 ± 0.89
1996 and later	7.20 ± 0.36	6.67 ± 0.40	12.67 ± 0.48

Table 1: The average mean, median and 90th percentile values for wind speed before and after 1996, with standard deviation, to two decimal places.

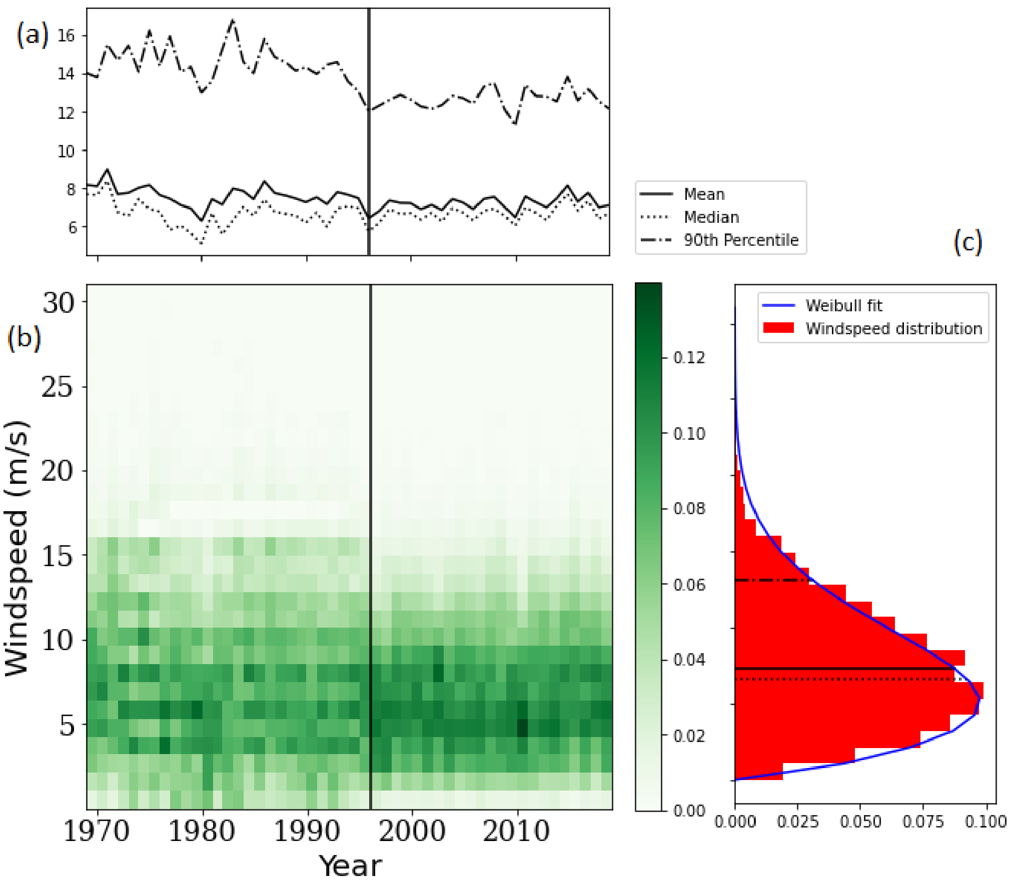

Figure 5: (a): A plot showing the mean, median and 90th percentile wind speed, in metres per second, as a function of year. These lines were generated by fitting a Weibull distribution to the wind speeds for each given year, resulting in a shape and scale parameter which could be used to calculate the values for mean, median and 90th percentile. The vertical black line is drawn at the year 1996, which is the first year for which all data are obtained via newer measuring techniques.
(b): A two-dimensional histogram over year and wind speed in metres per second. The histogram is normalized to show frequencies rather than raw observations, as the number of observations differed each year, with later years having far more observations. The normalization was thus done year by year (so all the frequencies for each year sum to one) rather than overall (in which case all the bins in the figures for all the years would have to sum to one). The vertical black line is drawn at the year 1996, the first year for which all data are obtained via newer measuring techniques.
(c): A one dimensional normalized histogram combining the wind speed data from all years, with a best fit Weibull distribution. This distribution has shape parameter 1.75 and scale parameter 8.27 m/s. The mean, median and 90th percentile wind speeds for the Weibull fit are depicted as horizontal black lines, and have respective values of 7.35, 6.69 and 13.3 metres per second.

12.2 Wind directions

For each wind speed noted in the SMHI data used in the previous section, there is a corresponding wind direction provided. In the older data set prior to October 1995, wind direction measurements were given to a precision of ten degrees. In the newer data from after October 1995, measurements are given to the nearest degree.

We wish to find which wind directions are the most dominant near the Gullmar Fjord, and in order to depict a possible correlation between wind speed and direction (as wind may be stronger in certain directions, regardless of the frequency with which we observe a specific wind direction) we use a wind rose. We combine the older and newer data into one figure by rounding the degree measurements for the newer data to the nearest ten; as the bins in the wind rose are larger than ten degrees, we do not expect to lose very much accuracy from this. The resulting image can be seen in figure 6. Note that the wind rose follows the meteorological convention in that it depicts the direction which the wind comes from.

We see from the figure that the three preferred directions which wind comes from, especially for stronger winds, are west-southwest, west and southwest. This fits well with what we might expect from the geographical layout of the Måseskär measuring station at which data was collected – this location is on the West coast of Sweden, and is therefore exposed to sea from the west and the south, and land from the east and the north. As the ocean is smoother and provides less friction than land (Possner and Caldeira 2017), we would thus think that the wind coming from the west to southwest would be stronger.

We can further apply this principle to the Gullmar Fjord, which is roughly between 34 and 41 degrees east, and so we would expect the strongest winds to come from a direction 180 degrees away from this, so between 214 and 221 degrees, corresponding to the compass directions south-southwest and southwest. Additionally, the fjord is more exposed to the sea from the west, rather than the eastern direction at which there is more landmass. We would therefore expect the wind direction results from Måseskär to hold for the Gullmar Fjord as well, even though the wind speeds observed at Måseskär may be higher than those in the Fjord.

12.3 Wind steadiness

We have now taken a look at the wind speeds and directions that are the most frequently occurring on the island of Måseskär, which is important if we wish to model currents. Another relevant aspect, however, is the steadiness of the wind – that is, if we know that at a certain time the wind is blowing at a specific velocity, for how long would we expect the wind to remain somewhat steady?

Over a shorter period of time, we would expect that the wind tends to be more steady than over a longer time, and so we wish to know that whichever time scale selected in simulation is realistic. If we for example simulate the same wind velocity over several days, when in fact the wind is only steady for several hours, then the resulting current will not be realistic.

We will proceed in calculating wind steadiness as in the paper Singer 1967. First, we find the mean scalar wind k, given by

$$k = \frac{\overline{(\overrightarrow{V})}}{|\overline{V}|},$$

where $\overline{\overrightarrow{V}}$ is the mean vector velocity, and $\overline{V}$ is the mean scalar speed. A value of $k = 1$ is the maximum, and indicates that the wind has been constant over the given averaging time, whereas the minimum value is $k = 0$, indicating that there has been no preferred wind direction over the averaging time. If we however vary the angular deviation of the wind between 0 and 180 degrees (representing complete steadiness, and total symmetry of wind directions, respectively), we see that k decreases in a non-linear way as a function of the deviation. If we wish to map k so that the resulting deviation becomes linear, we can use the function S given by

$$S = \frac{2 \arcsin(k)}{\pi},$$

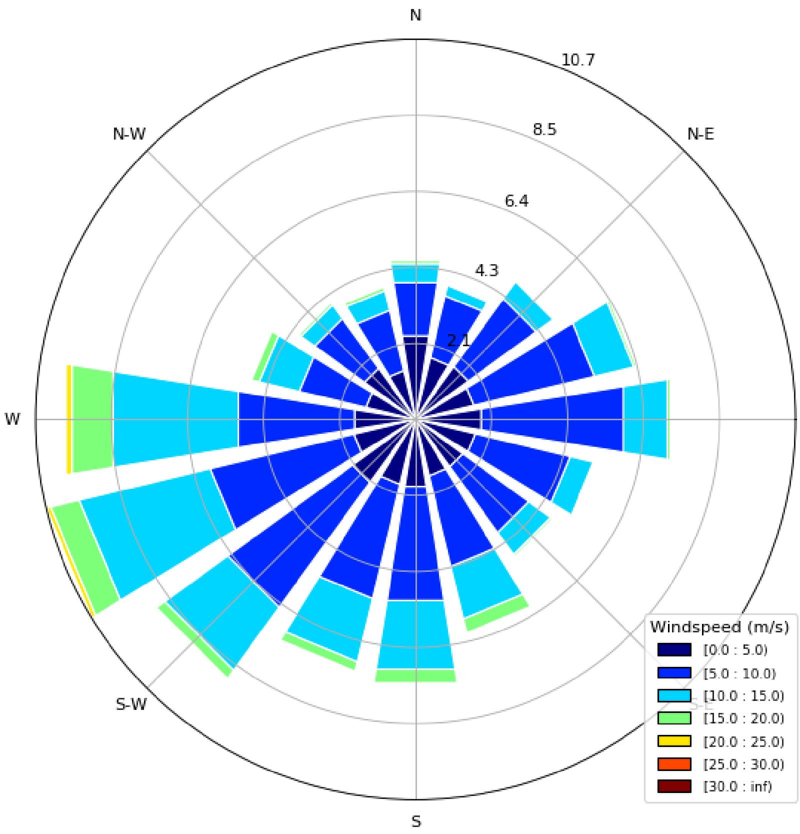

Figure 6: A wind rose depicting the frequency of wind coming from different directions at different speeds. The bars on the graph represent directions of wind, with the coloured regions indicating different wind speeds. The size of each coloured section and each bar indicates the percentage frequency of how often that combination of wind direction and wind speed occurs.

which like k will have a range of 0 to 1, and since arcsine is monotonically increasing, 0 once again represents complete symmetry of wind direction, and 1 represents perfect steadiness. Since S is linear in the angular deviation, a depiction of which can be seen in figure 7, a change of 0.1 in S corresponds to a change in the angular deviation of 18 degrees.

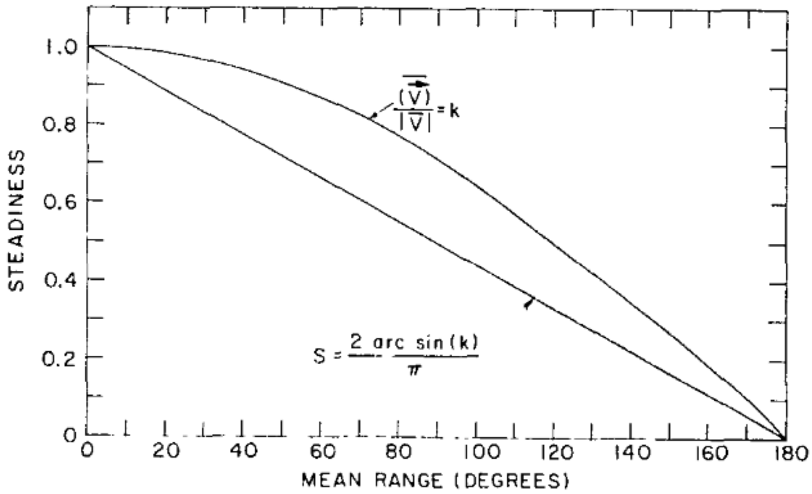

Figure 7: A graph from (Singer 1967) depicting the steadiness values S and k as a function of angular deviation in degrees. We see that k is a curved line, whereas S is a straight line.

In our case, we computed running means in order to calculate values of S for the following time intervals: 2, 4, 12, 24, 48, 96, 192, 348 and 720 hours. For each averaging period examined, we will have a value of S for each running mean, which will give us a distribution of S values for each of the nine periods. Before calculation, we would expect that the wind is more steady for shorter time intervals, but that as the time interval increases, we would see lower values for S.

In figure 8 we can see the result of this analysis represented as histograms of S values at different averaging periods. We indeed see that distribution starts off being very skewed towards the higher value of $S = 1$ when we average over two hours, but that with each added time increment, the distribution moves towards the direction of $S = 0$. Each histogram is normalized so that the total area of the bars is equal to 1, and they are all set along the same x and y-axes. This makes it apparent that lower maximum frequencies are observed for larger time scales, which is due to the fact that the running mean for shorter time scales produces more observations. We also observe that the distribution becomes flatter for longer periods. The minimum variance in the distributions of S was $7.89 \cdot 10^{-3}$ for the period of 2 hours, and the maximum was $4.26 \cdot 10^{-2}$ for the period of 48 hours, after which we do see the distribution getting more clustered towards lower values of S.

Breaking down the result for each individual histogram, we see the following characteristics:
2 hours: The values for S are very high, with the majority being above 0.9. This indicates an angular deviation of 18 degrees or less in these cases.
4 hours: Similar in shape to the distribution seen for 2 hours, but with the modal value of S somewhat lower (0.965 rather than 0.985).
12, 24 and 48 hours: The shape remains similar to the previous two histograms, and the trend of lowering values of S continues.
96, 192, 348 and 720 hours: The variance lowers with each of these histograms after the highest variance distribution for 48 hours. The modal values of S shift to be lower for each histogram, and the distribution becomes more symmetrical.

Using these histograms for S values at different times, we can find the modal value of S, which is useful as a single value which can represent the general trend of what we could expect to occur at different time scales. We can furthermore plot the modal value of S for different hours, as can be observed in figure 9. The plot has a log scale on both the x and the y axis, and on this scale the relationship between S and the averaging period appears piecewise linear.

In the figure one can observe two linear least squares lines fitted to certain hourly ranges of the data – one line for the range of 2 to 24 hours with four points, and another in the range of 48 to 720 hours with five points. The fitted slopes are -0.043 for the first line (2-24 hours), and -0.298 for the second line (48-720 hours). Both slopes are negative, which fits well with our expectation that the angular deviation, and thus S, would be smaller for shorter averaging periods. We additionally see that the second line is steeper, indicating that the steadiness decreases more rapidly for these time scales. In fact, the linear relationship on the log axes indicates that S goes as t^m, where t is the time scale, and m is the slope of the fitted straight line, and so this decrease in steadiness is much more rapid than linear. This means that if we simulate a scenario where the wind is steady over the course of several days, this will be somewhat unrealistic.

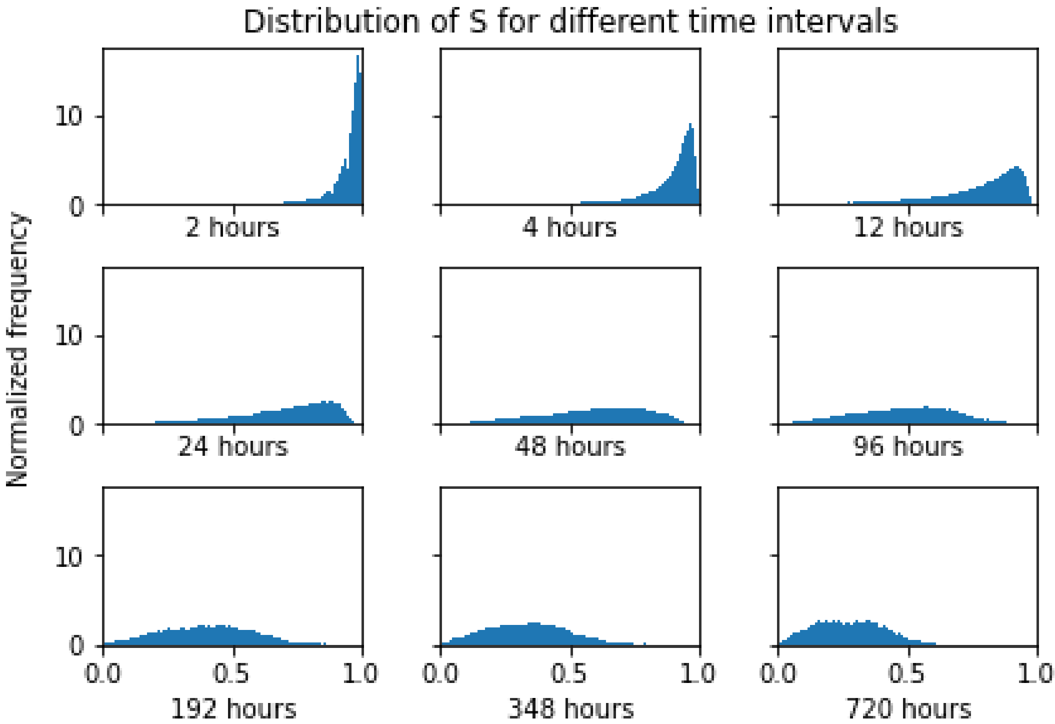

Figure 8: A histogram depicting the distribution of different values of S for each of the nine selected averaging periods. Each histogram is normalized so that the sum of the area of the bars equals to one.

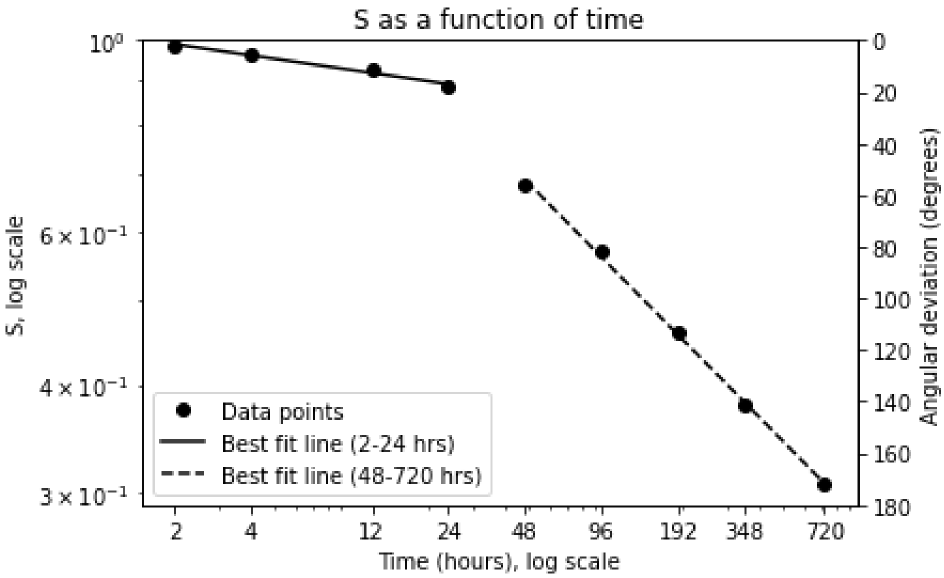

Figure 9: A graph of the logarithm of S as a function of the logarithm of the averaging period. There are two best fit straight lines fitted to different parts of the data: between 2 and 24 hours the line $-0.043x + 0.019$, and between 48 and 720 hours the line $-0.30x + 0.78$. The former line is indicated as a continuous black line, whereas the latter is indicated as a dashed line. An extra y-axis indicates the angular deviation which corresponds to each value of S.

13 Numerical simulations

Now that we are more knowledgeable about the properties of the wind in the Gullmar fjord, we can proceed to simulate the motion of tracer particles for different wind properties. This involves first obtaining ocean currents which result from different wind conditions, and then simulating particle drift using these currents. The former simulations, obtaining ocean currents from a wind profile, was done using A General Estuarine Transport Model (GETM). The latter, of simulating tracer particles using given wind currents, was done using OceanParcels.

In the following, we will begin by describing ocean models theoretically. First we will look at GETM, and then Lagrangian ocean modelling of tracer particles as used in OceanParcels. After describing the theory, we will describe the specific simulations used in greater detail. Finally, we will present and discuss results of these simulations.

13.1 General Estuarine Transport Model (GETM)

The first step in simulating tracer particles is to obtain ocean current fields from different wind profiles in the Gullmar Fjord, which we do using A General Estuarine Transport Model (GETM). In this section, we will describe GETM more closely.

The physical theory underlying GETM is the three-dimensional Reynolds averaged hydrostatic Navier-Stokes equations, making use of the Boussinesq approximation. The General Ocean Turbulence Model (GOTM) is used for vertical turbulence closure (Burchard, Bolding, and Ruiz-Villarreal 2004; Hofmeister, Burchard, and Beckers 2010). The model captures tides, wind-driven currents and estuarine circulation. It has already been successfully used to model several scenarios at various spatial scales in the North

Sea (Gräwe, Flöser, et al. 2016; Chegini et al. 2020) and the Baltic Sea (Gräwe, Holtermann, et al. 2015; Lange, Klingbeil, and Burchard 2020).

For our purposes, current fields were simulated through forcing with wind speed of 7 m s^{-1} in several of the different cardinal and intercardinal directions. This wind speed was selected as it was shown to be near the median when examining the wind profile of the region in the previous section. The resolution in the simulations was high, with a time step of 0.5 s run on 432 cores. The grid was spherical with a resolution of 60 m by 120 m in the longitudinal and lateral directions. The vertical dimension was split into 60 adaptive layers, which were tuned to minimize errors in calculation of pressure gradients and have extra resolution where vertical pressure gradients were larger, as in (Chegini et al. 2020; Gräwe, Holtermann, et al. 2015).

13.2 OceanParcels

OceanParcels is a set of Python classes and functions which make it easier to run Lagrangian ocean particle tracking simulations. The input to these simulations is current fields which can be user-defined, or inputted from another simulation like GETM. The particles in the OceanParcels simulations can represent passive particles such as plastics, which is the purpose of our simulations, or active agents such as fish. One of the main functions of OceanParcels is to provide an interpolation scheme to take current fields defined on a discrete time and spatial grid, so that values can be accessed between these times and locations. Once this is done, OceanParcels has some inbuilt advection and other functions which can use the interpolated values, as well as the option for the user to define their own functions. (Delandmeter and Sebille 2019)

13.3 Implementation details

We run a simulation in OceanParcels of the Gullmar Fjord, with a latitude of between 58.1039039190777 and 58.4789039202777 degrees North and a longitude of between 11.1894406455531 and 11.7029823138631 degrees East. This extent captures the Gullmar Fjord, as well as a small part of the North Sea. The simulation uses input files which contain a current field. These files are outputs from GETM which are obtained by running GETM with a single wind velocity. Although the currents are obtained from a three-dimensional run using GETM, we take only a surface cross-section and run the simulations with the assumption that particles float.

Each simulation was run for a time period of 168 hours (one week). The GETM simulations which produced the input current fields were run for 169 hours, which is why this time period was selected. Each GETM filed contains zonal velocity variable and a meridional velocity variable. These both have the same dimensions, of a new velocity value every hour (that is, 169 values), a value at 364 different latitudes, and a value at 494 different longitudes. The OceanParcels simulation was set to update every 20 seconds, in order to comfortably satisfy the CFL criteria with the maximum values of velocity which gave a maximum time step of around 90 seconds. Outputs from the OceanParcels simulation were saved every hour.

Particles were released in the simulation at two general locations. The first location was near Bornö Marine Research Station, and the second was near Lysekil, which is the largest city on the Gullmar Fjord. The research station is of interest to oceanographers at the University of Copenhagen, which is why it was selected. The location near Lysekil was selected because it is reasonable to assume that more densely inhabited areas are more likely to be significant sources of plastic pollution, and we have seen this confirmed in the literature data on the Baltic Sea. There were 100 particles released from each of these locations, which were set at random locations within a pre-defined region. For Lysekil this was between a latitude of 58.258628 and 58.263640 degrees North and between a longitude of 11.423181 and 11.436399 degrees East. For the Bornö Marine Research Station this was between 58.376735 and 58.379030 degrees North and 11.573965 and 11.576711 degrees East. The release locations were kept constant for each run, and can be seen in fig. 10.

The algorithm used to propagate the particles during the run was a simple Euler update scheme using the velocity fields provided in the GETM files and interpolation done using OceanParcels. Boundary conditions were set for two different cases: in the first case for particles which left the bounds of the simulation into the North Sea, and in the second case for particles colliding on land. For the case of particles leaving to the North Sea, they were kept in place on the boundary and not transported further. Particles that collided with land, on the other hand, were kept in place, under the assumption that these had bounced off the coast and returned to their position. The other alternative would be to remove the particles from the simulation by letting them beach on land. Which of these boundaries is more realistic depends heavily on the coastal features of the simulated region. The Gullmar Fjord has many cliffs, and we would expect for plastic objects not to beach in this case.

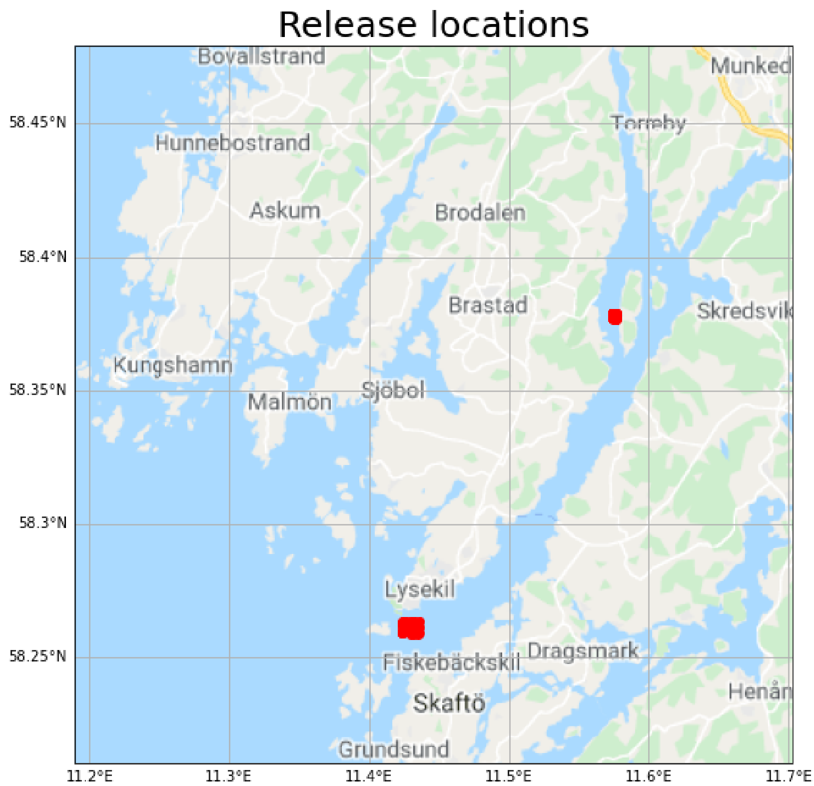

Figure 10: A map of the Gullmar Fjord with release locations of plastics in the OceanParcels simulation indicated as red dots.

14 Results

We ran simulations to test several different factors of plastic transport in the Gullmar Fjord. The first of these is wind direction. We will run the simulation for a few different wind directions, with special focus on the most common wind directions for 7 m s^{-1} wind, which are West and Southwest. The second is the effect of different transport mechanisms. As previously mentioned, the current fields which we use as an input to our simulations capture the effects of tides, wind and estuarine circulation. By performing several different simulations it is possible to isolate which of these is most relevant in different scenarios.

There are several factors to the results which will be of interest. One of these is where particles end up or accumulate in the simulation, which can be seen by examining a map of results. In connection with this it may be relevant to look at how quickly particles accumulate at a given location, or if they might drift further if the simulation was run for a longer period of time. Another factor which could be relevant is how far the particles travel under different conditions. It may also be of relevance to split up the particles by release location, as these may behave differently.

14.1 Wind directions

We have input current fields for several different wind directions. In the following, we will examine the trajectory patterns for these wind directions, focusing on the most frequently occurring in this area, which are wind from the Southwest, and from the West. The wind speed in each direction was 7 m s^{-1} in all cases, other than the instance with no wind.

14.1.1 No wind

We first examine the case where there is no wind present, to see what our baseline movement is. We recall that in the case of no wind, the transport mechanisms reflected by the current fields are tides and estuarine circulation. The particle locations at the end of the simulation run can be seen in figure 11.

We observe from this figure that particles released near Bornö stayed close to the island and spread out between Bornö and the western coast of the Gullmar Fjord. None of the particles released fom Bornö left the Fjord, and particles on average travelled 13.99 km with a standard deviation of 5.98 km. The median distance travelled was 16.65 km, with a minimum of 1.91 km and a maximum of 20.36 km.

On the other hand, particles released by Lysekil spread out outside of the Fjord. The mean distance traveled for these particles was 12.68 km, which seems odd as it is smaller than the average for particles released at Bornö, where it appears from glancing at figure 11 that particles spread out less. This is presumably because many particles got stranded at the coastline of the islands at the opening of the Fjord to the North Sea, or at other coasts. The median distance travelled was even smaller at 7.43 km, however the standard deviation was very large at 13.25 km. As the standard deviation is larger than the mean, and the distance travelled must be weakly positive, this indicates that we have some large outliers. This is confirmed by examining the maximum and minimum distances travelled from Lysekil, which are 51.32 km and 0.53 km, respectively.

In addition, we can see on the map that some particles seem to be arrayed at the western edge. These are particles which have exited the bounds of the simulation at some point during the run. Due to the way boundary conditions were implemented, these were kept in place and not updated once they had crossed this bound, which is why they are all located on the same vertical line. In all, there were 11 such particles, and they left the simulation after between 38 and 149 hours had elapsed. This could be skewing the distance metric somewhat, as the particles may have travelled further given a larger available simulation domain.

We could also observe the particles not just at the endpoint of a run, but also throughout to see the pattern there. In the interest of brevity, we examine a figure for each day in figure 12. From these figures we see that after 24 hours, the particles have moved significantly from both Lysekil and Bornö. From Lysekil, the spread is in the direction of the North Sea, whereas in Bornö it appears that the particles have moved farther apart in each direction. We note that some particles reach eastern coast of a small island near Lysekil, and remain there for the rest of the run. After 48 hours, the particles spread further out from both release locations. We observe that a single particle has reached the North Sea. Some particles reach the coast of Sweden by this point and stay there for the remainder of the simulation.

After the first 48 hours, particles from Bornö do not appear from the figure to move very far, although there does seem to be some back and forth motion. Particles released from Lysekil, however, moved farther and farther out with each day, with the exception of particles that gathered near a coast early on in the run and remained in place. In this figure we do not clearly see any effects from eddies or a back and forth motion; it appears that the particles spread in different directions throughout the run. On the other hand, this could easily be due to viewing snapshots only every 24 hours, rather than more frequently, and so we cannot form such definitive conclusions from this figure.

It is noteworthy, however, how particles seem to get stuck along coastlines. This is likely due to a combination of the specific velocity fields in this run and the boundary conditions in the program. We recall that the boundary conditions specify that when a particle would hit land in the next time update, it instead stays in place as though it had bounced off the coast to the exact same location. This boundary condition is likely too simple to capture reality, and was selected it was not possible to find information on what a more realistic scenario would look like exactly. Whether this meaningfully alters the simulation to be less accurate is hard or impossible to tell.

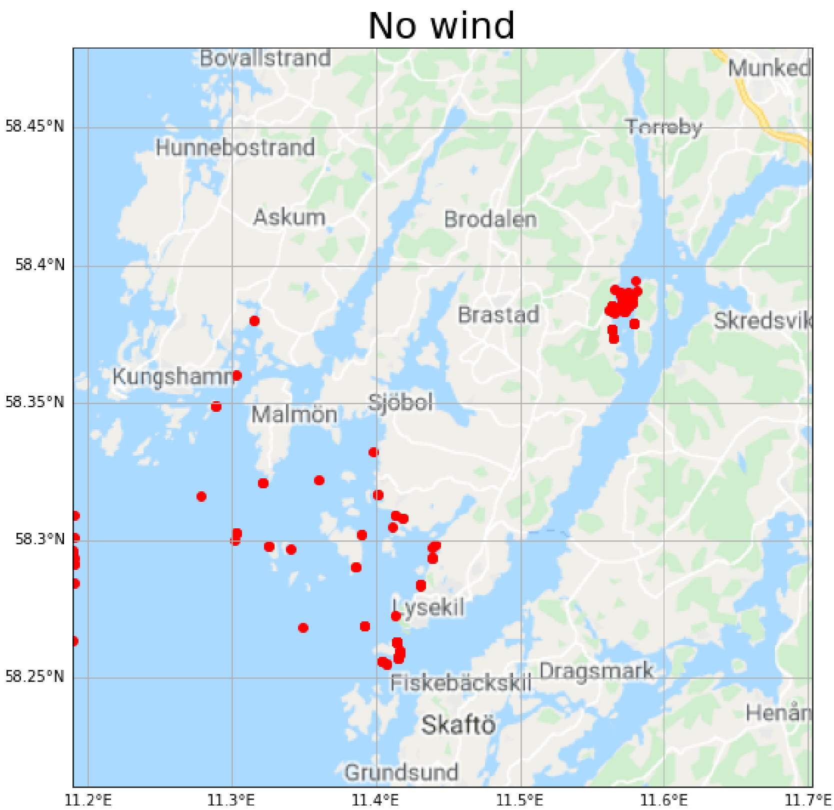

Figure 11: A map of the Gullmar Fjord with the endpoints of the simulation run with no wind for 168 hours indicated as red dots.

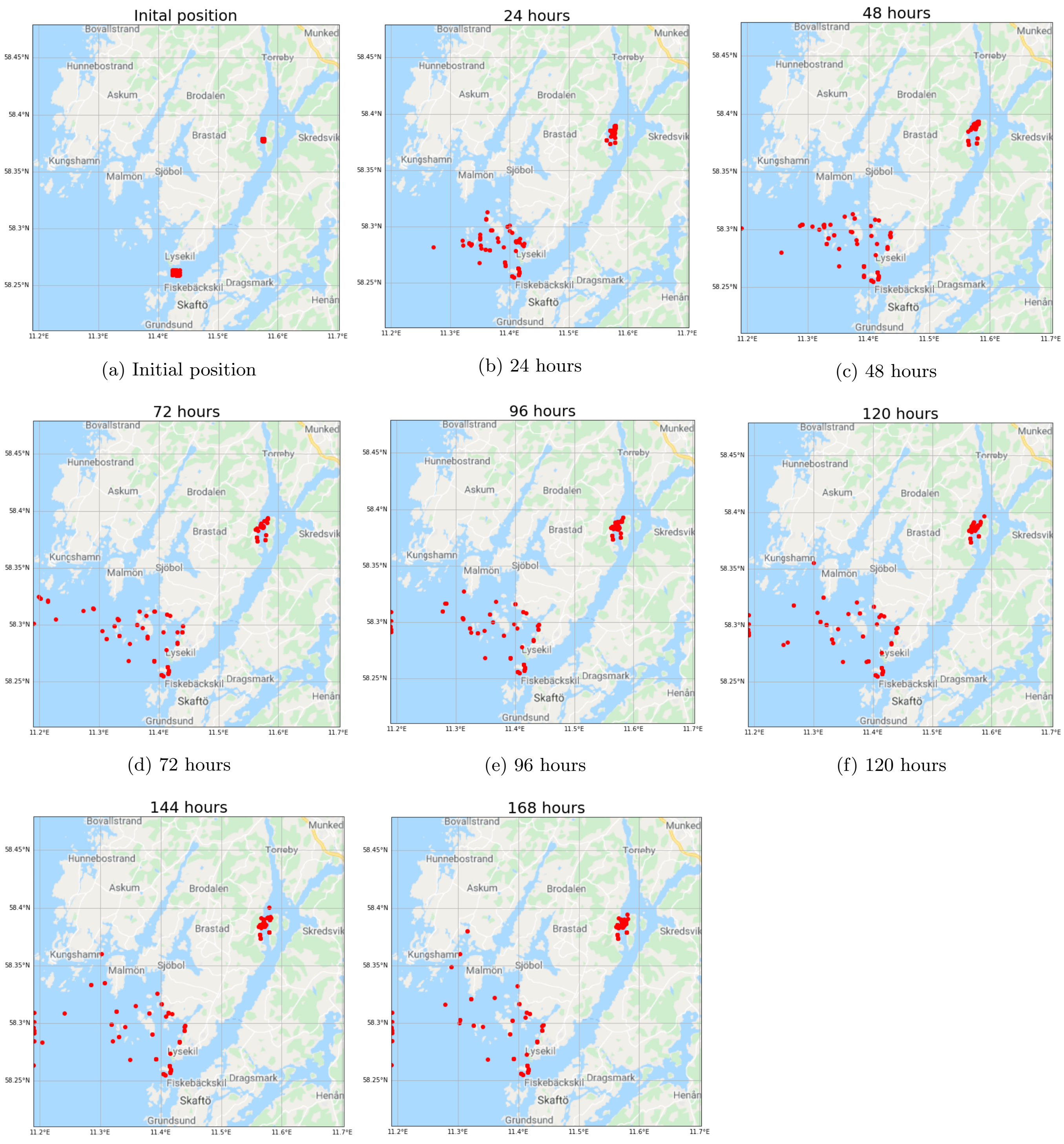

(a) Initial position

(b) 24 hours

(c) 48 hours

(d) 72 hours

(e) 96 hours

(f) 120 hours

(g) 144 hours

(h) 168 hours

Figure 12: The Gullmar Fjord with simulated plastic particles indicated in red, after different amounts of time had elapsed during the run with no wind.

14.1.2 Southwestern wind

As can be observed in figure 13, the particles accumulated in three general areas during this run. The first is near Bornö, the second is near Lysekil, and the third is along the coastline in the northeastern direction from Lysekil. When examining the corresponding data from the run, it becomes clear that the third accumulation zone is due to particles from Lysekil, which makes sense considering that the wind is blowing from the southwest to the northeast. On average, particles from Lysekil travel 6,356 m with a median of 7,104 m, presumably reflecting the fact that some particles remain near their starting point in Lysekil and do not travel very far, causing a skewed data set.

Particles released near Bornö did not travel very far, only 321 m on average. We suppose that this is due to the fact that the particles are released between Bornö on its western coast and another small island. Due to the way that boundary conditions are implemented in the simulation, it could be that particles bounce along the coast many times in the duration of the run rather than travelling far distances.

Other than knowing where particles accumulate, we are interested in how long it takes for them to accumulate in these locations. As the particles released near Bornö are fairly static, we will focus on those released from Lysekil. In fig. 14, we can observe the average distance travelled from Lysekil as a function of time. It appears that the particles travel around 6 km in the first day, and then travel only a small amount in the remaining six days of the simulation, on average. This makes it seem as though the accumulation zones seen in fig. 13 are indeed accumulation zones, and that the particles would not necessarily travel much farther if we had run a longer simulation.

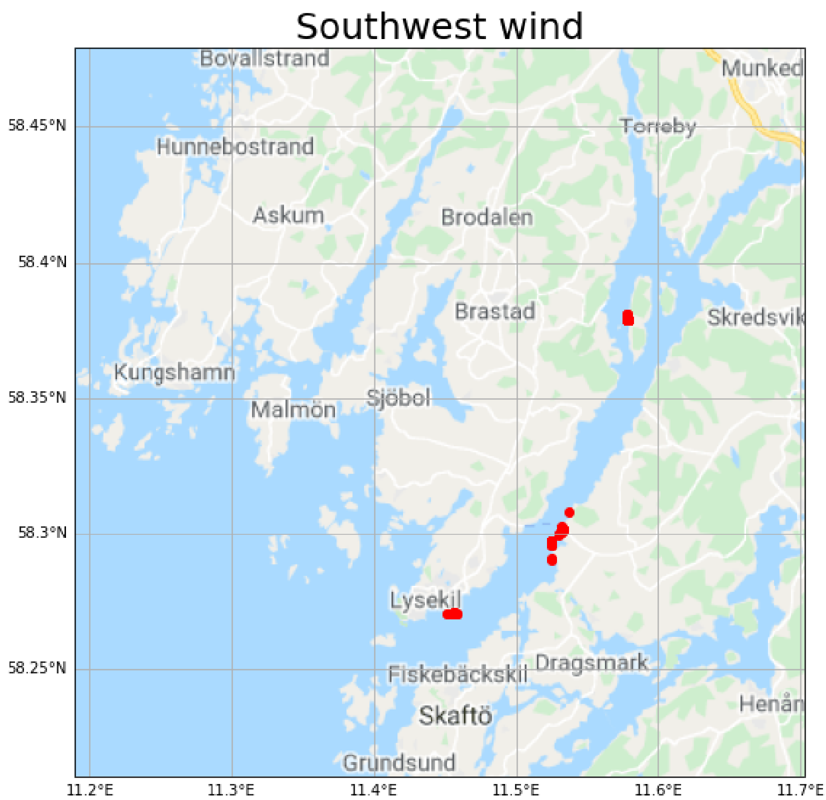

Figure 13: A map of the Gullmar Fjord with the endpoints of the simulation run with southwestern wind for 168 hours indicated as red dots.

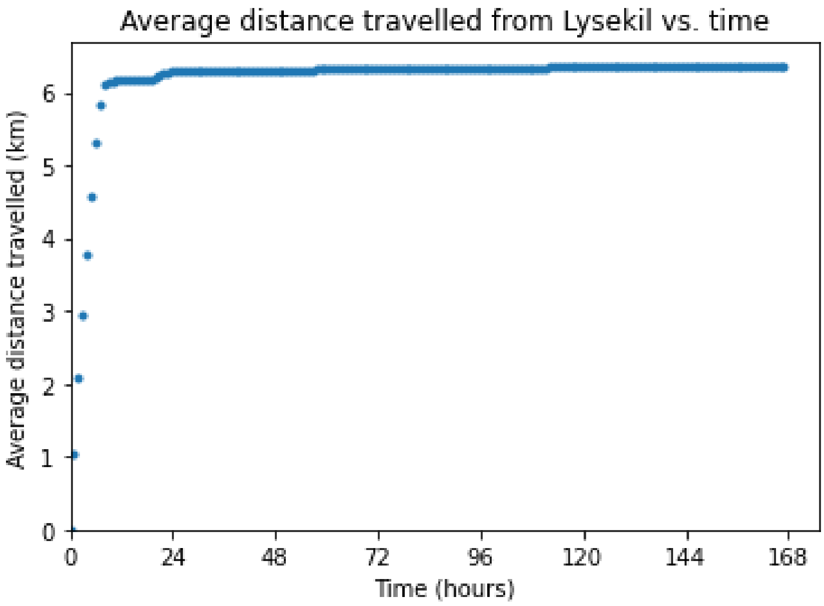

Figure 14: A graph depicting the average distance which particles released near Lysekil have travelled as a function of time for a southwestern wind.

14.1.3 Western wind

Western wind was also very common in the Gullmar Fjord, and so we examine this wind direction as well. The results with a southwestern wind direction indicate that particles from Bornö mostly stay in the same region of the Fjord, whereas those from Lysekil either circulate near Lysekil, or more commonly move to the opposite coast of the Fjord and accumulate there. Before running the simulation, we would expect the results with a western wind to be similar.

By examining figure 15, we see that this prediction appears to be almost accurate. The particles released at Bornö do indeed show a similar pattern to the run with a southwestern wind. The particles released at Lysekil, on the other hand, show a slightly different pattern – particles did end up accumulating at a coast, although not the same coastal region as before, and no particles remained near Lysekil.

Particles from Lysekil travelled around 2,813 m on average, whereas those from Bornö travelled only 247 m on average. Both of these values are smaller than for the simulation with southwestern wind. When looking at the distance data for this wind direction, we observe that particles travelled most of their distance in the first 12 hours of the simulation, and afterwards stayed in place for the most part. This indicates that the endpoints in figure 15 could represent accumulation zones of plastic.

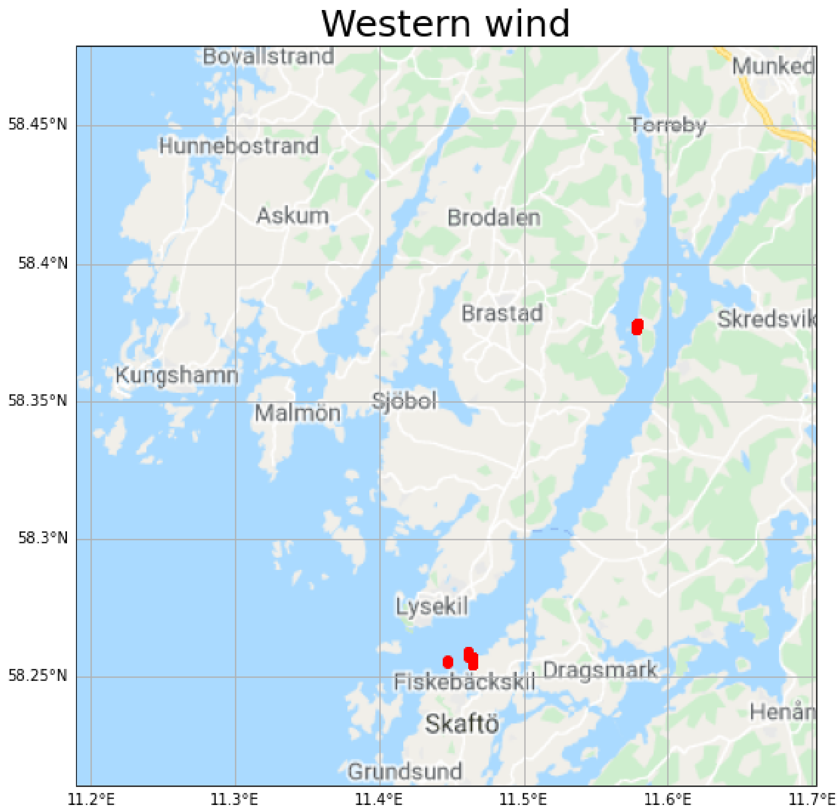

Figure 15: A map of the Gullmar Fjord with the final locations of particles after a run for 168 hours with a western wind indicated as red dots.

14.1.4 Eastern wind

Eastern wind also occurs somewhat frequently in the Gullmar Fjord, about 7% of the time, with an additional 6% in the ENE direction, as can be seen from figure 6. We therefore are interested in knowing what happens in this case.

Looking at figure 16 reveals that particles from Bornö remain near the release location. Presumably they become stuck at a small island directly west of Bornö. Some particles travel around this small island and arrive at the nearest western coast. These particles travel on average 454 m, most of which is covered within the first several hours of the run. The particles from Lysekil are similar, except they instead arrive at the coast of an island near Lysekil. These travel on average 1.49 km, and reach almost this distance within the first two hours of the simulation.

It appears that the trajectory of the particles tracks well with the wind direction.

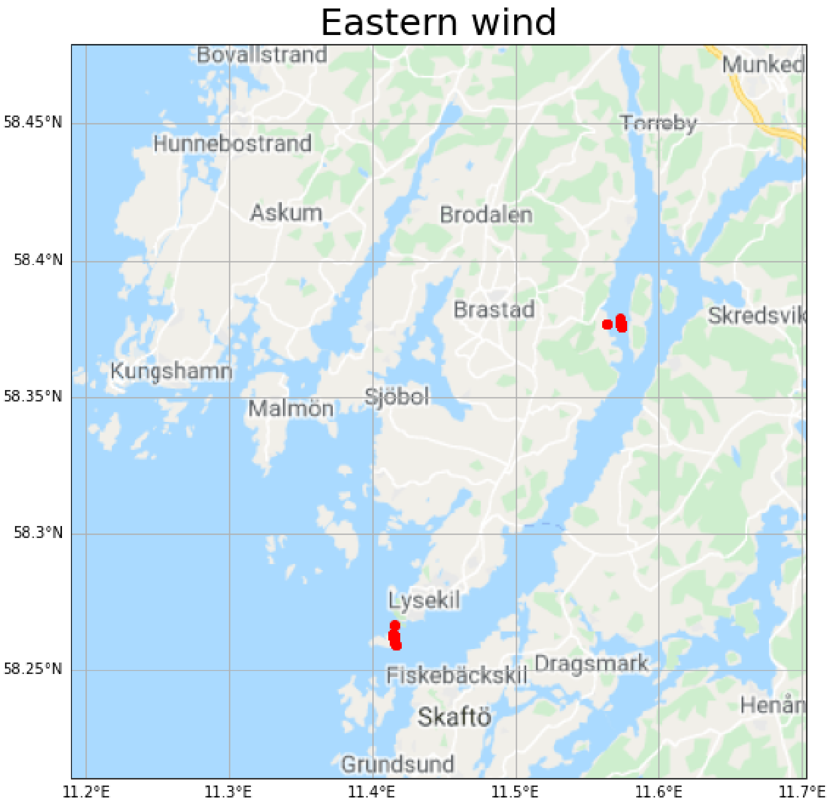

Figure 16: A map of the Gullmar Fjord with the final locations of particles after a run for 168 hours with an eastern wind indicated as red dots.

14.1.5 Northeast wind

As we can see from figure 6, the wind direction of Northeast does not occur very frequently, only about 5% of the time. In spite of this, it is relevant to see what happens in this case as a contrast to the case with southwestern wind, and to further examine the role of wind transport in this simulation.

We see from figure 17 that the particles released from Bornö stay near the island, although they move in the direction of the wind. Particles released from Lysekil leave the Fjord, and from examining the figure they appear to reach the coast of several islands near the opening of the Fjord. Particles from Bornö travel on average 0.43 km, while those from Lysekil on average travel 1.46 km. In both of these cases, particles tend to travel very rapidly for the first two hours or so of the simulation, reaching almost their full total distance travelled, and then remain very close to this for the rest of the simulation duration. This fits with the pattern of what we have seen from other simulations, and indicates that the particles have settled; we would not necessarily expect them to travel much farther if the simulation were longer.

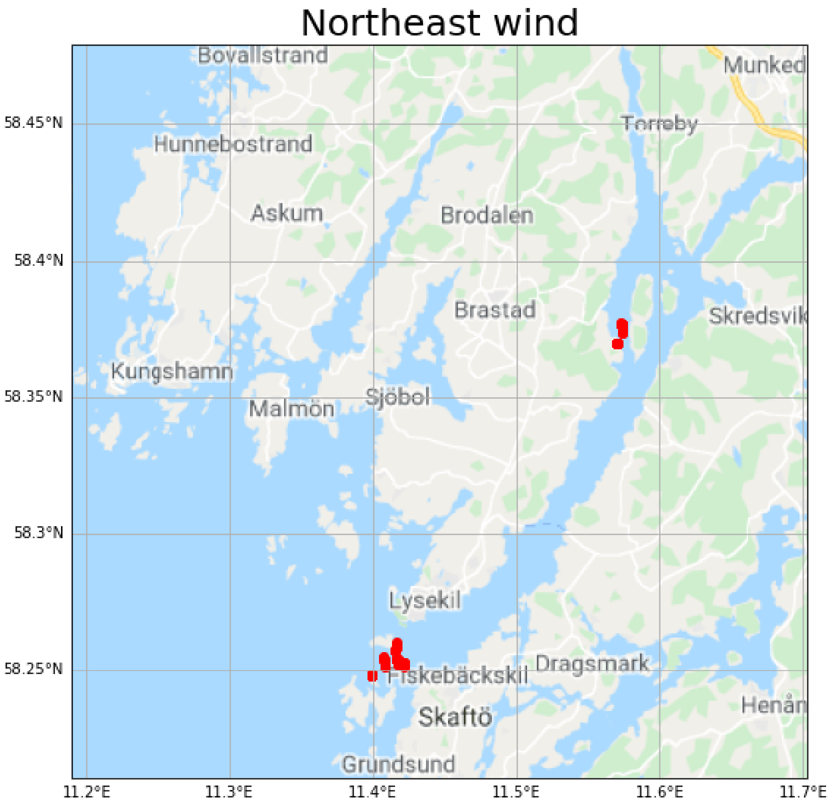

Figure 17: A map of the Gullmar Fjord with the final locations of particles after a run for 168 hours with a northeastern wind indicated as red dots.

14.2 Transport mechanisms

The relevant transport mechanisms for our simulations are transport due to wind, tides and estuarine transport. We can isolate these different effects through two means. The first way can isolate wind, as we have available a current field obtained using no wind forcing, which thus captures only the effect of tides and estuarine circulation. The second way involves taking a boxcar average of the current input fields over the time axis. This leaves us with fewer input fields than we started with, and if we select an averaging window which is greater than the tidal period (about 12 hours and 25 minutes for lunar tides) we can average over the tidal effects.

We make two different comparisons: in one, we have a simulation run with a Southwestern wind with and without a boxcar average, and in another we have a simulation run with no wind with and without a boxcar average. Both boxcar averages were chosen to have a window of 60 hours, as this is longer than several tidal periods and may significantly shorten the number of inputs to the simulation, shortening the run time. We also conducted an extra simulation using current fields in the case of no wind with a boxcar average of 30 hours. In each case we wish to know the relative effect of the different transport mechanisms.

The first comparison involves Southwestern wind, the results of which are depicted in maps in figure 18. Plastic particles are indicated in red after a week-long simulation (though the 60 hour boxcar average simulation involves a run of only 109 hours to capture the full week, due to removal of boundary points). From a cursory glance at both figures, it appears that the drift pattern in both cases is very similar. Particles released by Bornö appear to stay near the island in both cases. Particles released at Lysekil have a similar drift pattern in both cases, although those that accumulate by the coast appear slightly more spread out along the coastline in the case with no boxcar average.

When looking more closely at the average difference in the final locations of particles in the two scenarios, there is in fact a larger difference observed. The difference between the endpoints of the particles released in the two scenarios is 66 m on average for those particles released near Bornö, but 1,321 m on average for particles released near Lysekil. On the other hand, in the original simulation running over the full time interval, particles released near Bornö travelled only 321 metres on average, whereas particles released near Lysekil travelled 6,356 metres on average. In both cases the accuracy calculated using these numbers is just under 80%. The particles travelled a bit farther from Lysekil in the simulation with the boxcar average, 6,545 m. On the other hand they travelled a shorter distance from Bornö with the boxcar average, about 282 m.

We note that the average distance travelled in the two scenarios is closer than the average difference between final particle locations would suggest. What may be happening here is that the general pattern of final distribution is similar, captured in the average distance travelled being similar, even though where individual particles in the distribution end up can be very different in the two cases. An example of this is that one of the particles in the simulation with no boxcar average remained near Lysekil for the whole run, while in the simulation with a boxcar average it ended up near the coastline in a different cluster of particles.

The accumulation zones did not change in the two runs, but which particles ended up in which zone was altered. Unfortunately, due to the way data is stored in OceanParcels, the exact number of particles which end up in each of the two locations would need to be checked manually. We instead use another method to compare the two runs, by examining the "center of mass" of the final configuration at the end of the run, i.e. the average location of particles at their final location. We focus on the particles released from Lysekil, as it seems somewhat clear that in both runs the particles which started near Bornö did not move very much, and they both had only one identical accumulation zone. The particles released near Lysekil at the end of the original run were on average at a latitude of 58.29398 and a longitude of 11.51507, whereas in the run where the boxcar average was taken, the end location had an average latitude of 58.294212 and an average longitude of 11.520564. These locations can be observed on a map in figure 19. The distance between the two points is 322 m, which is consistent with the difference in average distance travelled over the two runs, however it once again does not shed much light onto the relative sizes of the two accumulation zones when particles are released from Lysekil.

We repeated the run with a 60 hour boxcar average in the case of no wind. In figure 20 we see a side-by-side comparison of the run with no wind with and without the boxcar average. The difference in the end locations of particles in both runs appears quite dramatic. The main property of note is that in the run with the boxcar average, particles spread out less and clustered more. This is apparent both for the particles released near Bornö, which do not appear to have spread out at all from glancing at the map, and for the particles released near Lysekil, which appear to cluster at fewer locations.

This difference seen in the maps is borne out in the statistics for the two cases. The average difference between the particles released in both locations was 1.05 km for particles from Bornö, and 6.42 km for particles from Lysekil. In the original simulation, carried on without the boxcar average, particles from Bornö travelled on average 13.99 km, while those from Lysekil travelled 12.68 km on average. Especially in the case of the release from Lysekil, the 6.42 km error represents a significant deviation between the run with and without a boxcar average.

We see that in the boxcar averaged run the accumulation zones appear more stable than in the original run. We also know from figure 12 that there were significant differences in particle location throughout the original run. The question then becomes whether the travel at different rates throughout the duration of both simulations. By examining figure 21, which contrasts the average distance travelled as a function of time between the two release locations and the release with and without a boxcar average, we can conclude that there is a large difference in how the particles travel. In the original simulation, the rate of distance travelled appears to be either linear or close to linear, and particles continue to travel non-trivial distances for the entire run. Presumably if we ran the simulation for longer than a week, the particles would travel even further.

This is not the case for the run with a boxcar average. We see from figure 21d that the particles released near Lysekil travel around 2 km on average, and that the travel flattens out after around three days. It seems possible that the particles have settled into final locations, although of course the simulation was run for only a brief period of one week and so we cannot know for sure either way. The pattern in figure 21b is more peculiar, since the particles appear to move in jumps and then the motion flattens for a long period of time. The particles also only move around a hundredth of the distance in the run with no boxcar average. This comparison seems to make it clear that there is a significant difference between having no wind with or without tidal effects, although of course there could also be a loss in accuracy due to the averaging itself. Either way, if we want to predict how particles move accurately, we should not rely on using a boxcar average with 60 or more hours in the case of no wind.

We could however wonder whether the case with a boxcar average of only 30 hours would give more accuracy. This is enough time that we have averaged over a tidal period, but involves a smaller error due to the averaging itself compared to when we use 60 hours. It is therefore relevant to see whether a run with a 30 hour boxcar average appears closer to the pattern of distribution with no averaging than the pattern with 60 hour averaging. The result of this simulation, and the figures without averaging and with a 60 hour average, can be seen in figure 20.

It appears when glancing at the figures that the results for the boxcar average with only 30 hours are slightly closer to those of the original simulation. In particular, we note that there was greater spreading around Bornö and that several plastic particles floated outwards rather than clustering when we compare with the 60 hour boxcar average results. On the other hand, there was still a great deal of clustering, and by eye it seems clear that these results differ substantially from those of the original run.

The average distance travelled in this run for particles released near Bornö was 277 m (in contrast with 13.99 in the original simulation and 1.05 km for the 60 hour average). For particles released near Lysekil it was 2.52 km on average (in contrast with 12.68 for the original simulation and 6.42 km with the 60 hour average). We see that both average distances are lower than in the simulations with a 60 hour boxcar average and the original run. This mismatch with the original run indicates that the 30 hour boxcar average is not useful either in the case with no wind, as it gives significantly different results. It also indicates that the tidal effects are significant when wind is not present.

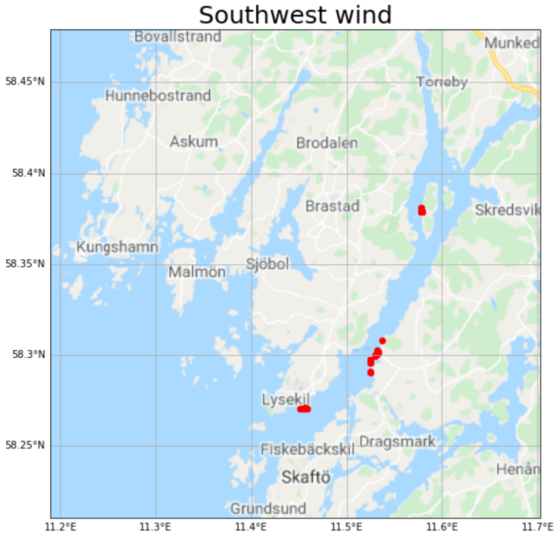

(a) Drift of plastic in the Gullmar Fjord for 168 hours with current fields forced by a Southwestern wind.

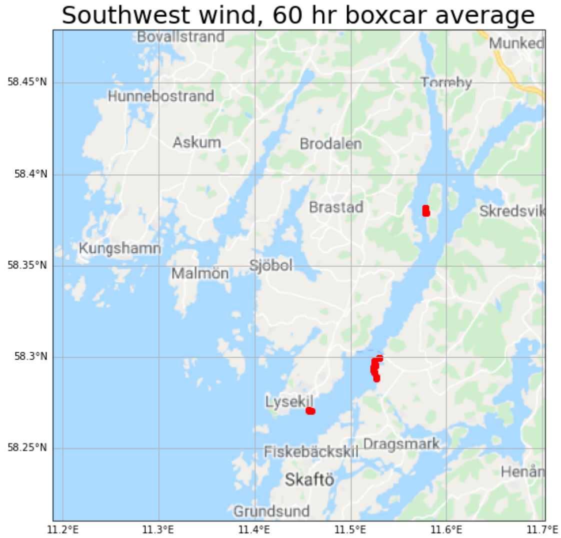

(b) Drift of plastic in the Gullmar Fjord for 109 hours due to a 60 hour boxcar average, with current fields forced by a Southwestern wind. (The time was shortened as a boxcar average results in fewer current field maps to sample from.)

Figure 18: Maps of the Gullmar Fjord with red dots indicating plastic particle locations after a simulation run with wind coming from the Southwest, with and without a 60 hour boxcar average taken over the current input fields.

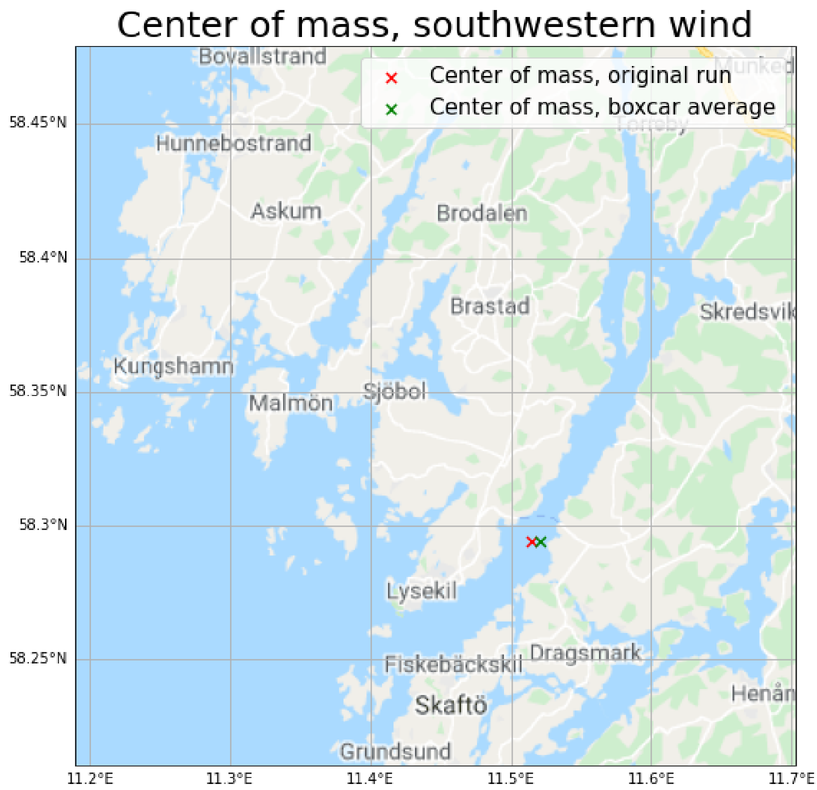

Figure 19: A graph the final average location of the particles (denoted their "center of mass" for the two runs with southwestern wind direction, with and without a 60 hour boxcar average.

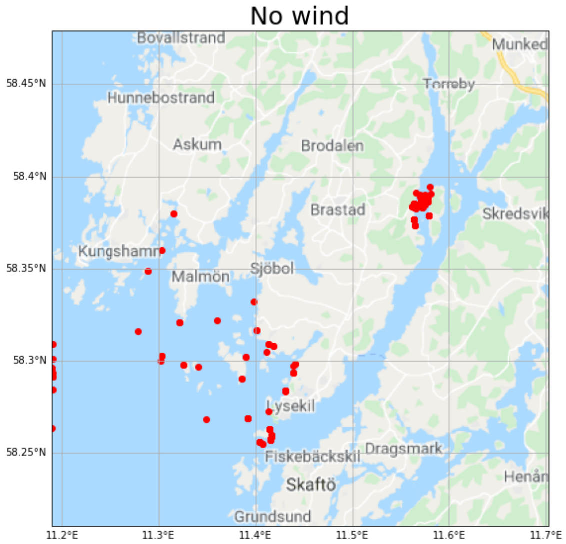

(a) Drift of plastic in the Gullmar Fjord for 168 hours with current fields with no wind.

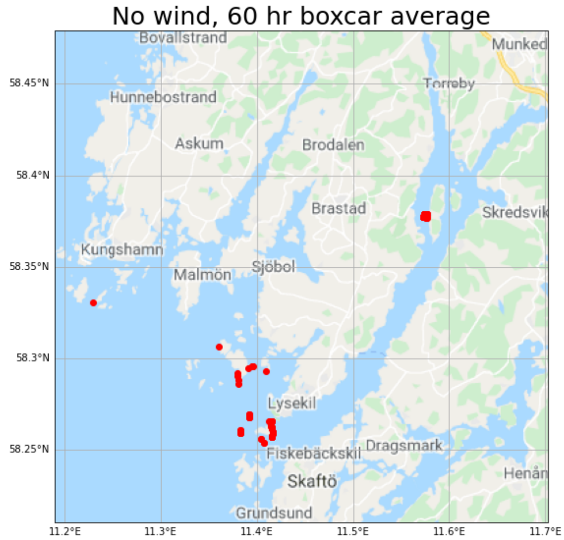

(b) Drift of plastic in the Gullmar Fjord for 109 hours due to a 60 hour boxcar average, with no wind forcing. (The time was shortened as a boxcar average results in fewer current field maps to sample from.)

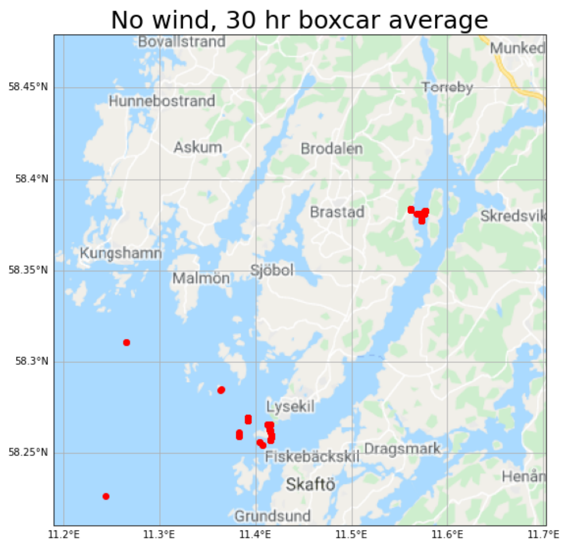

(c) Drift of plastic in the Gullmar Fjord for 139 hours due to a 30 hour boxcar average, with no wind forcing. (The time was shortened as a boxcar average results in fewer current field maps to sample from.)

Figure 20: Maps of the Gullmar Fjord with red dots indicating plastic particle locations after a simulation run with no wind, first with no wind, then with a 60 hour boxcar average and a 30 hour boxcar average taken over the current input fields.

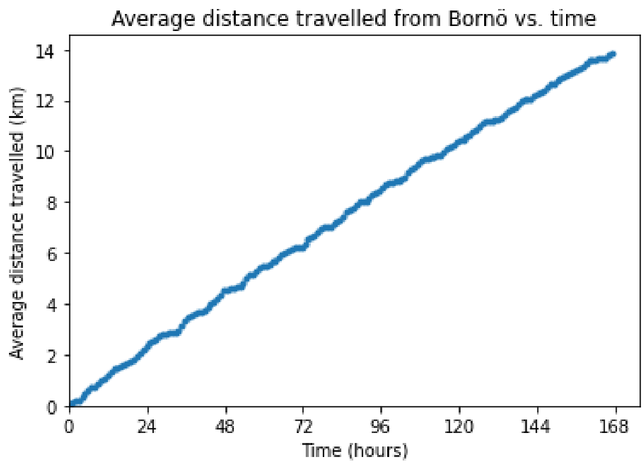

(a) Average distance travelled as a function of time for particles released from Bornö.

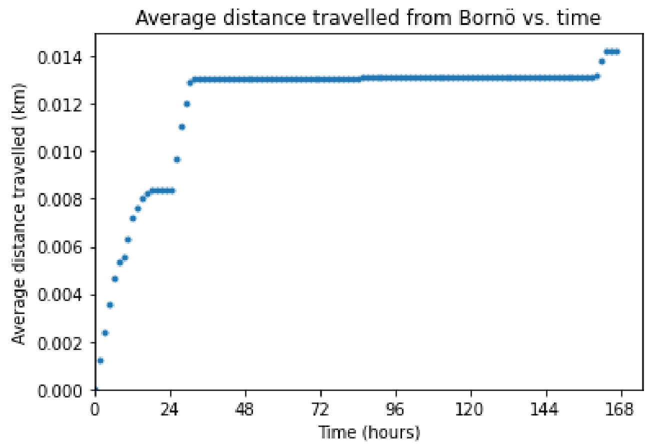

(b) Average distance travelled as a function of time for particles released from Bornö, with a boxcar average.

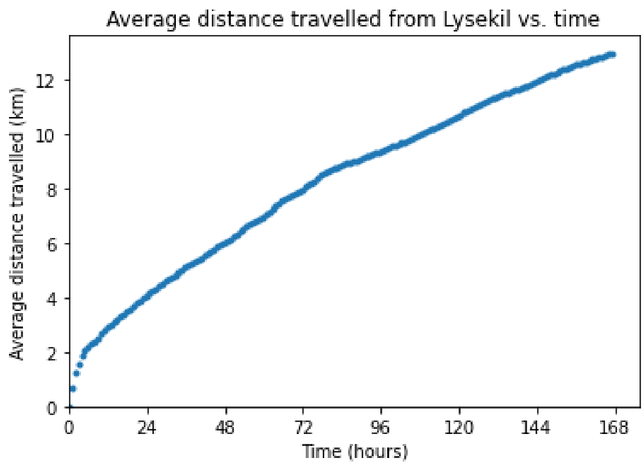

(c) Average distance travelled as a function of time for particles released from Lysekil.

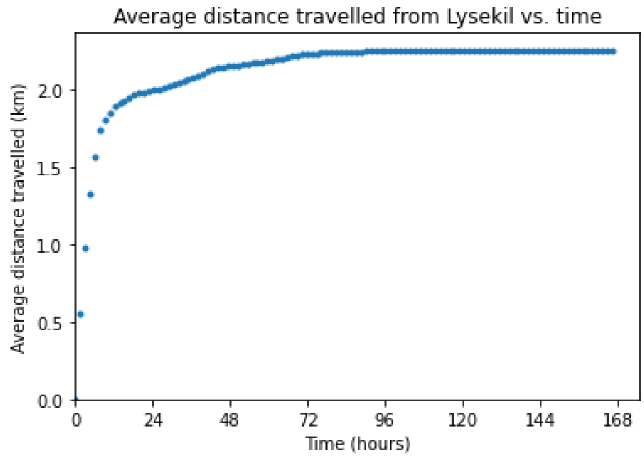

(d) Average distance travelled as a function of time for particles released from Lysekil, with a boxcar average.

Figure 21: Average distance travelled as a function of time for particles released from both Bornö and Lysekil, with and without a boxcar average.

14.3 General patterns

We wish now to summarize some of the findings from the simulations above. We first focus on conclusions from varying the wind direction, and then from the runs with a boxcar average.

It appears that the trajectory of particles in simulations with different wind directions is determined largely by the wind direction and the location of coasts. Particles tend to move in the wind direction until reaching a coast, which often happens within the first 24 hours, whereupon they often stay by the coast for the remainder of the run. This result of course depends on the implementation of boundary conditions, as we could also have erased the particles from the simulation, allowing them to beach – if this were done, practically all particles would be removed from the simulation at some point.

The contrast between the case with no wind and the results for each of the wind directions included is large. When there is no wind present, particles tend to drift and spread out, even leaving the simulation domain into the North Sea. They tend to travel at a similar rate throughout the course of the run. In contrast to this, when wind is applied, particles tend to accumulate near a coastal region quite close to other particles released from the same location, and they accumulate rapidly. This indicates that transport by wind is a significant effect compared to other transport mechanisms captured by the model.

We have also applied a boxcar average to the simulations run with both a southwestern wind and no wind. This resulted in significant differences from the original result in these two cases. In the case with southwestern wind, the difference was less pronounced, with the particle accumulation zones being the same with and without a boxcar average, even though which particles ended up in which accumulation zone differed, and the average final location of particles was different. If it is important to use a simulation to predict the exact final locations of particles under certain conditions, then it is preferable to use the full simulation results. If one only wishes to find general accumulation zones, though, then it seems that in this case the simulation with a boxcar average is sufficient. We note that the simulation with a boxcar average takes less time to run (in this case around 8 minutes and 30 seconds, as opposed to 12 minutes and 30 seconds for the full run), and this is preferable in some cases. In our case, the full run did not take very much time, and so sacrificing accuracy for a shorter run time would not be necessary.

In the run with no wind, taking the boxcar average did significantly alter the results. Rather than spread out and continue travelling throughout the run, the particles tended to accumulate, and in general moved less. The movement pattern as a function of time was especially strange for particles released from Bornö, with long periods of no motion and then staircase hops. None of the particles exited the simulation domain into the North Sea, in contrast with the original run. All of this indicates that the boxcar average resulted in a substantial loss of accuracy compared to the original result in the case of no wind.

Taking a boxcar average with the period which we have selected, which was 60 hours, involves averaging over more than a tidal period. This allows us to make some preliminary conclusions about the relative importance of the different transport mechanisms for plastics in the Fjord. From the simulations where we varied between wind directions and no wind, it seems that the most significant transport mechanism is through wind-driven currents. This is because the results seemed to depend heavily on the wind direction, where particles drifted in the same direction as the wind, and since the results differed in a significant way between the cases with and without wind. Following this, it seems that tidal effects are significant, especially in the case with no wind. This is because when we average over a tidal period, we see a large difference in the results. On the other hand, eddies and estuarine circulation seem to play a role as well. One major shortcoming of these conclusions is that we are unsure if the big difference is entirely because of averaging over tides, or if some portion of it is due to a loss of accuracy when we average.

Finally, we note that the presence of islands and other coastal features play a major role in where particles end up. This can be observed as the particles released from Bornö are initially between two islands, with a large coastal perimeter to collide with, and for much of the runs seem to move between the two islands. The particles from Lysekil sometimes accumulate by nearby islands as well. This is also indicated by the fact that in some simulations, e.g. for western or southwestern wind, it appears that particles move in the wind direction until colliding with a coast. It therefore seems that the results might be somewhat different if we conducted the simulations in a more open area of the sea.

14.4 Shortcomings

The simulations which we have run for the Gullmar Fjord give us some information on the likely relative importance of different transport mechanisms for plastics, particularly for partially enclosed bodies of water, and on how plastics accumulate depending on wind direction. On the other hand, they simulations also have a number of shortcomings which limit there inferential use.

One of the biggest of these shortcomings is that only surface currents were considered, rather than a full three dimensional map. This was done in order to save computational time, and it also simplifies the implementation of boundary conditions considerably. It does, however, mean that the simulation only applies to floating plastic litter, and especially to larger plastic items, which are less likely to sink due to biofouling. In papers that detail the abundance of microplastic particles in the Baltic Sea water column such as Bagaev, Khatmullina, and Chubarenko 2018, they find that the highest abundance of microplastics is near the sea surface, followed by near the sea floor, and that the abundance in the rest of the water column appears lower. This provides some evidence that merely considering a two dimensional model of plastic accumulation is insufficient in the case of microplastics. Sedimentation may be a significant sink for microplastic particles, and the simulation as conducted here cannot be used to test how significant it is under different parameters.

In a more complete three dimensional description of the Fjord, biofouling could be implemented by considering the rate of algae growth, which depends on sunlight and temperature (S. Singh and P. Singh 2015), and estimating other variables such as typical plastic surface area and volume. We could then use algorithms such as in the paper (Kooi et al. 2017) to simulate the sinking behaviour of microplastics. If one were to implement this, it would be relevant to consider seasonal variations, as temperature and sunlight are seasonally dependent variables.

Another shortcoming of our simulations is that the wind in the Gullmar Fjord does not tend to be steady over the course of entire weeks, as we saw in section 12 on wind velocity statistics. In some cases, such as for southwestern wind, it did appear (e.g. in figure 14) that particles accumulated relatively fast, within a day of simulation time. In other cases, the particles continued to travel significant distances throughout the simulation time, and many did not appear to accumulate. This is useful to know, however it may be inaccurate to real life as the wind conditions likely would have varied more.

The problem is difficult to fix, because as we allow the wind to vary in direction and speed throughout the run, we get a large number of possible combinations of different wind velocities, with difficulty in discerning which should be preferred over others. One way to proceed could be to find a week with a meteorological profile near the average for the area, and select the wind conditions for that week. This has the drawback of being more difficult to generalize than the simulations done in this report, where we selected a single wind velocity for each run.

We should also consider if the results from our simulations can generalize to other regions. The Gullmar Fjord is small, enclosed, and has low population density. We would not expect there to be a large amount of plastic pollution coming from the Gullmar Fjord. Without repeating simulations in other areas, for example where there are fewer islands or a larger distance between coasts, it is difficult to tell whether the results found in these simulations are replicable. Presumably some of the fundamental behaviour, such as particles moving in the general wind direction, is more general, but there could for example be large-scale behaviour that we do not see when running simulations for the Gullmar Fjord.

Finally, the simulations which we have run are not easily verifiable. We have limited data for plastic pollution in the Baltic Sea, and this data mostly covers microplastic collection, which as we have just discussed is less relevant to the simulation in the Gullmar Fjord. The data for the Gullmar Fjord itself is even more limited. Even with more data, though, the experiments and the simulation do not show the same thing. The experiments attempt to determine abundance of plastic at a specific place and time, and of course this is in part a result of realistic meteorological conditions. On the other hand, the simulation predicts transport pathways and endpoints, but under less realistic conditions and after a week of release. When data is collected in an experiment, there is no reliable way to know exactly when particles had been released and trace them back to a source. The simulations can therefore provide some information on what might realistically happen, but it is difficult to know how much stock we should put in the results.

All of these shortcomings mean that we should be careful when generalizing the simulation results. The dynamics could be significantly different using a three dimensional model with biofouling, using a more realistic wind profile, or in a different region.

14.5 Ideas for further work

There are several things which we could do to work more with this simulation set-up in OceanParcels, from which we could learn more about the possible transport of plastics in the Gullmar Fjord.

Firstly, we could do simulations with different wind strengths. We have conducted all of the above simulations for a wind strength of 7 m s^{-1}, which is close to the mean and median in the region (7.35 and 6.69 m s^{-1}, respectively). We could add extra simulations with the 90th percentile wind speed of 13.3 m s^{-1}, for example. From examining the results obtained with 7 m s^{-1} wind, we would predict that the results for stronger wind might be that particles arrive at a coast more rapidly. We could also use a weaker wind, to see whether particles with for example a western wind would still beach in the same location, or if there might be larger observed effects due to tides and estuarine circulation.

Another option would be to take different boxcar averaging periods, especially for the simulation with no wind as it is there we see the largest difference. We wished to take averaging periods which were larger than the tidal period, which of course is satisfied by taking ones of 60 and 30 hours. On the other hand, though, we would expect that taking a boxcar average for any period would make results less accurate, and though some of the results do appear due to an absence of tidal effects for the simulation with no wind, we also cannot exclude that the loss of accuracy could be due to the averaging itself. It would thus be relevant to repeat the simulations with a boxcar average for more averaging periods, and try to ascertain what the loss of accuracy is as a function of the averaging period.

As we have discussed above in the section on shortcomings of the simulations, the Gullmar Fjord is not necessarily a good place to conduct a representative simulation of how plastic travels in the sea. For one, it is a narrow body of water, with a short distance to the nearest coast on average relative to for example the Baltic Sea. It is also not densely populated, and therefore unlikely to be a major source of plastic contamination. A next step could be to conduct further simulations over different bodies of water.

One more thing which we could do is examine the wind profiles that are typical for different seasons. Here we have used a wind velocity which is near the annual mean in the region, however the seasonal mean could be different. Additionally, we know that the Gullmar Fjord freezes in January and February (Länsstyrelsen Västra Götaland n.d.), and we recall from section 5 that formation and melting of ice can alter tracer transport pathways. We could attempt to simulate this process as well, and examine its effects on plastic particles released in different locations of the Fjord.

Part V

Conclusions

At the outset of the project, we had two aims. Now in the conclusion, we will recall what these aims were, and discuss whether we succeeded in fulfilling them with the methods used.

The first aim was to determine the patterns of concentration of microplastic particles in the Baltic Sea in space and time. The methodology in this part was an analysis of the existing literature on this topic, wherein samples were collected through various means, and particles were counted for a given sample volume.

Overall, we learned several things from this analysis. The first is that different sampling methods of marine microplastics produce meaningfully different results. The biggest difference was seen when different mesh sizes were used in collection, where the finer mesh sizes were associated with the collection of far more particles than a coarser mesh. This could give some indication that most microplastics in the Baltic Sea are of a size scale smaller than the coarsest meshes of 300 μm. We also saw meaningful differences between samples taken with a manta trawl and using bulk sampling techniques, though there were not clear differences between manta trawl samples and water pump samples. When samples were taken with a similar technique and mesh size, results tended to be of comparable magnitudes. This all indicates that we should have reservations when comparing studies using different methodologies.

Another conclusion from the literature was that there seemed to be high concentrations at or near the surface of the sea, followed by at the sea floor, and that there were low concentrations found in intermediate layers. This conclusion is mostly based on a single study (Bagaev, Khatmullina, and Chubarenko 2018) which involved 95 samples. The study was not all controlled, with samples taken at a variety of times, locations and depths, however the results even as they are seem strong.

Finally, we could not form any definitive conclusions on the horizontal distribution of plastics, or the change in abundance over time. This is due to a number of factors: different methodologies which are not directly comparable, too few samples, and lack of controls in experiments. This is unfortunate, as when so many studies are conducted in nonuniform ways which cannot be compared, the total sum of knowledge does not improve by very much. This means that we did not quite meet our aim of forming a profile of the Baltic Sea microplastic distribution, and more data is needed in this area.

The second aim of the project was to learn more about the transport mechanisms of plastics. To limit the scope, we focused on the Gullmar Fjord, conducting simulations of particle releases from Bornö and Lysekil which ran over a week. The simulations were run in OceanParcels using current fields from another simulation in GETM, with a wind speed of 7 m s^{-1} with a number of different directions, and a simulation with no wind. We also conducted simulations with southwestern and no wind with a boxcar average over the current fields, which reduced the number of current fields as a function of time.

From comparing the simulation with no wind with those of different wind directions, we saw that wind played a significant role in transport. When no wind was applied, particles appeared to spread more, whereas when wind was applied at 7 m s^{-1}, particles appeared to travel in the wind direction until they reached a coastline where they accumulated.

We also ran a couple of simulations with a boxcar average of 60 hours. The purpose of this was to average over several tidal periods and see if transport patterns were altered with no tides. The first of these simulations involved wind blowing from the southwest. In this simulation, we did see a loss of accuracy when considering the boxcar averaged current fields as compared to the original ones. The accumulation zones remained the same, however, and so it seemed that wind transport was a more significant factor than tides.

After examining the effects of this averaging with a southwestern wind, we examined the effects with no wind. Here there was a large loss of accuracy, and rather than spreading out more and more, particles tended to cluster and accumulate near coastlines. Particles released from Bornö barely appeared to spread at all. From this it seems as though tides have an impact by spreading particles and acting in a nonuniform manner on particles in different locations. After observing the large differences between the simulation with no wind before and after applying the boxcar average, we also attempted another simulation with a shorter averaging period of 30 hours, in case the loss of accuracy with the previous boxcar average was mainly due to the averaging itself rather than any tidal effects. After examining the results of this simulation, we still see a large difference compared to when we used the original current fields. This makes it seem as though it is indeed due to the lack of tidal effects that we see a difference.

We have to some extent fulfilled the second aim of the project, as we have seen that when wind is present at a typical magnitude for the region, transport due to wind is the most significant mechanism of those captured in the GETM current fields. When no wind was present, tidal effects played a larger role in particle spreading. On the other hand, there are a number of shortcomings in our simulation which prevent us from taking these results at face value. We have conducted the simulation with a single wind direction for an entire week, which is unrealistic as the wind does not tend to be stable for these periods of time. We have also simulated only buoyant particles and not included any mechanisms for particles to sink in the water column by including only 2D current fields in OceanParcels.

There are many further avenues of study in the area of marine microplastics. More coordinated data collection is needed in the area, preferably using smaller mesh sizes of 10 μm. This would make an analysis of plastic concentrations in the Baltic Sea more meaningful. We could also conduct simulations in a variety of different ways, using different wind strengths, directions and boxcar averaging periods to obtain more robust results. Another important extension of this project would be to conduct a more detailed source mapping for plastics entering the Baltic Sea, which would provide a more realistic starting point for any simulations. We could also extend the work in this project by using algorithms for more transport mechanisms such as biofouling and ice formation and melting.

A Simulation code

In this appendix, we include some of the code used in order to run the simulation in OceanParcels. The main code is the following:

```
from parcels import *
import netCDF4 as nc
import numpy as np
from operator import attrgetter
from datetime import timedelta
import math
import pandas as pd
import random

file_input    = r'C:/documents/theseus/parcels_tutorials/gul50m.ZZ.nc4'
file_output   = 'C:/documents/theseus/parcels_tutorials/results.ZZ.nc'
release_locations = 'C:/documents/theseus/parcels_tutorials/release_points.txt'

run_time      = 168 #hours
time_step     = 20 #seconds
out_step      = 60*60  #seconds

#%% DEFINING PARTICLE CLASS AND UPDATE ALGORITHM

class PlasticParticle(JITParticle):
   active    = Variable('active'  , initial=1     , dtype=np.float32)
   inside    = Variable('inside'  , initial=1     , dtype=np.float32)

   dx        = Variable('dx',       initial=0.0   , dtype=np.float64)
   dy        = Variable('dy',       initial=0.0   , dtype=np.float64)

   u         = Variable('u',        initial=0.0   , dtype=np.float32)
   v         = Variable('v',        initial=0.0   , dtype=np.float32)

   prev_lon = Variable('prev_lon', dtype=np.float32, to_write=False,
                                   initial=attrgetter('lon'))  # the previous longitude
   prev_lat = Variable('prev_lat', dtype=np.float32, to_write=False,
                                   initial=attrgetter('lat'))  # the previous latitude.
   distance = Variable('distance', initial=0., dtype=np.float32)  # the distance travelled


def AdvectionEuler_2D(particle, fieldset, time):
    #NOTE: THIS FUNCTION CALCULATES POSITION UPDATE
    if particle.active == 1 and particle.inside == 1:

      (u1, v1) = fieldset.UV[time, particle.depth, particle.lat, particle.lon]

      particle.u  = u1
      particle.v  = v1

      particle.dx = u1 * particle.dt
      particle.dy = v1 * particle.dt

      particle.lon   += particle.dx
      particle.lat   += particle.dy
```

```


def UpdatePosition_2D(particle, fieldset, time):
    #NOTE: THIS FUNCTION UPDATES THE POSITION
    if particle.active == 1 and particle.inside == 1:

      tmp_x = particle.lon + particle.dx
      tmp_y = particle.lat + particle.dy
      #NOTE: THIS FOLLOWING CONDITION IS FOR WHEN THE PARTICLES MOVE OUT TO THE OCEAN
      if fieldset.Landmask[time,0,tmp_y,tmp_x] <= -1:
        particle.inside = 0
      #NOTE: AND THIS CONDITION IS SUPPOSED TO BE FOR WHEN THE PARTICLE GOES ON LAND
      elif fieldset.Landmask[time,0,tmp_y,tmp_x] >= 1:
        particle.inside = 0
        dx = -particle.dx
        dy = -particle.dy

      else:
        dx = particle.dx
        dy = particle.dy

      particle.lon   += dx
      particle.lat   += dy

def RecoveryKernel(particle, fieldset,time):
    #NOTE: DEFINES WHAT SHOULD HAPPEN IN CASE OF AN OUTOFBOUND ERROR
    dx = -particle.dx
    dy = -particle.dy

    particle.lon += dx
    particle.lat += dy

def TotalDistance(particle, fieldset, time):
    # Calculate the distance in latitudinal direction (using 1.11e2 kilometer per degree latitude)
    lat_dist = (particle.lat - particle.prev_lat) * 1.11e2
    # Calculate the distance in longitudinal direction, using cosine(latitude) - spherical earth
    lon_dist = (particle.lon - particle.prev_lon) * 1.11e2 * math.cos(particle.lat * math.pi / 180)
    # Calculate the total Euclidean distance travelled by the particle
    particle.distance += math.sqrt(math.pow(lon_dist, 2) + math.pow(lat_dist, 2))

    particle.prev_lon = particle.lon  # Set the stored values for next iteration.
    particle.prev_lat = particle.lat

def BrownianMotion2D(particle, fieldset, time):
    r = 1/3.
    m_to_degree = 1#9e-6 #NOTE: This constant should be 9e-6; have played with order of magnitude
    kh_meridional = fieldset.Kh_meridional[time, particle.depth, particle.lat, particle.lon]
    particle.lat += m_to_degree*random.uniform(-1., 1.) * math.sqrt(2*math.fabs(particle.dt)*kh_meridional/r)
    kh_zonal = fieldset.Kh_zonal[time,particle.depth, particle.lat, particle.lon]
```

```python
    particle.lon += m_to_degree*random.uniform(-1., 1.) * math.sqrt(2*math.fabs(particle.dt)*kh_zonal/r)


#%% DEFINING THE GRID

filenames  = {'U': file_input, 'V': file_input, 'Landmask': file_input, 'Kh_zonal': file_input, 'Kh_meridional':  file_input}
variables  = {'U': 'uu',       'V': 'vv',       'Landmask': 'landmask0',    'Kh_zonal':'Am_3d',     'Kh_meridional':'Am_3d'}

dimensions = {'lat': 'lat', 'lon': 'lon','time': 'time'}

with nc.Dataset(file_input,'r') as ncdata:
  lon = ncdata.variables['lon'][:]
  lat = ncdata.variables['lat'][:]

fieldset = FieldSet.from_netcdf(filenames, variables, dimensions, allow_time_extrapolation=True)
fieldset.add_constant('dres', 0.1)

#%% SETTING PARTICLE RELEASE LOCATIONS

release_loc = pd.read_csv(release_locations,sep=",")
#RELEASING 100 PARTICLES FROM EACH OF THE TWO LOCATIONS:
x=release_loc.iloc[:, 1]; y=release_loc.iloc[:,0]
pset = ParticleSet.from_list(fieldset=fieldset, pclass=PlasticParticle, lon=x, lat=y)

pset.show(field=fieldset.U)

#%% EXECUTING THE RUN

Kernel = pset.Kernel(AdvectionEuler_2D) + pset.Kernel(UpdatePosition_2D) + pset.Kernel(TotalDistance) #+ pset.Kernel(BrownianMotion2D)

pset.execute(Kernel, runtime=timedelta(hours=run_time), dt=timedelta(seconds=time_step),
             output_file = pset.ParticleFile(name=file_output, outputdt=timedelta(seconds=out_step)),
             recovery={ErrorCode.ErrorOutOfBounds: RecoveryKernel})

pset.show(field=fieldset.U)
```

This is however not the only code file which we have used. We also used a Python script to add a boxcar average to our files:

```python
import numpy as np
import netCDF4 as nc
from scipy.signal import fftconvolve

file_input  = r'C:/documents/theseus/parcels_tutorials/gul50m.ZZ.nc4'
file_output = nc.Dataset('C:/documents/theseus/parcels_tutorials/gul50m.ZZconv30.nc4', mode='w', format='NETCDF4')

with nc.Dataset(file_input,'r') as ncdata:
  U = ncdata.variables['uu'][:]
  V = ncdata.variables['vv'][:]

```

```
  lon = ncdata.variables['lon'][:]
  lat = ncdata.variables['lat'][:]

  time = ncdata.variables['time'][:]
  Am_3d = ncdata.variables['Am_3d'][:]

#defining the kernel
N = 30 #boxcar average length

#defining the kernel for the velocity array convolution
kern = np.ones((N, 1,1))
kern /= kern.sum()
#defining the kernel for the time convolution
kern_time = np.ones((N,))
kern_time /= kern_time.sum()

#doing a convolution of the necessary arrays
U_convolve = fftconvolve(U,kern,mode='valid')
V_convolve = fftconvolve(V,kern,mode='valid')
Am_3d_convolve = fftconvolve(Am_3d,kern,mode='valid')
time = fftconvolve(time,kern_time,mode='valid')

#adding the necessary masks to the arrays
U_mask = np.isfinite(U_convolve)
U_convolve = np.ma.masked_array(U_convolve, mask=~U_mask)

V_mask = np.isfinite(V_convolve)
V_convolve = np.ma.masked_array(V_convolve,mask=~V_mask)

Am_3d_mask = np.isfinite(Am_3d_convolve)
Am_3d_convolve = np.ma.masked_array(Am_3d_convolve,mask=~Am_3d_mask)

#creating the dimensions for the output file
time_var = file_output.createDimension('time', None)

lat_var = file_output.createDimension('lat', 364)

lon_var = file_output.createDimension('lon', 494)

#creating the variables for the output file
u_var = file_output.createVariable('uu', 'f4',('time', 'lat','lon'))
u_var[:] = U_convolve[:,:,:]

v_var = file_output.createVariable('vv', 'f4',('time', 'lat','lon'))
v_var[:] = V_convolve[:,:,:]

Am_3d_var = file_output.createVariable('Am_3d', 'f4',('time', 'lat','lon'))
Am_3d_var[:] = Am_3d_convolve[:,:,:]

time_variable = file_output.createVariable('time', 'f8',('time',))
time_variable[:] = time[:]

lat_variable = file_output.createVariable('lat', 'f8',('lat',))
lat_variable[:] = lat[:]

lon_variable = file_output.createVariable('lon', 'f8',('lon',))
```

```
lon_variable[:] = lon[:]
```

The final pre-processing script was created in order to add a mask on our velocity arrays where there were NaN values due to land. This additional mask is necessary in order to run the main script with no errors:

```
import netCDF4 as nc
import numpy as np
#import matplotlib.pyplot as plt

#%% Importing the relevant file

file_input = r'C:/documents/theseus/parcels_tutorials/gul50m.ZZconv30.nc4'
file_output = nc.Dataset('C:/documents/theseus/parcels_tutorials/gul50m.ZZconv30.nc4', '
    r+', format='NETCDF4')

with nc.Dataset(file_input,'r') as ncdata:

  U = ncdata.variables['uu'][:]
  V = ncdata.variables['vv'][:]

  lon = ncdata.variables['lon'][:]
  lat = ncdata.variables['lat'][:]

  time = ncdata.variables['time'][:]

#%% Extracting the land-sea mask

mask = np.ma.getmask(U)
landmask0 = mask.astype(int)
landmask0[landmask0 == 1] = 2

A=landmask0[:,:,0]
A[A==0] = -2

landmask0[:,:,0] = A

#%% Adding the Landmask as an extra variable to the file

mask_var = file_output.createVariable('landmask0', 'i4',('time', 'lat','lon'))
mask_var[:] = landmask0[:,:,:]
```

References

Faller, Alan J. (1964). “The angle of windrows in the ocean1”. In: *Tellus* 16.3, pp. 363–370.

Singer, I. A. (1967). “Steadiness of the Wind”. In: *Journal of Applied Meteorology* 6, pp. 1033–1038.

Maxey, Martin R. and James R. Riley (1982). “Equation of motion for a small rigid sphere in a nonuniform flow”. In: *The Physics of Fluids*.

Weber, Jan Erik (1983). “Attenuated wave-induced drift in a viscous rotating ocean”. In: *Journal of Fluid Mechanics* 137, pp. 115–129.

Ryan, P.G. and M.W. Fraser (1988). “The Use of Great Skua Pellets as Indicators of Plastic Pollution in Seabirds”. In: *Emu - Austral Ornithology* 88.1, pp. 16–19.

HELCOM (1992). *Convention on the Protection of the Marine Environment of the Baltic Sea Area, 1992 (Helsinki Convention).*

Ribic, Christine A., Trevor R. Dixon, and Ivan Vining (Apr. 1992). *Marine Debris Survey Manual.* NOAA.

Kubota, M. (May 1994). “A Mechanism for the Accumulation of Floating Marine Debris North of Hawaii”. In: *Journal of Physical Oceanography* 24.5, pp. 1059–1064.

Doering, J.C. and A.J. Bowen (1995). “Parametrization of orbital velocity asymmetries of shoaling and breaking waves using bispectral analysis”. In: *Coastal Engineering* 26.1, pp. 15–33.

The Open University (1999). “Chapter 2 - Tides”. In: *Waves, Tides and Shallow-Water Processes.* Ed. by The Open University. Open University Oceanography. Oxford: Butterworth-Heinemann, pp. 50–86. ISBN: 978-0-08-036372-1.

Acha, Eduardo M. et al. (2003). “The role of the Rio de la Plata bottom salinity front in accumulating debris”. In: *Marine Pollution Bulletin* 46.2, pp. 197–202.

Arneborg, Lars et al. (2004). “The rate of inflow and mixing during deep-water renewal in a sill fjord”. In: *Limnology and Oceanography* 49.3, pp. 768–777. DOI: https://doi.org/10.4319/lo.2004.49.3.0768.

Burchard, Hans, Karsten Bolding, and Manuel Ruiz-Villarreal (May 2004). “Three-dimensional modelling of estuarine turbidity maxima in a tidal estuary”. In: *Ocean Dynamics* 54, pp. 250–265. DOI: 10.1007/s10236-003-0073-4.

Maccready, Parker (Aug. 2004). “Toward a unified theory of tidally-averaged estuarine salinity structure”. In: *Estuaries and Coasts* 27, pp. 561–570. DOI: 10.1007/BF02907644.

Thorpe, S. A. (2005). *The Turbulent Ocean.* Cambridge University Press.

UNEP (2005). *Marine litter, an analytical overview.*

Norén, Fredrik (Jan. 2007). *Small plastic particles in Coastal Swedish waters.* Tech. rep. N-Research.

Eames, Ian (Dec. 2008). “Settling of Particles beneath Water Waves”. In: *Journal of Physical Oceanography* 38.12, pp. 2846–2853.

Martinez, Elodie, Keitapu Maamaatuaiahutapu, and Vincent Taillandier (June 2009). “Floating marine debris surface drift: Convergence and accumulation toward the South Pacific subtropical gyre”. In: *Marine pollution bulletin* 58, pp. 1347–55.

Tedesco, Letizia (July 2009). “Modelling coupled physical-biogeochemical processes in ice-covered oceans”. PhD thesis. University of Bologna.

Thompson, Richard C. et al. (July 2009). “Plastics, the environment and human health: current consensus and future trends”. In: *Philosophical transactions of the Royal Society of London. Series B, Biological sciences.*

Hanley, Kirsty E., Stephen E. Belcher, and Peter P. Sullivan (June 2010). “A Global Climatology of Wind–Wave Interaction”. In: *Journal of Physical Oceanography* 40.6, pp. 1263–1282.

Hofmeister, Richard, Hans Burchard, and Jean-Marie Beckers (Dec. 2010). “Non-uniform adaptive vertical grids for 3D numerical ocean models”. In: *Ocean Modelling - OCEAN MODEL* 33, pp. 70–86. DOI: 10.1016/j.ocemod.2009.12.003.

Breivik, Øyvind et al. (Apr. 2011). “Wind-induced drift of objects at sea: The leeway field method”. In: *Applied Ocean Research* 33.2, pp. 100–109.

Magnusson, Kerstin and Fredrik Norén (2011). *Mikroskopiskt skräp i havet - metodutveckling för miljöövervakning.* Tech. rep. N-Research.

Akan, Cigdem (Jan. 2012). “Surface Mass Transfer in Large Eddy Simulation (LES) of Langmuir Turbulence”. PhD thesis. University of Florida.

Mehlhart, Georg and Markus Blepp (Jan. 2012). *Study on Land-Sourced Litter (LSL) in the Marine Environment: Review of sources and literature.* Tech. rep. Öko-Institut e.V.

Skóra, Michał et al. (Sept. 2012). “Diet of the twaite shad Alosa fallax (Lacépède, 1803) (Clupeidae) in the Gulf of Gdansk, the Baltic Sea”. In: *Oceanological and Hydrobiological Studies* 41, pp. 24–32.

Programme, Interreg Central Baltic (2013). *Final Report of Baltic Marine Litter Project MARLIN.*

Santamaria, Francesco et al. (Apr. 2013). “Stokes drift for inertial particles transported by water waves”. In: *Europhysics Letters* 102, p. 14003.

Sørensen, Thomas Kirk et al. (2013). “Analyse af marint affald i sild og hvilling fra det nordlige Storebælt”. Released by DTU Aqua; sponsored by the Danish government.

Obbard, Rachel W. et al. (2014). “Global warming releases microplastic legacy frozen in Arctic Sea ice”. In: *Earth’s Future* 2.6, pp. 315–320.

Argyropoulos, C.D. and N.C. Markatos (2015). “Recent advances on the numerical modelling of turbulent flows”. In: *Applied Mathematical Modelling* 39.2, pp. 693–732. ISSN: 0307-904X. DOI: https://doi.org/10.1016/j.apm.2014.07.001.

Gräwe, Ulf, Peter Holtermann, et al. (June 2015). “Advantages of vertically adaptive coordinates in numerical models of stratified shelf seas”. In: *Ocean Modelling* 92. DOI: 10.1016/j.ocemod.2015.05.008.

Kukulka, T. and K. Brunner (2015). “Passive buoyant tracers in the ocean surface boundary layer: 1. Influence of equilibrium wind-waves on vertical distributions”. In: *Journal of Geophysical Research: Oceans* 120.5, pp. 3837–3858.

Norén, Katja, Kalle Haikonen, and Fredrik Norén (Dec. 2015). *Marint mikroskopiskt skräp längs Skånes kust.* Tech. rep. IVL Svenska Miljöinstitutet.

Reisser, J. et al. (2015). “The vertical distribution of buoyant plastics at sea: an observational study in the North Atlantic Gyre”. In: *Biogeosciences* 12.4, pp. 1249–1256.

Singh, Satendra and Priyanka Singh (Oct. 2015). “Effect of temperature and light on the growth of algae species: A review”. In: *Renewable and Sustainable Energy Reviews* 50.

Stolte, Andrea et al. (2015). “Microplastic concentrations in beach sediments along the German Baltic coast”. In: *Marine Pollution Bulletin* 99.1, pp. 216–229.

Strand, Jakob et al. (2015). *Marine Litter in Nordic Waters.* Tech. rep. Nordic co-operation.

Cheung, Pui Kwan, Lewis Ting On Cheung, and Lincoln Fok (2016). “Seasonal variation in the abundance of marine plastic debris in the estuary of a subtropical macro-scale drainage basin in South China”. In: *Science of The Total Environment* 562, pp. 658–665.

Cole, Matthew et al. (2016). “Microplastics Alter the Properties and Sinking Rates of Zooplankton Faecal Pellets”. In: *Environmental Science & Technology* 50.6, pp. 3239–3246.

FMI (2016). *Ice season in the Baltic Sea*. https://en.ilmatieteenlaitos.fi/ice-season-in-the-baltic-sea. [Published by Finnish Meteorological Institute, accessed November 2020].

Gräwe, Ulf, Götz Flöser, et al. (2016). "A numerical model for the entire Wadden Sea: Skill assessment and analysis of hydrodynamics". In: *Journal of Geophysical Research: Oceans* 121.7, pp. 5231–5251. DOI: https://doi.org/10.1002/2016JC011655.

Kowalski, Nicole, Aurelia M. Reichardt, and Joanna J. Waniek (Aug. 2016). "Sinking rates of microplastics and potential implications of their alteration by physical, biological, and chemical factors". In: *Marine Pollution Bulletin* 109.

Setala, Outi et al. (2016). "Distribution and abundance of surface water microlitter in the Baltic Sea: A comparison of two sampling methods". In: *Marine Pollution Bulletin* 110.1, pp. 177–183.

Bergmann, Melanie et al. (2017). "High Quantities of Microplastic in Arctic Deep-Sea Sediments from the HAUSGARTEN Observatory". In: *Environmental Science & Technology* 51.19, pp. 11000–11010.

Boucher, Julien and Damien Friot (2017). *Primary Microplastics in the Ocean: a Global Evaluation of Sources*. Tech. rep. International Union for Conservation of Nature (IUCN).

Bråte, Inger Lise N. et al. (2017). *Micro- and macro-plastics in marine species from Nordic wates*. Tech. rep. Nordic Council of Ministers.

Esiukova, E. (2017). "Plastic pollution on the Baltic beaches of Kaliningrad region, Russia." In: *Marine pollution bulletin* 114 2, pp. 1072–1080.

Gewert, Berit et al. (2017). "Abundance and composition of near surface microplastics and plastic debris in the Stockholm Archipelago, Baltic Sea". In: *Marine Pollution Bulletin* 120.1, pp. 292–302.

Hinata, Hirofumi et al. (2017). "An estimation of the average residence times and onshore-offshore diffusivities of beached microplastics based on the population decay of tagged meso- and macrolitter". In: *Marine Pollution Bulletin* 122.1, pp. 17–26.

Houghton, E.L. et al. (2017). "Chapter 1 - Basic Concepts and Definitions". In: *Aerodynamics for Engineering Students (Seventh Edition)*. Ed. by E.L. Houghton et al. Seventh Edition. Butterworth-Heinemann, pp. 1–86.

Iwasaki, Shinsuke et al. (2017). "Fate of microplastics and mesoplastics carried by surface currents and wind waves: A numerical model approach in the Sea of Japan". In: *Marine Pollution Bulletin* 121.1, pp. 85–96.

Kaiser, David, Nicole Kowalski, and Joanna Waniek (Sept. 2017). "Effects of biofouling on the sinking behavior of microplastics". In: *Environmental Research Letters* 12.

Khatmullina, Liliya and Igor Isachenko (Jan. 2017). "Settling velocity of microplastic particles of regular shapes". In: *Marine Pollution Bulletin* 114.

Kooi, Merel et al. (July 2017). "Ups and Downs in the Ocean: Effects of Biofouling on Vertical Transport of Microplastics". In: *Environmental Science and Technology*.

Lebreton, Laurent C. M. et al. (2017). "River plastic emissions to the world's oceans". In: *Nature Communications*.

Possner, Anna and Ken Caldeira (Oct. 2017). "Geophysical potential for wind energy over the open oceans". In: *Proceedings of the National Academy of Sciences of the United States of America*.

Vallis, Geoffrey K. (2017). *Atmospheric and Oceanic Fluid Dynamics: Fundamentals and Large-Scale Circulation*. 2nd ed. Cambridge University Press. DOI: 10.1017/9781107588417.

Zobkov, M and E Esiukova (2017). "Microplastics in Baltic bottom sediments: Quantification procedures and first results". In: *Marine Pollution Bulletin* 114.2, pp. 724–732.

Bagaev, Andrei, Liliya Khatmullina, and Irina Chubarenko (2018). "Anthropogenic microlitter in the Baltic Sea water column". In: *Marine Pollution Bulletin* 129.2, pp. 918–923.

Brach, Laurent et al. (2018). "Anticyclonic eddies increase accumulation of microplastic in the North Atlantic subtropical gyre". In: *Marine Pollution Bulletin* 126, pp. 191–196.

Bremer, T. S. van den and Ø. Breivik (2018). "Stokes drift". In: *Philosophical Transactions of the Royal Society A: Mathematical, Physical and Engineering Sciences* 376.2111.

DiBenedetto, Michelle H. and Nicholas T. Ouellette (2018). "Preferential orientation of spheroidal particles in wavy flow". In: *Journal of Fluid Mechanics* 856, pp. 850–869.

Ilyas, Muhammad et al. (Dec. 2018). "Plastic waste as a significant threat to environment – a systematic literature review". In: *Reviews on Environmental Health* 33.4, pp. 383–406.

Röhrs, J. et al. (2018). "The effect of vertical mixing on the horizontal drift of oil spills". In: *Ocean Science* 14.6, pp. 1581–1601.

Song, Young Kyoung et al. (2018). "Horizontal and Vertical Distribution of Microplastics in Korean Coastal Waters". In: *Environmental Science & Technology* 52.21, pp. 12188–12197.

Tamminga, Matthias, Elena Hengstmann, and Elke Kerstin Fischer (2018). "Microplastic analysis in the South Funen Archipelago, Baltic Sea, implementing manta trawling and bulk sampling". In: *Marine Pollution Bulletin* 128, pp. 601–608.

Turrell, W.R. (2018). "A simple model of wind-blown tidal strandlines: How marine litter is deposited on a mid-latitude, macro-tidal shelf sea beach". In: *Marine Pollution Bulletin* 137, pp. 315–330.

van Sebille, Erik, Stephen M. Griffies, et al. (2018). "Lagrangian ocean analysis: Fundamentals and practices". In: *Ocean Modelling* 121, pp. 49–75. ISSN: 1463-5003. DOI: https://doi.org/10.1016/j.ocemod.2017.11.008.

Zhao, Shiye et al. (2018). "Field-Based Evidence for Microplastic in Marine Aggregates and Mussels: Implications for Trophic Transfer". In: *Environmental Science & Technology* 52.19, pp. 11038–11048.

Atwood, Elizabeth C. et al. (2019). "Coastal accumulation of microplastic particles emitted from the Po River, Northern Italy: Comparing remote sensing and hydrodynamic modelling with in situ sample collections". In: *Marine Pollution Bulletin* 138, pp. 561–574.

de Haan, William P., Anna Sanchez-Vidal, and Miquel Canals (2019). "Floating microplastics and aggregate formation in the Western Mediterranean Sea". In: *Marine Pollution Bulletin* 140, pp. 523–535.

Delandmeter, P. and E. van Sebille (2019). "The Parcels v2.0 Lagrangian framework: new field interpolation schemes". In: *Geoscientific Model Development* 12.8, pp. 3571–3584. DOI: 10.5194/gmd-12-3571-2019.

GESAMP (2019). *Guidelines for the monitoring and assessment of plastic litter and microplastics in the ocean.* GESAMP.

Gove, Jamison M. et al. (2019). "Prey-size plastics are invading larval fish nurseries". In: *Proceedings of the National Academy of Sciences* 116.48, pp. 24143–24149.

Hsu, Wen-Yang et al. (2019). "Laboratory Observation of Turbulence and Wave Shear Stresses Under Large Scale Breaking Waves Over a Mild Slope". In: *Journal of Geophysical Research: Oceans* 124.11, pp. 7486–7512.

Karlsson, Therese M. et al. (2019). "Comparison between manta trawl and in situ pump filtration methods, and guidance for visual identification of microplastics in surface waters". In: *Environmental Science and Pollution Research.*

Meyerjürgens, Jens et al. (2019). "A State-of-the-Art Compact Surface Drifter Reveals Pathways of Floating Marine Litter in the German Bight". In: *Frontiers in Marine Science* 6, p. 58.

Näkki, Pinja, Outi Setälä, and Maiju Lehtiniemi (June 2019). "Seafloor sediments as microplastic sinks in the northern Baltic Sea - Negligible upward transport of buried microplastics by bioturbation". In: *Environmental Pollution*.

Onink, Victor et al. (Feb. 2019). "The Role of Ekman Currents, Geostrophy, and Stokes Drift in the Accumulation of Floating Microplastic". In: *JGR Oceans* 124.

Chamas, Ali et al. (2020). "Degradation Rates of Plastics in the Environment". In: *ACS Sustainable Chemistry & Engineering* 8.9, pp. 3494–3511.

Chegini, Fatemeh et al. (2020). "Processes of Stratification and Destratification During An Extreme River Discharge Event in the German Bight ROFI". In: *Journal of Geophysical Research: Oceans* 125.8. DOI: https://doi.org/10.1029/2019JC015987.

Lange, Xaver, Knut Klingbeil, and Hans Burchard (2020). "Inversions of Estuarine Circulation Are Frequent in a Weakly Tidal Estuary With Variable Wind Forcing and Seaward Salinity Fluctuations". In: *Journal of Geophysical Research: Oceans* 125.9. DOI: https://doi.org/10.1029/2019JC015789.

Mahmood, Faleh H., Ali K. Resen, and Ahmed B. Khamees (2020). "Wind characteristic analysis based on Weibull distribution of Al-Salman site, Iraq". In: *Energy Reports* 6. Technologies and Materials for Renewable Energy, Environment and Sustainability, pp. 79–87.

Monismith, Stephen G. (2020). "Stokes drift: theory and experiments". In: *Journal of Fluid Mechanics* 884.

Statistikmyndigheten SCB (2020). *Population*. https://www.scb.se/en/finding-statistics/statistics-by-subject-area/population/population-composition/population-statistics/pong/tables-and-graphs/quarterly-population-statistics--municipalities-counties-and-the-whole-country/quarter-13-2020/. [Accessed December 2020].

van Sebille, Erik, Stefano Aliani, et al. (2020). "The physical oceanography of the transport of floating marine debris". In: *Environmental Research Letters* 15.2.

Webb, Paul (2020). *Introduction to Oceanography*. Pressbooks.

Alistair Adcroft, Stephen Griffies, Robert Halberg (n.d.). *Ocean Mesoscale Eddies*. https://www.gfdl.noaa.gov/ocean-mesoscale-eddies/. [Published by Geophysical Fluid Dynamics Library, accessed November 2020].

Flanders Marine Institute (VLIZ) (n.d.). *Niskin bottle*. http://www.vliz.be/en/Niskinbottle. [Accessed November 2020].

Länsstyrelsen Västra Götaland (n.d.). *Gullmarn*. https://www.lansstyrelsen.se/vastra-gotaland/besoksmal/naturreservat/gullmarn.html. [Accessed December 2020].

RMB Environmental Laboratories, Inc. (n.d.). *How to Use an Integrated Sampler*. https://www.rmbel.info/training/how-to-use-an-integrated-sampler/. [Accessed November 2020].

Alice F.A. Mutton, Alastair Dougal Couper (December 2019). *Baltic Sea*. https://www.britannica.com/place/Baltic-Sea. [Published by Encyclopaedia Britannica, accessed October 2020].